DI Dorith Meischler

Polymer Composites – Characterisation and Synthesis

Dissertation

zur Erlangung des akademischen Grades eines Doktors der technischen Wissenschaften

erreicht an der

Technischen Universität Graz

Betreuer:

Ao. Univ.-Prof. DI Dr. Robert Saf

Institut für Chemische Technologie von Materialien

Technische Universität Graz

April 2008-Juli 2011

Für meine Familie

Falls Gott die Welt geschaffen hat,

war seine Hauptsorge sicher nicht,

sie so zu machen,

dass wir sie verstehen können.

Albert Einstein

Englische Fassung:

STATUTORY DECLARATION

I declare that I have authored this thesis independently, that I have not used other than the declared sources / resources, and that I have explicitly marked all material which has been quoted either literally or by content from the used sources.

…… (date)

…….. (signature)

Abstract

The main topic of this thesis is the characterisation of polymer composites. Characterisation focused on scanning electron microscopy and various other techniques. In addition, syntheses of precursors for a low bandgap polymer, for the use in hybrid solar cells, were carried out.

The first part of the work deals with the characterisation of the surface of medical gloves by means of scanning electron microscopy. Samples prepared with different production parameters, *i.e.* coating systems, coagulants and degrees of chlorination, and the influence on ageing were investigated. It was found, that chlorination had an impact on the ageing behaviour, but the coagulants not.

The second part deals with experiments to improve compounds of hybrid nanocomposite solar cells.

Therefore, several precursors and the monomer for Poly[Bis(4,4-dihexyl-*4H*-cyclopenta[1,2-*b*:5,4-*b'*]dithiophene)-2-yl-*co*-benzo[*c*][1,2,5]thiadiazole] (pTTTTBT) were synthesised successfully. The envisaged polymer, that contained a rigid backbone of thieno[3,2-*b*]thiophene and thiophenes, is a promising candidate for the use in solar cells. Within this work a route towards the desired monomer Bis(4,4-dihexyl-4*H*-cyclopenta[1,2-*b*:5,4-*b'*]dithiophene) (TTTT) is shown.

Additionally, inorganic semiconducting nanoparticles ($CuInS_2$, CIS) were characterised by means of mass spectrometry. Two different precursor systems, one with metal salts and thiourea and one with novel metal-xanthates, were used due to their different decomposition pathways towards semiconducting metal sulphides. It was found, that the use of thiourea as sulphur source leads to an undesired side-product, remaining in the active layer of solar cells. With metal-xanthates an alternative was found.

Kurzfassung

Diese Arbeit beschäftigt sich mit der Charakterisierung von Polymer-Kompositen mittels Rasterelektronenmikroskopie und diversen anderen Methoden. Zusätzlich wurden eine Vorstufen für ein low bandgap Polymer, welches in Solarzellen zur Verwendung kommen soll, hergestellt.

Der erste Teil der Arbeit behandelt die Charakterisierung der Oberfläche von medizinischen Handschuhen mittels Rasterelektronenmikroskopie. Verschiedene Herstellungsparameter, wie zum Beispiel Beschichtungen, Koagulantien und der Chlorierungsgrad, und deren Einfluss auf das Alterungsverhalten wurden untersucht. Dabei wurde festgestellt, dass die Chlorierung einen wesentlichen Einfluss auf die Alterung hat, Koagulantien hingegen nicht.

Im zweiten Teil der Arbeit wurden Versuche zur Verbesserung der Bestandteil von Hybrid-Nanokomposit-Solarzellen behandelt.

Deshalb wurden mehrere Vorstufen und das Monomer für Poly[Bis(4,4-dihexyl-*4H*-cyclopenta[1,2-*b*:5,4-*b'*]dithiophen)-2-yl-*co*-benzo[*c*][1,2,5]thiadiazol] (pTTTTBT) erfolgreich hergestellt. Das geplante Polymer, das ein starres Grundgerüst aus Thieno[3,2-*b*]thiophen und Thiophenen beinhaltet, gilt als vielversprechender Kandidat für die Verwendung in Solarzellen. In dieser Arbeit wird eine Route zur Herstellung des gewünschten Monomers Bis(4,4-dihexyl-4H-cyclopenta[1,2-b:5,4-b']dithiophen) (TTTT) gezeigt.

Zusätzlich wurden anorganische Nanopartikel mittels Massenspektrometrie charakterisiert. Zwei unterschiedliche Precursor-Systeme, eines aus Metallsalzen und Thioharnstoff und eines aus Metallxanthaten, wurden aufgrund ihrer verschiedenen Zersetzungsreaktionen zu Metallsulfiden verwendet. Es konnte gezeigt werde, dass Thioharnstoff unerwünschte Nebenprodukte bildet, welche in der Aktivschicht von Solarzellen verbleiben. Eine Alternative stellt die Verwendung von Metallxanthaten dar.

Acknowledgments

Many people contributed to this work. I want to thank …

…Ao.Univ. Prof. Dipl.-Ing. Dr. Robert Saf, who was my advisor, for his patience and guidance throughout my projects. We had lots of helpful discussions and I learned a lot from you.

…O.Univ. Prof. Dipl.-Ing. Dr. Franz Stelzer for the opportunity to work on this thesis and for financial support.

…Assoc.Prof. Dipl.-Ing. Dr. Gregor Trimmel for the possibility to be part of his group as well and for his financial support throughout my TTTT project.

…Ao.Univ.-Prof. Mag. Dr. Wolfgang Kern and Dipl.-Ing. Dr. Sandra Schlögl for their support during my glove project. Thanks go to the PCCL for financial support of this project.

…Karin und Olivia for many conversations and the nice working atmosphere.

…the solar cell group, who helped me to make progress within my project and made working in the lab a pleasure. It was a great time being part of this group. Special thanks go to Achim and Alex for the preparation of MS samples and to Stefan for his help in solar cell preparation.

…all the people that I have worked with on a daily basis.

…Karin Bartl for her help with MS measurements.

…Dipl.-Ing. Dr. Petra Kaschnitz for her support with NMR measurements.

…Prof. Iain McCulloch for the opportunity to work on TTTT and all the support he gave me throughout my internship.

…the McCulloch group, who made working in labs so enjoyable and pleasant. I want to thank especially David James and Dr. Hugo Bronstein for being such great colleagues and for their support and patience during my stay in London. It was a great time with you!

…my friends for their motivating words in hard times, their friendship and all the fun we had.

…my family for all the support they gave me throughout all the years.

…Alex for being on my side, his appreciation, tireless support and motivation.

This would not have been possible without any of you!

Table of Contents

1 Preface 12

2 Introduction 14

2.1 Composites based on natural rubber - Surface characterisation of medical gloves 14

2.1.1 Natural rubber - Origins and Properties 14

2.1.2 Production of natural rubber gloves 16

2.1.3 Ageing of natural rubber 22

2.2 Electroactive composites - Contributions to improved nanocomposite solar cells 25

2.2.1 Semiconducting polymers 26

2.2.2 Fundamentals of nanocomposite solar cells 29

3 Methods 34

3.1 Principles in electron microscopy 34

3.1.1 Fundamental processes and Interactions 34

3.1.2 Specimen 37

3.1.3 Sample preparation in SEM 37

3.2 Scanning electron microscopy 38

3.3 Influences on the performance 45

3.3.1 Acceleration voltage 45

3.3.2 Working distance 46

3.3.3 Optics 46

3.3.4 Specimen 47

3.4 Mass spectrometry 48

3.4.1 Ion source 48

3.4.2 Mass analyser 49

3.4.3 Detector 50

4 Experimental 52

4.1 Instruments and Materials 52

4.1.1 Scanning electron microscope 52

4.1.2 Sputter coater 52

4.1.3 Mass spectrometer 52

4.1.4 NMR spectrometer 53

4.1.5 Microwave 53

4.1.6 Infrared spectroscopy 54

4.1.7 Materials 54

4.2 Composites based on natural rubber 56

4.2.1 Sample preparation 56

4.3 Electroactive composites - Nanocomposite solar cells 59

4.3.1 Synthesis of precursors for a low bandgap polymer - Poly[Bis(4,4-dihexyl-*4H*-cyclopenta[1,2-*b*:5,4-*b'*]dithiophene)-2-yl-*co*-benzo[*c*][1,2,5]thiadiazole] (pTTTTBT) 59

4.3.2 CIS nanoparticles - Sample preparation for mass spectrometry 64

5 Results and Discussion 65

5.1 Surface characterisation of medical gloves 65

5.1.1 Powder coated gloves 65

5.1.2 Gloves with a low degree of chlorination 80

5.1.3 Gloves with a high degree of chlorination 89

5.2 Contributions to improved nanocomposite solar cells 98

5.2.1 Synthesis of precursors for a low bandgap polymer 98

5.2.2 Characterisation of CIS nanoparticles 111

6 Summary and Conclusion 117

6.1 Surface characterisation of medical gloves 117

6.2 Contributions to improved nanocomposite solar cells 118

7 Bibliography 123

8 Appendix 132

8.1 Abbreviations 132

8.2 Used Chemicals 133

8.3 List of Figures 133

8.4 List of Schemes 137

8.5 List of Tables 138

1 Preface

The aims of this work were the characterisation of polymer composites by means of different analytical techniques, as well as the synthesis of new materials for functional composites.

Composites in general are materials consisting of a certain, discontinuous material in a continuous phase, the so called matrix. The discontinuous phase can be of different shape, such as lamellar or particular shape. It should improve and support the physical properties - *e.g.* thermal, mechanical and electrical - of the continuous phase. In polymer composites the matrix is a polymer. In nanocomposites at least one part is in the nanometre scale. Polymer composites and nanocomposites gained high interest over the last years, especially in the field of renewable energies. Generally, polymer composites offer a lot of advantageous features such as low cost, good processability, combined with higher strength and improved physical properties, depending on the polymeric matrix and the discontinuous material. [1-4]

This thesis is divided in two parts: i) Characterisation of natural rubber gloves and ii) Contributions to improved nanocomposite solar cells.

The first part of this work deals with the characterisation of latex gloves. This work was carried out in cooperation with the Polymer Competence Center in Leoben (PCCL) and Semperit Technische Produkte GmbH. Differently produced latex gloves were investigated by means of scanning electron microscopy, their surfaces as well as their bulk were examined. The influence of production parameters such as different coagulant baths, washing cycles and coatings were studied not only on fresh, but also on aged samples. The aim was to investigate and improve barrier properties and ageing behaviour of these medical gloves.

The second part of this work deals with well selected experiments that aimed on the improvement of hybrid nanocomposite solar cells. These nanocomposite solar cells contain a hybrid assembly of a conductive, organic polymer and inorganic nanoparticles. Both compounds play an important role with respect to the performance of solar cells.

Concerning the organic component, novel precursors for a low bandgap, semiconducting polymer were synthesised. In more detail, the synthesis focused on a rigid system of 6 fused rings containing thieno[3,2-*b*]thiophene monomer units. A route, including a Stille cross coupling, as well as a microwave reaction and several typical organic syntheses, was selected. The desired novel, thiophene based, semiconducting polymer, has theoretically very promising properties for solar cells. Most of the experiments were carried out in the course of a 4 month internship (Prof. McCulloch and his group, Imperial College London).

Concerning the inorganic part, $CuInS_2$ nanoparticles made from thiourea and metal salts were investigated by electron impact mass spectrometry (EI-MS). For the synthesis of these nanoparticles the corresponding metal salts and different amounts of thiourea were mixed together. The obtained precursor solutions were drop-cast onto suitable substrates and heated to different end temperatures. The resulting nanoparticles were investigated with respect to impurities volatile under high vacuum conditions. Additionally, the formation of $CuInS_2$ from other precursors (*e.g.* xanthates) was investigated by EI-MS.

2 Introduction

2.1 Composites based on natural rubber - Surface characterisation of medical gloves

2.1.1 Natural rubber - Origins and Properties

The milky juice of several plants serves as starting material for natural rubber products. The name *caoutchouc* derives from the ancient word *Caao-Chu*, which means "weeping tree". Beside *Hevea brasiliensis* some other species, such as *Ficus elastica* (rubber plant), *Parthenium argentatum* (guayule) and *Taraxacum* (kok-saghyz) are used for the recovery of the latex milk. However, about 99 % of the natural rubber used today comes from *Hevea brasiliensis* plantations from Malaysia, Indonesia, Thailand and Africa. [5,6]

The latex milk is extracted from the tree by cutting the bark diagonally. In this process, called tapping, a milky colloidal suspension (latex), which contains not only *cis*-1,4-polyisoprene but also some other components (see Table 1), is obtained. [6-8]

Table 1: Typical composition of natural rubber [6]

solids content (35.5-44.5 %)[a]	
***cis*-1,4-polyisoprene**	30-38 %
proteins and phosphoproteins	1-2 %
resins	2 %
fatty acids	1 %
carbohydrates	1 %
inorganic salts	0.5 %

[a] 55.5-64.5 % water

Within the milk, negatively charged proteins surround rubber particles in order to prevent coagulation. However, these protein anions can be easily decomposed, either by bacteria or air. Hence, the latex milk is preserved with ammonia (~0.7 %) as soon as possible, because it stabilises the natural rubber. After preservation the latex milk is concentrated. [6,9,10]

Since the proteins present in natural rubber products are responsible for type I allergic reactions, it is recommended to improve leaching and post-cure processes in order to remove the majority of proteins. Nevertheless, natural rubber products are widely used, especially in areas which demand high toughness, flexibility and a good elongation behaviour, *e.g.* diving gear, adhesives, condoms and medical devices. [6,7,11,12]

2.1.2 Production of natural rubber gloves

In the late 19th century latex gloves were first introduced by William S. Halsted (Johns Hopkins Medical School). After that it became a standard in medicine to wear latex gloves, mainly because of their elasticity and excellent barrier properties. [13-15]

This chapter gives a short overview on the main steps during production of natural rubber gloves.

Figure 1 shows a schematic diagram of process steps involved in the production of powder coated latex gloves. In general, most of the process steps can be carried out continuously.

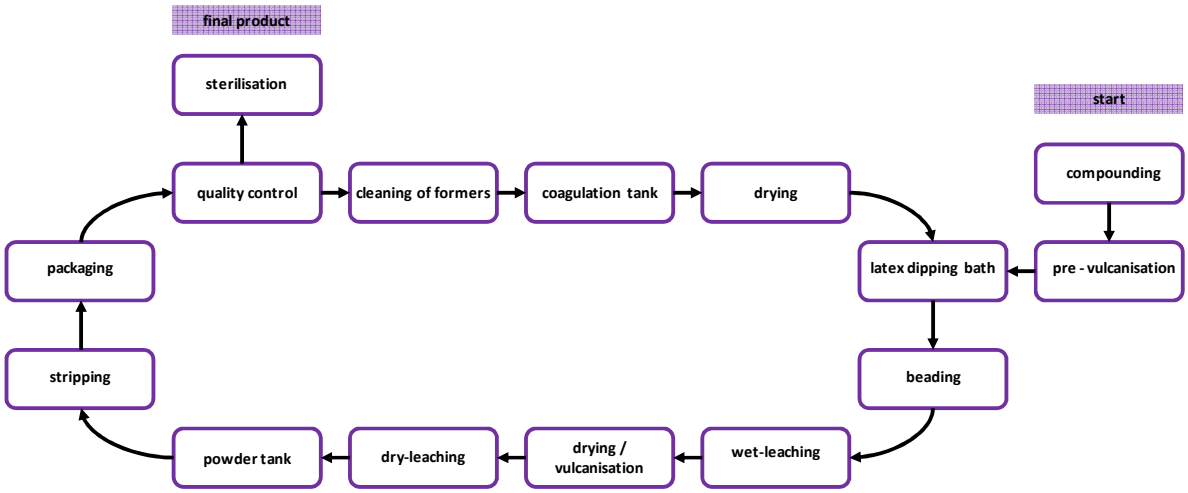

Figure 1: Production of powder coated latex gloves [8,14,16]

Compounding and Pre-vulcanisation

In the first step all compounding ingredients, including concentrated natural rubber, sulphur and additives are mixed together as aqueous solutions or dispersions. The first reported vulcanisation was attributed to Charles Goodyear in 1839. Vulcanisation, in general, is the cross-linking of the polymer chains in the natural rubber by vulcanising agents, *e.g.* sulphur or

peroxide-based systems. Without vulcanisation rubber exhibits less desirable mechanical properties and tends to be sticky. Depending on the curing mix, *i.e.* sulphur, activator, accelerator and anti-ageing reagents, and on vulcanising conditions, different properties of the rubber product can be obtained. After compounding, the mix is matured in large tanks and heated under stirring for several hours. The vulcanisation is finished during the drying step. [11,14,17-19]

Cleaning of formers

On a continuously moving chain the formers, mostly made of bone china, are cleaned. Several substances, including acidic baths, oxidising reagents, detergent solutions or combinations thereof, are employed. Without a proper cleaning of the formers it would not be possible to obtain the desired homogeneous deposition of latex in the following steps. [11,14]

Dipping processes

After cleaning, the formers are first dipped into the coagulant bath, usually containing either $CaNO_3$ or $CaCl_2$ and a wetting agent. The mix also includes a separating agent, *e.g.* $CaCO_3$ or polymers, in order to ensure that the final product can be easily removed from the formers. Following the coagulant bath the coagulant dipped formers are dried. [11,14,19,20]

In the next step the formers are lowered into the pre-cured latex bath, left for a certain time and then withdrawn from the dipping bath. Film thickness depends on the dwelling time in the latex bath and the consistency of the latex milk. Thicker films are usually obtained with a coagulant bath or by repeated dipping into the latex bath. Coagulant dipping results in colloidal destabilisation of the latex film and forms a thin gelled layer. [11,14,19,20]

Following the dipping process, the coated formers are dried.

Beading

The rim of gloves is mostly beaded at the open end. For this the edge of the deposit is rolled down mechanically with rotating brushes. Through the tackiness of the not yet fully dried material the bead is kept in the right position. [11]

Leaching

There are 2 leaching steps involved in latex glove production. First, wet gel leaching, which extracts proteins by washing the latex coated formers with warm water is carried out. After drying and vulcanisation, a dry leaching step of the already cured and dried latex film is carried out.

The quantity of removed substances depends mainly on water temperature and on extraction time. The more often and the longer the leaching processes are carried out, the fewer chemicals and allergens (proteins) are present in the glove. [19,21]

Drying and Vulcanising

Usually, these two steps occur simultaneously in hot air ovens (100-150°C). In addition to the drying of the deposited latex layer, the film also undergoes an after reaction due to the pre-vulcanisation of the latex. [11,14,20]

Post-cure treatment

To prevent the gloves from sticking together and to facilitate donning the inside of the gloves is powder coated (corn starch). This can happen in 2 different ways [14,19,22,23]:

- Powder-slurry:

  Cured gloves are dipped into a powder-slurry, dried and stripped off the formers. This is the most commonly used process by industry and also the simplest. The only problem is that there are lots of residues present, such as powder particles, chemicals and also proteins on the surface of the glove. This poses a big problem in terms of allergic reactions.

  To reduce the amount of chemicals and proteins there can be a leaching process between the curing process and the powder-slurry.

- Offline:

  After the last drying step the gloves are stripped off the formers, washed in huge tumblers and dried again. Afterwards they are powdered.

To reduce the amount of allergens present on the surface of medical gloves an alternative way is to produce non-powdered gloves. There are several processes which can be employed. Figure 2 shows the overall production process for powder-free gloves (highlighted section).

- Chlorination [14,19,22,23]:

  Some of the physical properties of natural rubber gloves can be changed by saturating the double bonds in polyisoprene with chlorine. On the one side the addition of chlorine leads to a tougher material with less tackiness. On the other side the material decolourises and an accelerated ageing process takes place. This ageing makes the gloves more prone to crack formation compared to powdered ones. Therefore the process has to be observed carefully to avoid too high chlorination.

Chlorination is most commonly carried out in huge tumblers in a batch process. Gloves are either treated with acidic (NaOCl with HCl, pH 2) or basic (NaOCl in water, pH 9) chloride solutions. Alternatively, chlorine is led into the washing water.

In each case, the chlorinated gloves are washed thoroughly with fresh water and dried afterwards.

In the above mentioned chlorination processes not only the inside of the gloves is treated, but also the outside. Alternatively, only the inside of the gloves can be chlorinated by manually turning the gloves inside out after stripping. To prevent these gloves from sticking together in the packaging, they are mostly chlorinated on the outside as well.

A third possibility is to chlorinate the latex gloves directly after curing in a continuous process.

- Inner coating [14,19,22,23]:

Coatings on the inside of gloves can be varied according to the desired properties, *e.g.* tendency to slide on wet hands. The outside is usually chlorinated with a lower concentration. The coating process can either be on-line or off-line. In the former process the wet glove is dipped into an inner coating bath. In the latter process the glove, stripped off the former, is washed in a tumbler with the coating material. Thereby both sides of the glove are coated.

In general coatings are based on silicones, polyurethanes or -acrylates.

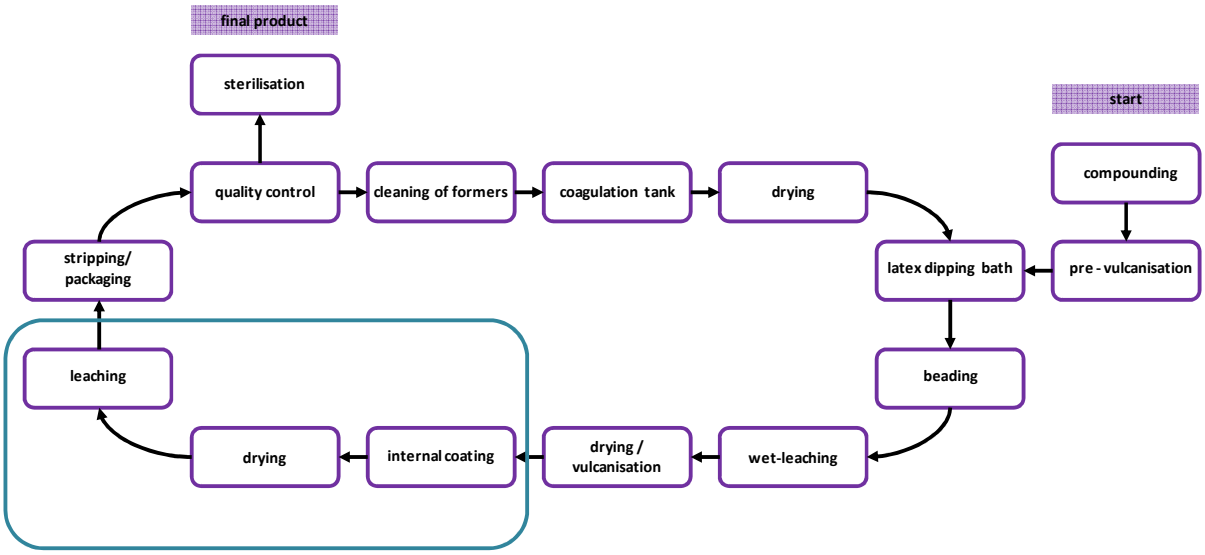

Figure 2: Production of powder-free latex gloves. [8,14,16] **The highlighted area (blue rectangle) shows the differences to powder-coated medical gloves.**

Stripping and Packaging

The last steps in the production of latex gloves are stripping and packaging including quality assurance.

For stripping the gloves off the formers, either compressed air or water jets are employed. Afterwards the gloves are classified and samples taken for inspection. Finally, the gloves are packed according to size. [11]

2.1.3 Ageing of natural rubber

Fundamentals about influences leading to ageing of natural rubber can be found in various literature reports. [10,18,19]

During ageing (*i.e.* degradation) the properties of natural rubber change due to environmental influences or usage. These changes include:

- Hardening and/or embrittlement
- Softening
- Loss of tensile and tear strength
- Cracking
- Loss of elasticity
- Surface changes (loss of colour, crazing, …)

Environmental influences, which can cause such changes, are:

- Heat
- UV-light
- Radiation
- Oxygen
- Moisture
- Ozone
- Stress
- Chemicals

The changes in natural rubbers depend strongly on the compounding process and on the type of exposure. Hence, during compounding antidegradants and antioxidants are added to the latex milk in order to prevent degradation of the products.

Oxygen

Degradation by oxygen is autocatalytic and simultaneous exposure to light accelerates the ageing effect. Different antioxidants, such as substituted phenols, diphenyl amines, *p*-phenylene diamines and benzimidazoles, are employed to prevent degradation caused by oxygen. Some antioxidants are used in combinations to yield a synergistic effect. Autoxidation is favoured in natural rubber due to the high double bond content and the methyl group next to it. During absorption of oxygen either degradation of the polymer chain can occur, which goes along with softening of the material, or cross linking takes place which is accompanied by hardening.

Metal poisoning (iron, manganese, cobalt, nickel) catalyses degradation in natural rubber products, too.

Ozone

Natural rubber is very sensitive towards ozone and tends to crack formation at slight elongation. Its ability to degrade latex is higher than that of oxygen. Formation of cracks depends on the concentration of ozone, elongation and time of exposure. Cracks deepen and the amount of cracks increases as ageing continues. Ozone attacks the double bonds in the polymer and ozonolysis takes place (Criegee mechanism [24]).

Paraffin is commonly used as antiozonant. It forms a protective layer on natural rubber. Other antiozonants are known too (butyl zimate, THIATE U, …).

UV-light

Crazing takes place when light-coloured latex products are exposed to UV-light. A network of cracks is formed on the surface which makes the natural rubber look like an elephant's skin. To prevent crazing, UV-light absorbers combined with light reflective materials (ZnO, TiO_2) are used.

Additionally, degradation products of vulcanisation accelerators can influence the degradation of natural rubber. Therefore, the amount of sulphur needed in vulcanisation, as well as vulcanisation temperature and time have to be considered to improve the ageing behaviour of latex products.

2.2 Electroactive composites - Contributions to improved nanocomposite solar cells

An ever increasing demand in energy supply is going to lead to a shortage in fossil fuels until 2050. [25]

The high demand of energy (approx. 10 TW/a [26]) is mostly covered by fossil fuels like oil, coal and gas (Figure 3). Only a small amount is supplied by renewable resources (wind, geothermal, sunlight) or nuclear energy. Furthermore, the awareness of mankind for depleting natural resources and conservation has led to a steady increase in the development of alternative energy technologies (*e.g.* photovoltaics).

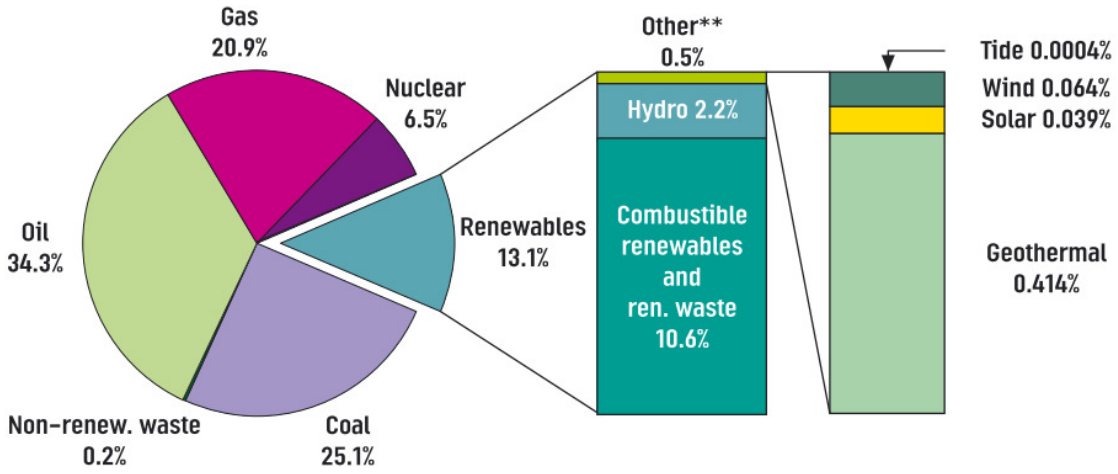

Figure 3: World primary energy supplies [27]

The sun as an inexhaustible and thus sustainable source of energy can provide $3x10^{24}$ J/a. This amount would cover the world's energy demand in 2050 (approx. 30 TW/a) 4000 times. According to Grätzel (2001) covering 0.1 % of the world's surface with solar cells having an efficiency of 10 % would be sufficient for 2050's energy demand. [26,28,29]

Generally, many different types of hybrid solar cells are known. [30] Hybrid nanocomposite solar cells consist of an organic and an inorganic part. Both parts are very important and have to be

well aligned with each other. In this chapter hybrid nanocomposite solar cells and their constituent parts are discussed.

2.2.1 Semiconducting polymers

Since the discovery of doped polyacetylene as semiconducting polymer, the field of conjugated polymers was extensively studied. [31,32]

Nowadays, many conjugated polymers are known to be semiconducting. Most of them are based on thiophenes [33-35], phenylenevinylenes [36,37], fluorenes [38-40], and carbazoles [40-43], respectively.

Responsible for conductivity in polymers is an extended π-system. Over parts of the polymer chain these π-electrons are delocalised leading to an overlap of orbitals. As a result, a bonding (π, HOMO) and an antibonding orbital (π*, LUMO) are formed. The energy difference between the HOMO and the LUMO is called bandgap (E_g). E_g determines the properties of a semiconducting polymer. Most polymers are in the range of E_g = 1.5-3 eV. For high efficiencies in solar cells low bandgap polymers (E_g<1.5 eV) are needed to match the solar spectrum. With decreasing bandgap the electron mobility, hence the conductivity, increases and the absorption spectra are red shifted. The oxidative stability of polymers is influenced by E_g, therefore low bandgap polymer containing solar cells are considered to be more stable to ambient conditions. [44-47]

In order to get low bandgap polymers, several points have to be considered: [40,45,46,48-53]

On the one side, the bandgap is lowered as the conjugation length is increased (Figure 4). This can be achieved by fusing aromatic units such as benzo- or thieno-rings. To further decrease the bandgap, twisting of the backbone should be reduced (Figure 4). Substituents (also hydrogen)

on the backbone can cause twisting though they might be necessary for the solubility. If side-chains are needed for better solubility regioregularity should be envisaged (see interchain coupling in Figure 5). To reduce twisting, a molecule can be rigidified by bridging adjacent aromatic rings together (chemical rigidification in Figure 5).

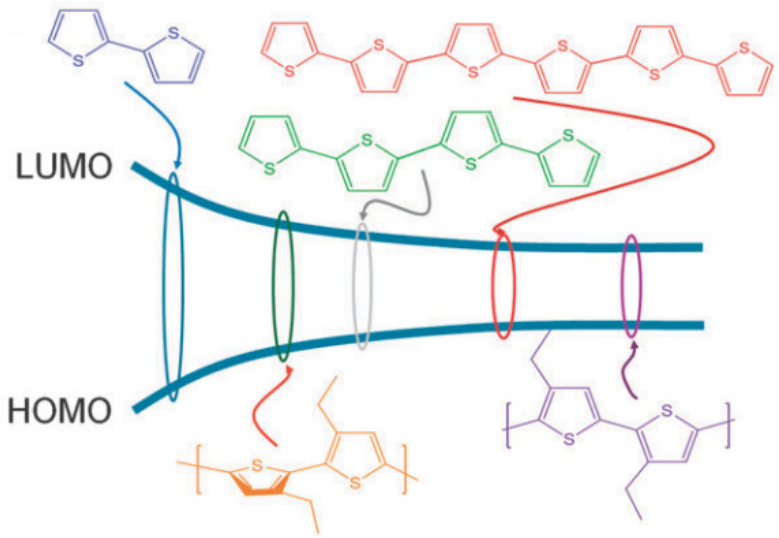

Figure 4: Influence of the conjugation length on the bandgap. [53] **LUMO (lowest unoccupied molecular orbital), HOMO (highest occupied molecular orbital)**

Higher planarity can lead to π-π stacking resulting in less steric hindrance and a lowered bandgap.

Another possibility to further decrease the bandgap of a polymer is the use the quinoidal and other mesomeric effects, whereby electrons are more delocalised (inductive or mesomeric effects and aromaticity in Figure 5).

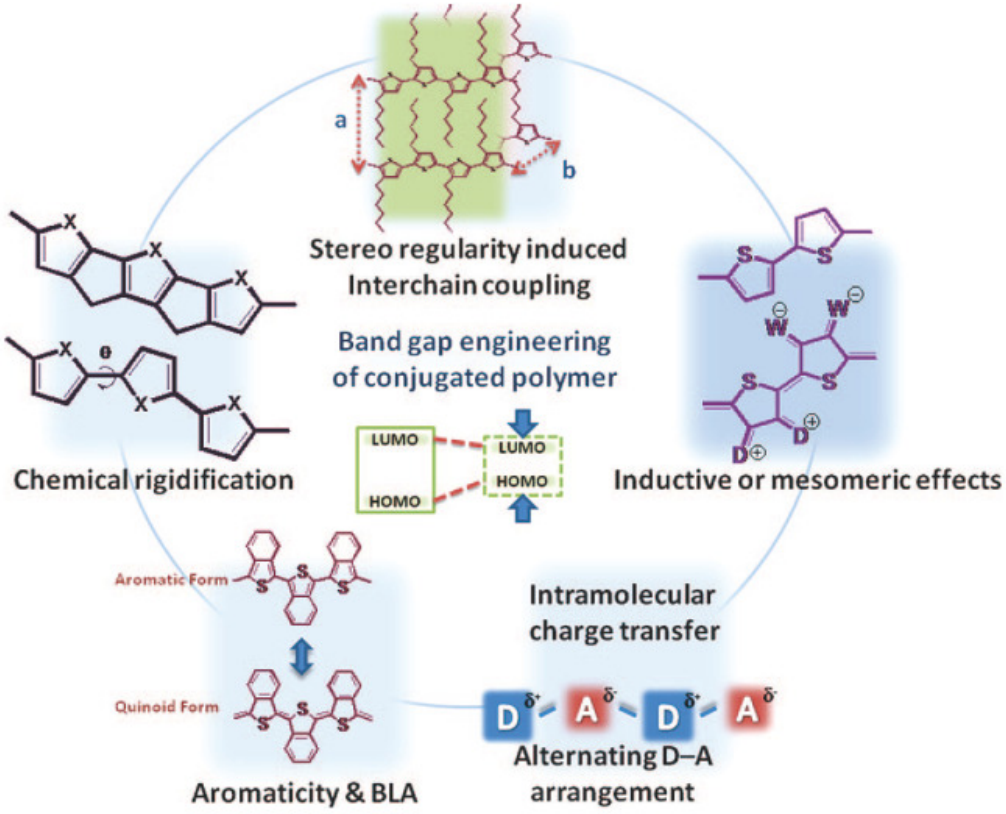

Figure 5: Effects leading to a low bandgap polymer. [40] **LUMO (lowest unoccupied molecular orbital), HOMO (highest occupied molecular orbital), D (donor), A (acceptor), BLA (bond length alternation)**

Another strategy is to use the push/pull effect of a donor/acceptor system. By using alternating donor and acceptor units within the polymer backbone the bandgap can be lowered (Figure 5 and Figure 6).

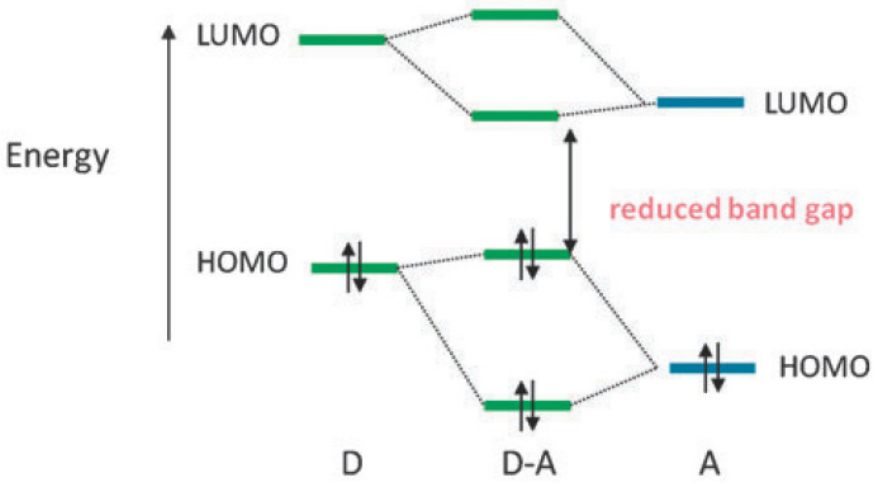

Figure 6: The bandgap can be lowered through the interaction of donor and acceptor units. [40,53] **LUMO (lowest unoccupied molecular orbital), HOMO (highest occupied molecular orbital), D (donor), A (acceptor)**

2.2.2 Fundamentals of nanocomposite solar cells

Generally, a photovoltaic device converts sunlight into electricity. Usually an organic solar cell consists of two different layers, a positive (electron donating) and a negative (electron accepting) semiconductor stacked or mixed together in different ways. There are several principles of building an efficient solar cell such as dye-sensitised, inorganic or hybrid solar cells. The latter will be discussed in this chapter. [30,54]

In a nanocomposite solar cell, containing a hybrid assembly, inorganic nanoparticles and an organic polymer, both semiconducting, are mixed together. These two phases form an interpenetrating network which is sandwiched between two electrodes (see Figure 7). [29,44,55,56]

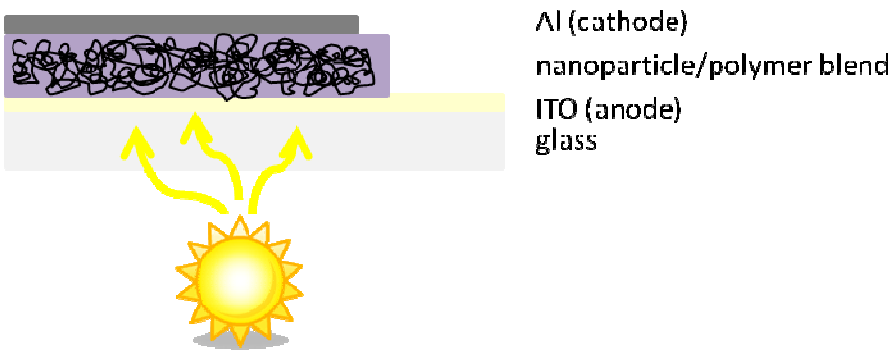

Figure 7: Schematic drawing of a nanocomposite solar cell

Once the electron-hole pairs are generated through light absorption, they have to be separated. This separation occurs at the organic/inorganic interface. Obviously, the larger the interface is, the greater is the chance for charge separation. A large interface is given in the bulk heterojunction concept shown in Figure 9 (right). After charge separation the electrons move to the cathode and the holes are transported to the transparent anode.

The main advantages of nanocomposite solar cells are their low weight, colour, low material costs and flexibility, which makes them interesting for various applications. Additionally, a roll-to-roll process is possible. [44,56-58]

The conversion of sunlight to electric power takes place in several steps according to literature. [59,60] The processes are schematically shown in Figure 8.

Firstly, *light is absorbed* in the device. The amount of absorbed sunlight limits the efficiency of solar cells and is influenced by many factors. Most polymers have bandgaps above 2.0 eV which is not ideal for light harvesting. To circumvent this problem, low bandgap polymers (E_g<1.5 eV [45,47]) are employed more often in the assembling of solar cells. Also the bandgap of the nanoparticles can be adjusted by varying the size and material. [61,62] Due to relatively high absorption coefficients of polymers only thin films (approx. 100 nm) are necessary to harvest the majority of the sunlight. To optimise absorption, reflecting back contacts are used.

The energy of the light absorbed is used to *generate excitons*. These excitons are bound electron-hole pairs. The electron-hole pairs can diffuse within a polymer depending on the exciton *diffusion* length (usually a few nanometres) before recombination takes place. At a suitable junction, such as the polymer/nanoparticle interface within nanocomposite solar cells, *dissociation* can take place. In this system the polymer is the electron donor and the nanoparticles build the electron accepting phase. Continuous pathways, as in bulk heterojunction solar cells (Figure 9 right), ensure an efficient transport of the charges to the electrodes. [44,55]

As the charges get separated, the hole stays within the polymer and the electron is transferred to the acceptor (nanoparticle) (Figure 8). Both, electron and holes, are *transported on to the respective electrodes*. The driving force for the charges to move within the material is a gradient determined by the difference of the HOMO of the donor and the LUMO of the acceptor and the difference in work functions of the used electrodes (Figure 8). At the respective electrodes the *charges are collected*. In some cases the charges have to overcome a barrier layer (a thin oxide layer) formed or deliberately introduced at the low work function electrode (*e.g.* Al). [55,56,61]

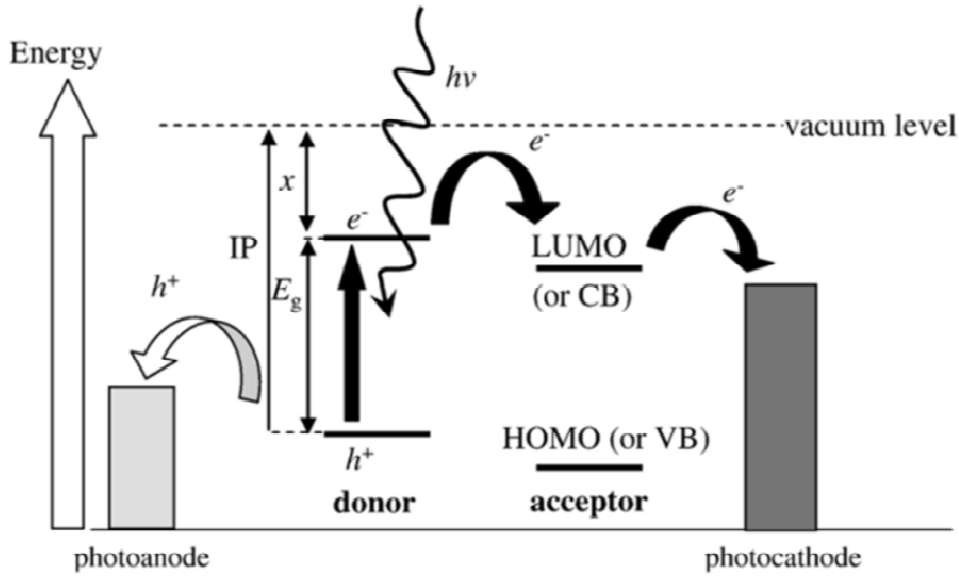

Figure 8: Transport of charges within a solar cell. [55] **HOMO (highest occupied molecular orbital), LUMO (lowest unoccupied molecular orbital), VB (valence band), CB (conduction band), h^+ (hole), e^- (electron), IP (ionisation potential), E_g (bandgap), hv (incident light), acceptor (inorganic nanoparticles), donor (organic polymer)**

The basis for hybrid nanocomposite solar cells is the well established principle of a bulk heterojunction (BHJ) (Figure 9 right). [63-65] This principle leads to a greater interfacial area and a decreased exciton diffusion length. [44,55,59,66]

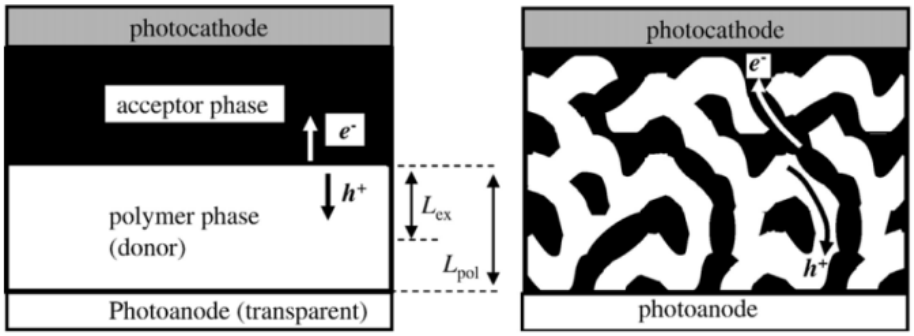

Figure 9: Schematic drawing of a bilayer heterojunction (left) and a bulk heterojunction (right). [55] **h^+ (hole), e^- (electron), L_{pol} (mean domain size of the polymer), L_{ex} (exciton diffusion length)**

The concept of nanocomposite solar cells was extensively studied by various groups with CdSe [67], CdS [68,69], $CuInSe_2$ [70,71], $CuInS_2$ [66,72,73], PbS [74-76], TiO_2 [77-79] or ZnO [80-82] as nanoparticles. Most of these nanoparticles are prepared via solvothermal or colloidal routes by utilising surfactants as shell. [66,67,83,84]

This work mainly focused on copper indium disulphide (chalcopyrite structure) as inorganic part of the nanocomposite solar cell. $CuInS_2$ (CIS) shows a high absorption coefficient and has a bandgap of 1.5 eV, which lies within the optimum range for light absorption. Major drawbacks are the price and the poor availability of indium. [85]

The nanoparticles are prepared in-situ without surfactants as capper (Figure 10).

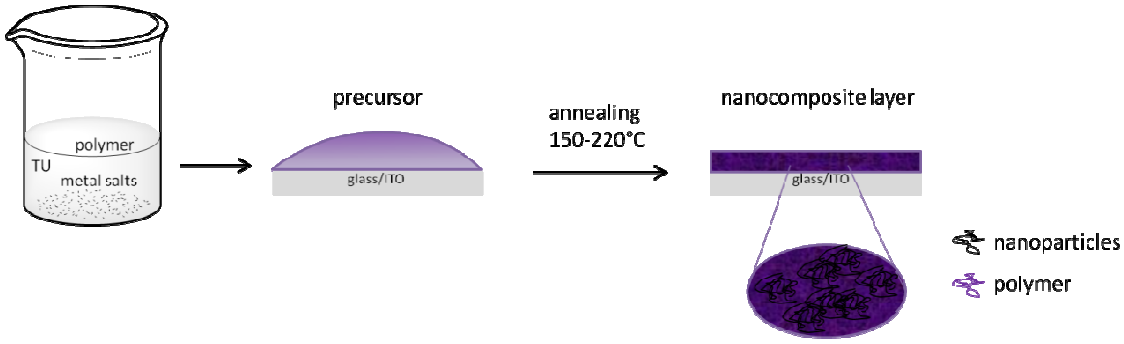

Figure 10: Schematic drawing for the production of CIS/polymer nanocomposite solar cells. ITO (indium tin oxide), TU (thiourea)

Corresponding metal salts, the polymer and thiourea - as sulphur source - are dissolved in an appropriate solvent (*e.g.* pyridine). The obtained solution is applied on a suitable substrate and annealed at different temperatures (150-450°C). During the annealing step the nanocomposite layer is formed.

3 Methods

The following methods were employed to characterise the investigated polymer composites.

3.1 Principles in electron microscopy

3.1.1 Fundamental processes and Interactions

Several interactions of primary electrons with atoms in the specimen are known (Figure 11).

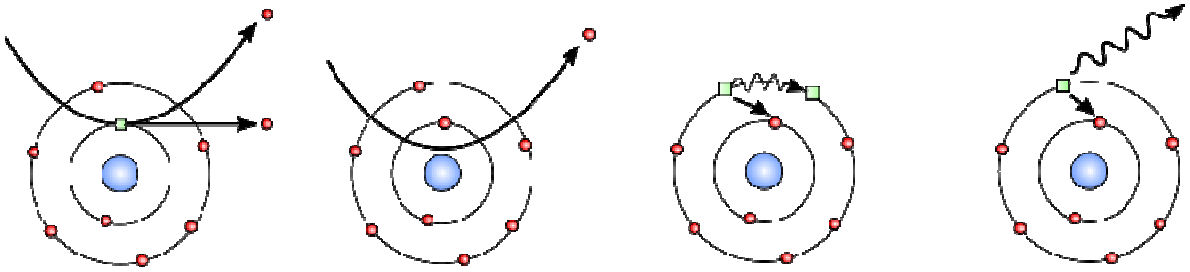

Figure 11: Interactions of primary electrons and specimen. [86] **a: secondary electrons (SE); b: backscattered electrons (BSE); c: Auger electrons; d: characteristic X-rays**

During the scanning process accelerated electrons hit the specimen surface. These electrons are scattered, either elastically or inelastically. Depending on the interaction with the atoms in the specimen different signals can be observed. Secondary electrons (SE), backscattered electrons (BSE) and characteristic X-rays are the most commonly used signals in scanning electron microscopy (Figure 11 and Figure 12). [87]

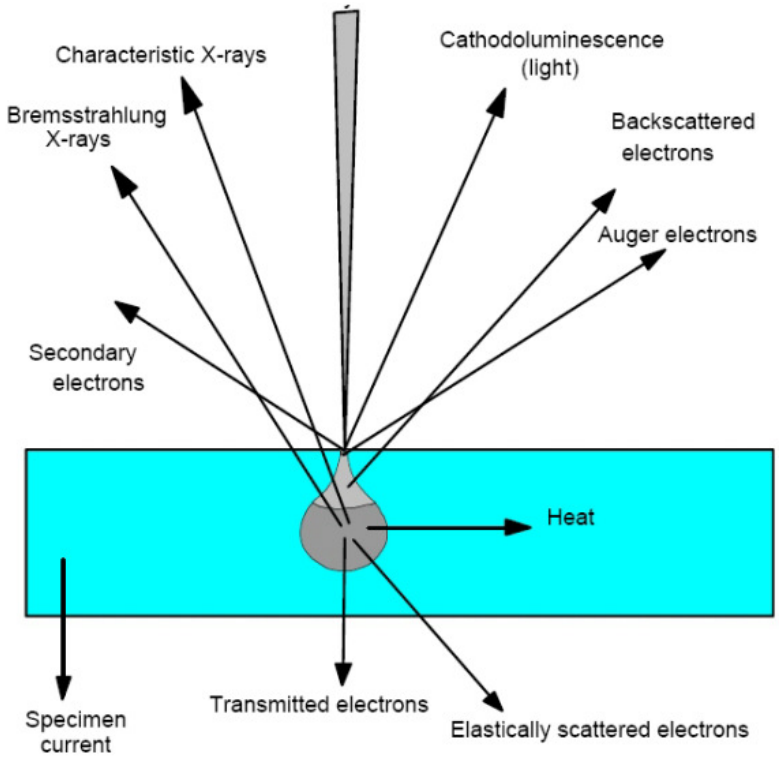

Figure 12: Interactions of the electron beam with the specimen [87]

As can be seen from Figure 12, SE originate from the topmost area of the specimen. This leads to higher resolution compared to BSE. BSE are either reflected or backscattered by interaction of the primary electrons with specimen atoms. They originate from deeper areas within the sample and have higher energies (Figure 12). BSE are used to detect different areas of chemical composition, due to a difference in atomic number of the specimen atoms. [87-89]

When the primary electron beam hits a specimen atom, a hole in the inner shell of the atom arises. This hole can be filled by an electron from an outer shell and X-rays can be detected (Figure 11). This X-rays have a characteristic energy, depending on the atom and the shell they come from. In some cases instead of emission of X-rays, the energy is transferred to another electron, which is ejected. This ejected electron is an Auger electron (Figure 11). [87-89]

The area in which the electrons are absorbed or scattered is called interaction volume. Its volume is influenced by acceleration voltage (E_0) and atomic number (Z) (Figure 13). [88-91]

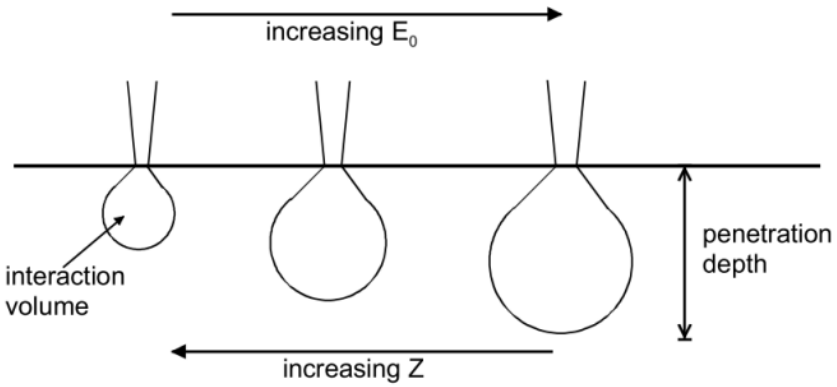

Figure 13: Dependence of atomic number (Z) and acceleration voltage (E_0) on the interaction volume [90]

Elastically scattering involves a small loss in primary energy and scattering angles > 90°. Due to their high kinetic energy these electrons (backscattered electrons, BSE) are more likely to leave the specimen and re-enter the vacuum, where they can be collected by a detector. Electrons which hit heavy atoms (high atomic number) are more scattered than these hitting light atoms (low atomic number). Thus heavy elements appear brighter in images and this contrast is used in imaging for the differentiation in elemental composition. [88-91]

Secondary electrons (SE) are produced by inelastically scattering interaction of primary electrons with atoms of the specimen. Inelastically scattering of electrons involves small scattering angles and SE have low kinetic energy (3-5 eV). Hence only secondary electrons originating from a few nanometers below the surface can escape the sample. Images derived from SE display topographical information of the specimen surface. In uneven samples some parts appear brighter than others due to facilitated escape of electrons from features present in the specimen (Figure 14). [88-91]

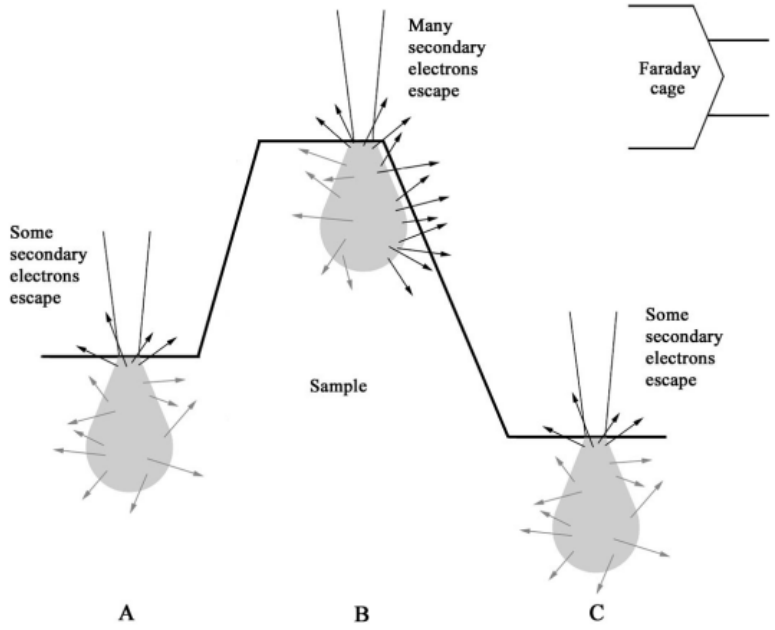

Figure 14: Edge effect in SEM. More electrons escape from morphological surface features. [92]

3.1.2 Specimen

In scanning electron microscopy samples do not have to be thin like in transmission electron microscopy (TEM). Samples can be thick and do not have to be permeable for the electron beam. [88]

3.1.3 Sample preparation in SEM

In general sample preparation for scanning electron microscopy is quite easy. Only a few things have to be considered. Firstly, the specimen has to be stable in vacuum and no solvents or particles should evaporate. Secondly, the sample should be conductive. If not, it has to be

coated with a conductive layer (Au, Pd, C) to prevent charging of the specimen by the electron beam, as this would lead to decreased image quality due to lower resolution. [88-91]

3.2 Scanning electron microscopy

One of the most important methods for imaging in material science and biology is electron microscopy. In this chapter a short overview on scanning electron microscopy is given. [88-91]

In scanning electron microscopy electrons are accelerated towards the specimen. Interactions with the atoms of the specimen produce secondary electrons, backscattered electrons or X-rays which are detected.

In Figure 15 a schematic diagram of a scanning electron microscope is shown. In principle, the electron gun produces an electron beam, which is focussed by lenses and scanned across the sample. The secondary electrons leaving the sample surface are collected by a detector. [88-91]

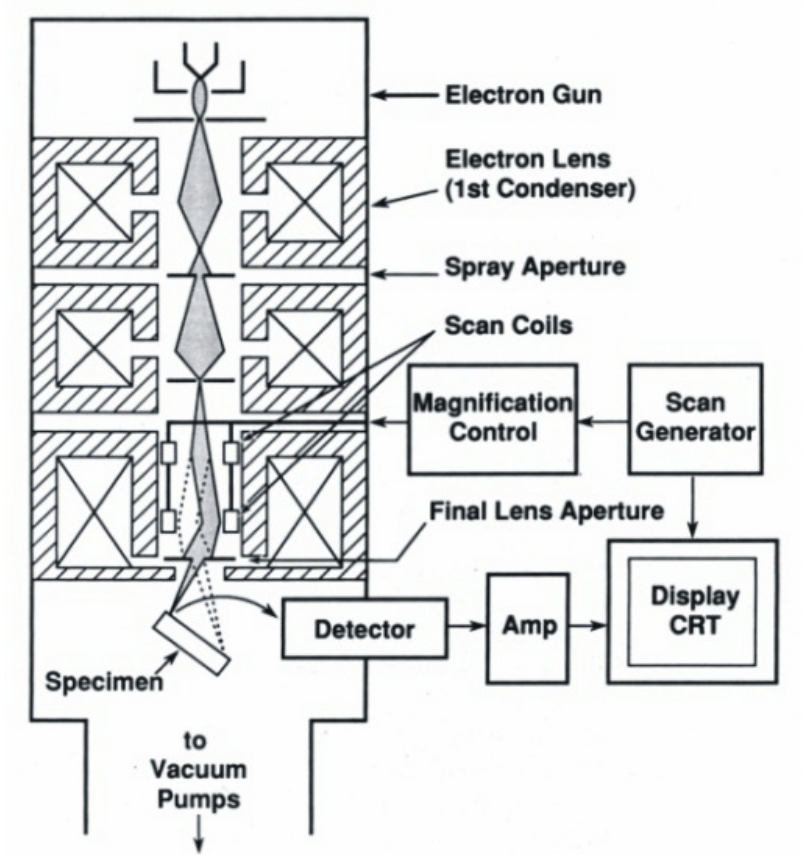

Figure 15: Schematic diagram of a scanning electron microscope (SEM) [87]

The main parts in a SEM are:

- Electron gun
- Lenses
- Vacuum system
- Scanning coils
- Detector

Electron gun

Generally, 3 types of electron sources are used in electron microscopy: tungsten filament, lanthanum hexaboride (LaB_6) cathode and field emission gun. In the majority of cases, the tungsten filament (cathode) is used, which is bent like a hairpin (Figure 16 right). An applied electric current effects heating of the filament, hence it is called thermionic cathode. At the tip of the tungsten filament electrons escape because of thermionic emission. They are accelerated towards the positively charged anode. An electron beam is established. The tungsten filament is situated in a Wehnelt cylinder (Figure 16 left), which is held at a negative potential compared to the filament. Because of this negative bias, electrons are repelled whereby the Wehnelt cylinder acts as electrostatic lens as well. [88-91]

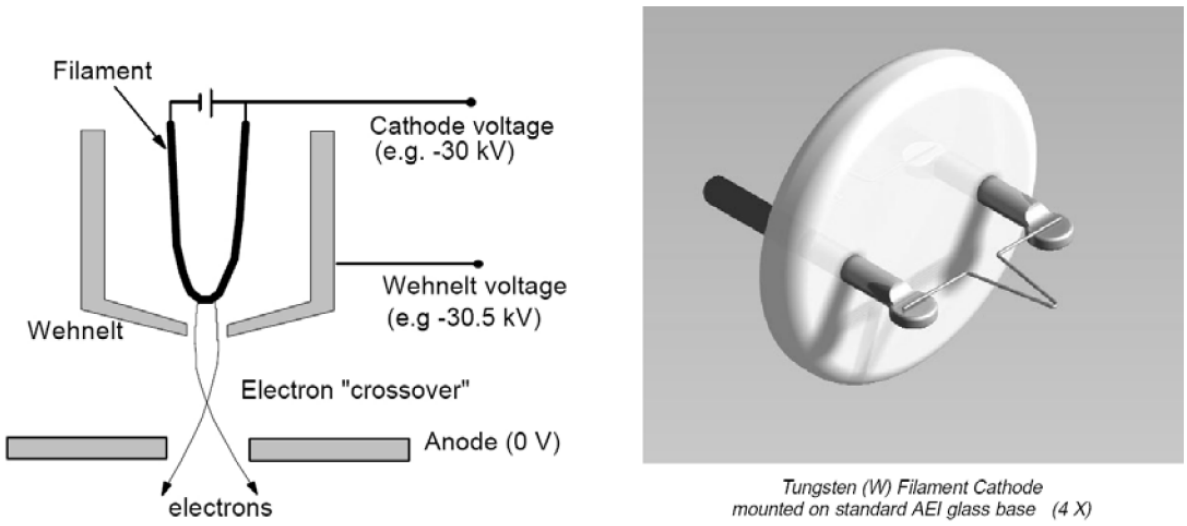

Figure 16: Schematic drawing of a Wehnelt cylinder (left) and a tungsten filament (right) [87]

The potential difference between filament and anode is called accelerating voltage (5-30 kV) and determines energy and consequently the wavelength of the electrons.

Advantageous are the stability, the cost-efficiency of the filaments and that no ultra-high vacuum is necessary. [88-90]

In a lanthanum hexaboride cathode a LaB_6 crystal is fitted in a Wehnelt arrangement. Again, a potential difference is applied and the crystal emits electrons. There are several advantages and disadvantages in comparison to the tungsten filament. The first advantage is that more electrons are emitted from a LaB_6 crystal which yields a brighter electron beam. Secondly, the electron beam is narrower. Both advantages yield a better resolution compared to a tungsten filament. As a matter of fact, the resolution of a scanning electron microscope is limited by its electron beam diameter. [88-90]

A major drawback of LaB_6 cathodes are higher maintenance costs. Moreover, higher vacuum is necessary and the crystal needs to be heated very slowly (approx. 30 minutes). [89]

The third type of electron guns is the field emission gun. It uses the principle of field emission which means that in strong electrostatic fields electrons are emitted from a tungsten tip. This type of electron gun is a cold cathode as there is no heat applied for electron emission. [88-91]

The advantages of the field emission gun are:

- The brightness of the electron beam is up to 1000 times higher compared to a tungsten filament.
- The electron beam is even narrower than the one in LaB_6 cathodes.
- Both advantages lead to a higher resolution.
- Field emission guns have a long life time.

But there are also disadvantages. Firstly, the vacuum should be approx. $1*10^{-8}$ Pa (tungsten filament: $1*10^{-4}$ Pa) which leads to more expensive electron microscopes.

Secondly, the microscope must be specially designed for field emission guns. [88-90]

Lenses

Lenses in modern electron microscopes are electromagnetic lenses. These lenses are operated by changing the current. In general there are 2-3 lenses in a scanning electron microscope. The

last lens in the scanning electron microscope is the objective lens. This lens limits the electron beam diameter and hence greatly influences the resolution of the SEM.

Aperture stops are situated at the end of electromagnetic lenses and are mainly used for further limitations of the electron beam diameter and to capture scattered electrons.

Comparable to optical microscopy, electromagnetic lenses show lens aberrations (astigmatism, spherical aberration, chromatic aberration) too, what reduces the resolution. [88-91]

Vacuum system

In electron microscopy the vacuum system is a crucial parameter due to collisions of electrons with gas molecules. This leads to ionisation of the gas molecules and to an unstable electron beam. Furthermore, the tungsten filament can react with oxygen what can cause damage. [88-91]

For these reasons the vacuum has to be high enough to get a stable electron beam and a reasonable contrast.

Usually two vacuum pumps are employed in an electron microscope. The first one is a rotary pump for low vacuum. The second pump is for high vacuum such as a diffusion pump, turbo molecular pump or getter pump. [88-90]

Scanning coils

To move the electron beam across the specimen two scanning coils are used. A generator supplies these coils with appropriate currents in order to control magnetic fields. This field "moves" the electron beam across the specimen in x- and y-direction, respectively (Figure 17). [90]

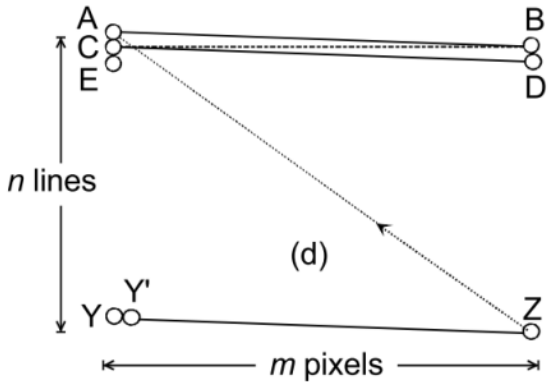

Figure 17: Scanning principle in a SEM [90]

Detector

In Figure 18 an Everhart-Thornley detector is depicted, which is used for detection of secondary electrons.

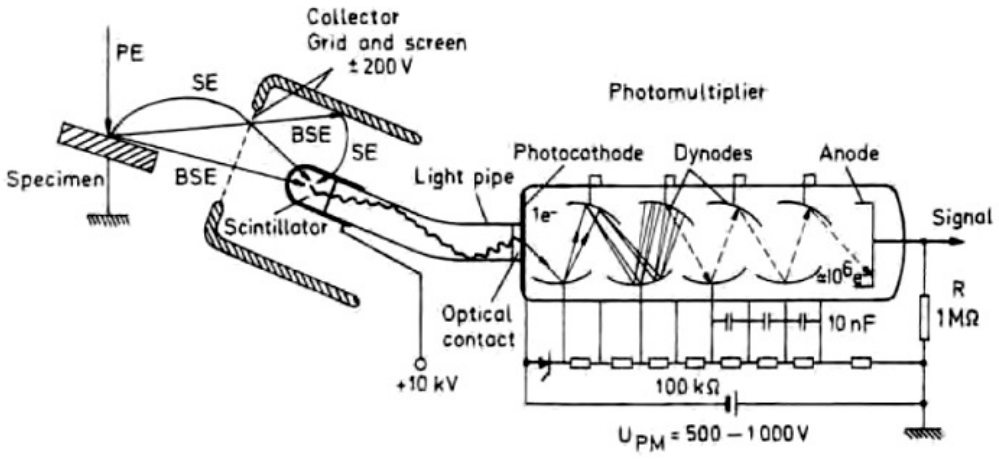

Figure 18: Everhart-Thornley detector [90]

Secondary electrons emitted from the specimen surface are attracted by the Faraday cage at the front of the detector, where a few hundred volts are applied. The electrons are accelerated

by several thousand volts towards the scintillator. Photons are generated when electrons hit the scintillator. The photons are transported to a photocathode by an optical fibre. Within the photomultiplier (PMT) the photons are converted to electrons, which are subsequently accelerated towards dynodes. A cascade process is used to multiply the incoming electrons. The signal produced by the PMT is amplified. [88-90]

Backscattered electrons are usually detected with other detectors, either a Robinson or a solid-state detector. The Robinson detector consists of a ring shaped scintillator which is mounted above the sample. When BSE hit the solid-state detector (silicon diode) free charge carriers (electrons and holes) are created which cause a current pulse. [90]

Image recording

In older electron microscopes a camera was mounted in front of a cathode ray tube (CRT) to take pictures, scanned line by line, of the specimen surface. Nowadays images are recorded digitally. [88-90]

3.3 Influences on the performance

Several parameters influence the resolution and the overall performance of a scanning electron microscope. Resolution of a scanning electron microscope lies within the range of >1-2 nm (Figure 19).

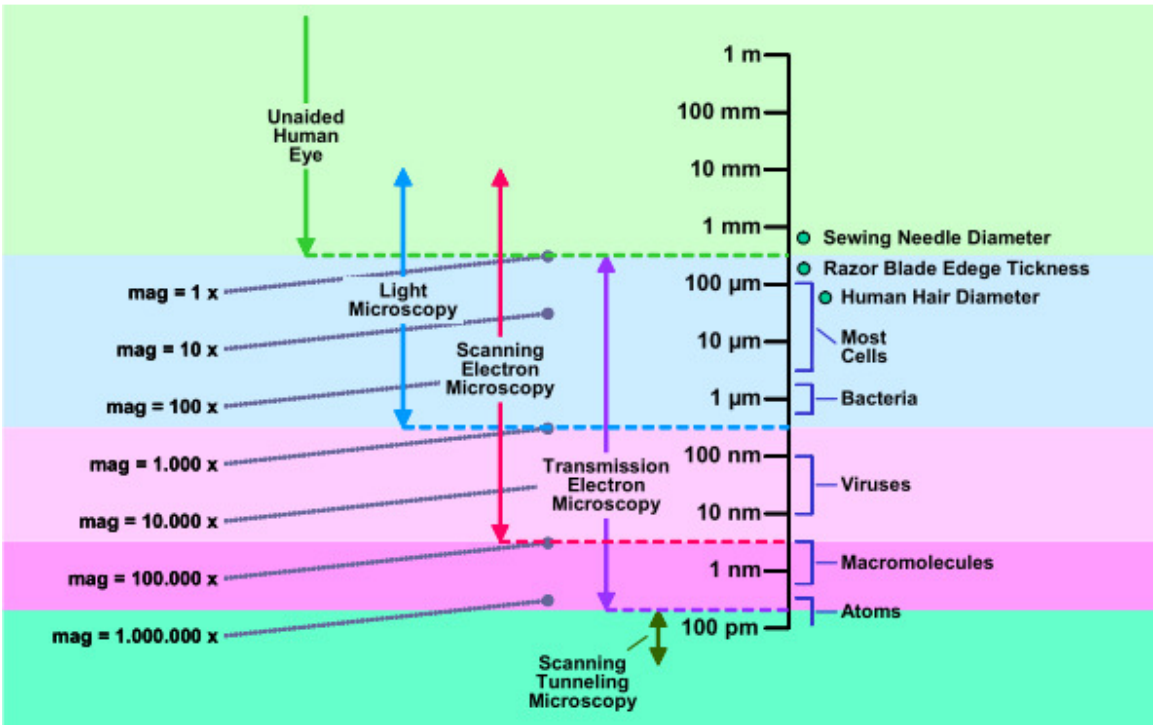

Figure 19: Resolution and magnification areas in microscopy [93]

3.3.1 Acceleration voltage

Usually, the acceleration voltage of a SEM is between 5 and 30 kV. In theory, a higher acceleration voltage leads to smaller wavelengths of the electrons. This should lead to a better resolution. But with increasing acceleration voltage also the interaction volume increases, which results in a poor resolution (Figure 13). Therefore it is necessary to

adjust the accelerating voltage according to the type of specimen. Additionally, lens aberrations limit the resolution. [88-90]

3.3.2 Working distance

The distance between the objective lens and the sample is called working distance (WD). The working distance and the aperture of the objective lens determine the diameter of the electron beam. A large WD leads to a great depth of field. The depth of field is the area which can be focussed sufficiently. It is one of the striking advantages of scanning electron microscopes compared to optical microscopy.

Unfortunately, a good depth of field does not include good resolution. For good resolution the working distance has to be as low as possible. Hence, resolution and depth of field have to be brought in line for good quality images of the sample. [88-90]

3.3.3 Optics

Resolution in general is better, the narrower the beam diameter is. This diameter is largely influenced by the objective lens. Contrary the amount of secondary and backscattered electrons decreases with decreasing probe diameter. This problem can be solved by amplification of the signal, but this leads to granularity in images and restricts resolution. [88-90]

3.3.4 Specimen

Resolution also depends on the investigated sample. Non conductive samples lead to charging and this in turn results in a lower resolution, hence in poor image quality. If a sample is not conductive itself, it can be coated with a thin conductive layer (Au, Pd, C). [88-90]

3.4 Mass spectrometry

Over the last decades an increasing interest in the field of mass spectrometry was observed. This can be mainly attributed to new ionisation and analyser techniques. [94]

In mass spectrometry substances are transferred into the gas phase prior or during ionisation. Afterwards the produced ions are analysed with respect to their mass-to-charge ratio.

The main components of a mass spectrometer are:

- *Ion source*
- *Mass analyser*
- *Detector*

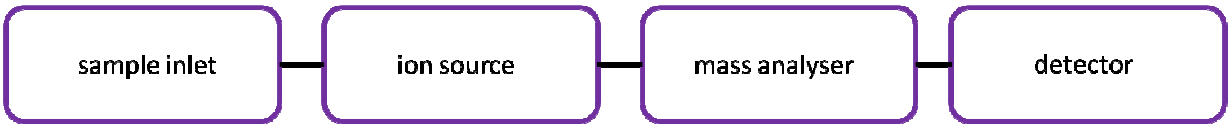

Figure 20: Schematic drawing of a mass spectrometer

3.4.1 Ion source

In the ion source molecules are ionised. In general there are two categories of ionisation techniques:

- *Ionisation of volatile compounds by electrons, electric fields or ions*
- *Ionisation of non-volatile compounds by strong electric fields, fast atoms, ions, heating or by the use of a laser*

One method to ionise volatile compounds is electron impact (EI) ionisation. Typical for this technique is, that the sample has to be evaporated thermally prior to ionisation with accelerated electrons (70 eV). The method is a rather hard ionisation technique and produces

molecular ions as well as fragment ions. A schematic drawing of an EI source is shown in Figure 21. Other popular ionisation techniques like electrospray (ESI), matrix assisted laser desorption/ionisation (MALDI) are not discussed, since they were not applied within this work. [94-96]

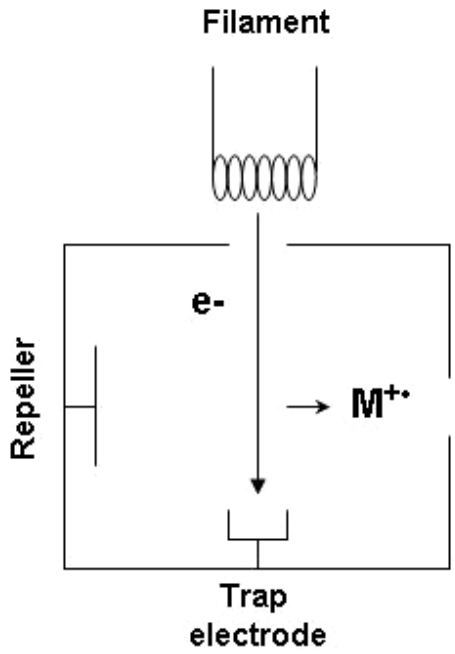

Figure 21: Schematic drawing of an EI source. [97] **e^-: electron; $M^{+\bullet}$: molecular ion**

3.4.2 Mass analyser

In a mass analyser ions are analysed with respect to their mass-to-charge ratio. Important characteristics of a mass analyser are the upper mass limit, resolving power, dynamic range, mass accuracy, transmission, operating pressure and resolution (Table 2). With appropriate resolution and mass accuracy isotope patterns can be resolved and the elemental composition of the ion can be determined. [94-96,98]

In a time-of-flight (TOF) mass analyser, generated ions are accelerated with a defined acceleration voltage resulting in the same kinetic energy for all ions having the same charge. Consequently, ions with small m/z values have higher velocities in comparison to the ions with an increased mass-to-charge ratio. The time an ion needs to get through a field free tube is measured and the mass-to-charge ratio of the respective ions can be determined. Flight times are very short hence spectra can be recorded fast. [94-96,98]

A quadrupole mass analyser consists of 4 parallel rods to which suitable voltages are applied generating an electric field. As this type of mass analyser is a scanning analyser, only ions of a certain mass-to-charge ratio pass the rods while others are eliminated. [94-96,98]

In a double focusing magnetic sector field ions are analysed by combination of an electric and a magnetic field. The instruments reach higher resolution, mass accuracy and sensitivity, but in scanning mode they are very slow when compared to a TOF. [94-96,98]

Table 2: Characteristics of different mass analysers [94]

	upper m/z limit	resolution (at m/z 1000)[a]	mass accuracy (at m/z 1000)	operating pressure / torr
TOF	$>10^6$	10^3-10^5	2-5 ppm	10^{-7}
Quadrupole	10^4	10^3-10^4	0.1%	10^{-5}
Sector field	10^4	10^5(double focusing)	<2ppm	10^{-7}

[a] Resolution is defined as the ability to distinguish between two neighbouring peaks . Two definitions are common, the 10% valley definition and "full width at half height" (FWHM).

3.4.3 Detector

In a detector an electrical signal is produced which is - in first approximation - proportional to the number of ions reaching the detector. For quadrupole and sector instruments electron multipliers or photon multipliers are employed.

TOF instruments are usually equipped with microchannel plates (MCP). In a MCP secondary electrons, generated at the entrance of the detector, are continuously multiplied within the channels, leading to current, which is finally measured. Thus, each channel of the plate acts as a miniature electron multiplier (Figure 22). [94-96]

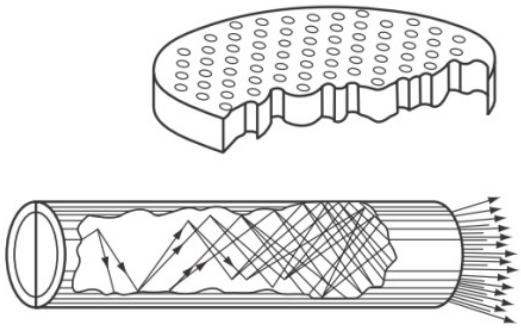

Figure 22: Micro channel plate (top) and signal amplification in a channel (bottom) [94]

4 Experimental

4.1 Instruments and Materials

4.1.1 Scanning electron microscope

JEOL JSM-5410 Scanning Microscope equipped with a SE and a BSE detector

Acceleration voltage: 5.0-30 kV

Image recording: SemAfore

4.1.2 Sputter coater

Biorad Microscience Division SC 502 SEM coating system

Coating material: Gold

4.1.3 Mass spectrometer

Waters GCT Premier

Mass analyser: orthogonal acceleration time-of-flight

Mass range: 2000 Da

Resolution: 7000 (FWHM)

Mass accuracy: better than 5 ppm RMS

Inlet system: direct insertion (DI)

Ionisation: electron impact (EI, 70 eV)

Data evaluation: Waters MassLynx V4.1

4.1.4 NMR spectrometer

^{1}H- and ^{13}C-NMR spectra: Bruker Ultrashield (300 MHz and 75 MHz, respectively)

Internal reference: TMS, solvent [99]

Temperature: 25 °C

^{119}Sn-NMR spectra: Varian Oxford (300 MHz)

Shifts (δ) are given in ppm.

4.1.5 Microwave

Microwave Synthesis System Initiator 8 by Biotage

Microwave reactions were carried out in sealed glass vials.

4.1.6 Infrared spectroscopy

FTIR spectrometer: Perkin Elmer Spectrum One IR spectrometer

Detector: DTGS detector

Mode: transmission

Substrate: CaF_2 windows

Abbreviations used for interpretation: s (strong), m (medium) and w (weak)

4.1.7 Materials

Chemicals and solvents were bought from Sigma Aldrich, Alfa Aesar, Merck, Fluka or Roth and used as obtained unless otherwise stated. For a detailed list of chemicals see Table 3.

Column chromatography was carried out on neutral alumina (0.05-0.15 mm) from Fluka.

Thin layer chromatography was carried out on aluminium supported alumina coated plates with UV fluorescence (254 and 366 nm).

Some of the reactions were carried out under inert atmosphere (Ar). In these cases the glassware was dried in a drying oven (80 °C), evacuated and flushed with Argon three times before start of the synthesis.

Table 3: Chemicals

name	company	product number	purity
Thieno[3,2-*b*]thiophene	Sigma Aldrich	702668	95 %
Trimethyltin chloride	Sigma Aldrich	146498	97 %
THF	Sigma Aldrich	401757	99.9 %, anhydrous, inhibitor free
DMF	Roth	6251	99.8 %
***n*-BuLi**	Sigma Aldrich	230707	2.5 M in hexanes
2-Bromothiophene-3-carboxylic acid	Sigma Aldrich	633011	97 %
Ethanol	Roth	T171.2	≥96 %, ca. 1 % MEK
***p*TSA**	Merck	9613	99 %
Acetone-d6	euriso-top	D009FE	99.80 %
Chloroform-d1	euriso-top	D007FE	99.80 %
Dichloromethane-d2	euriso-top	D023FE	99.90 %
Chlorobenzene	Sigma-Aldrich	270644	99.9 %
$Pd_2(dba)_3$	Sigma-Aldrich	32,877-4	-
Tri-*o*-tolylphosphine	Fluka	93415	≥97 %
Hexylmagnesium bromide	Sigma-Aldrich	255025	2.0 M in diethyl ether
Ethyl acetate	Roth	7338.2	≥99.5 %, for synthesis
DCM	Roth	8424.5	≥99.5 %, for synthesis
Acetonitrile	Sigma-Aldrich	27,100-4	99.8%
NaCl	Roth	71383	100 %
Sodium sulphate	Roth	8631.1	≥99 %, water free
HCl	Sigma Aldrich	258148	37 %
$NaHCO_3$	Roth	6885.2	≥99.5 %
Methanol	Sigma Aldrich	24229	puriss.
Hexane	Roth	3907.3	95 %, for synthesis
H_2SO_4	Roth	X945.1	98 %
TMEDA	Sigma-Aldrich	T2,250-0	99 %
Alumina	Fluka	06300	-

4.2 Composites based on natural rubber

4.2.1 Sample preparation

The aim of this work was to investigate the ageing of differently produced latex samples. All samples were analysed on their outer side and inner side by means of SEM. Additionally, the edge obtained after “breaking” of the samples was investigated, too.

First the samples, taken from approximately the same area of the glove, were cut into small strips (approx. 2x15 mm). In order to obtain a breaking edge of the samples they were either torn with tweezers until rupture (RT fracture) or dipped into liquid nitrogen before they were fractured (freeze fracture).

Most of the samples were aged for 21 days in Petri dishes with the outer side upwards (absence of direct sunlight, constant temperature). Later on the samples were stored under inert atmosphere to prevent uncontrolled ageing. Some samples were received as “already aged” (Semperit Technische Produkte Gesellschaft m.b.H., Wimpassing, for 17 days) (see Table 4, Table 5 and Table 6).

Powder coated samples were either carefully washed with deionised water or wiped dryly to minimise powder particles on the surface.

Prior to investigation, all samples were coated with a thin layer of gold to ensure conductivity of the specimens.

To investigate edges obtained after fracture, samples were placed on a bevelled specimen holder (approx. 45°).

Table 4: Investigated latex samples - Semperit

Number	Sample name[a]	Sample preparation[b]	Ageing[c]
1	Sempercare LF 2007	RT	0
2	Sempercare LF 2007	N_2[c]	21/TU
3	Sempercare LF 2006	RT	0
4	Sempercare LF 2006	N_2	21/TU
5	Sempercare IC 2007	RT	0
6	Sempercare IC 2007	N_2	21/TU
7	Sempercare IC 2006	RT	0
8	Sempercare IC 2006	N_2	21/TU
9	$CaCl_2$ coagulant, modified coating	N_2	0
10	$CaCl_2$ coagulant, modified coating	N_2	21/TU
11	$Ca(NO_3)_2$ coagulant, modified coating	N_2	0
12	$Ca(NO_3)_2$ coagulant, modified coating	N_2	21/TU
13	$CaCl_2$ coagulant	RT	0
14	$CaCl_2$ coagulant	N_2	21/TU
15	$Ca(NO_3)_2$ coagulant	RT	0
16	$Ca(NO_3)_2$ coagulant	N_2	21/TU
17	untreated material	RT	0
18	untreated material	N_2	21/TU
19	Supreme, without leaching	N_2	0
20	Supreme, without leaching	N_2	21/TU
21	Supreme, without leaching, modified coating	N_2	0
22	Supreme, without leaching, modified coating	N_2	21/TU
23	Supreme, NaOCl	N_2	0
24	Supreme, NaOCl	N_2	21/TU
25	Supreme, NaOCl, modified coating	N_2	0
26	Supreme, NaOCl, modified coating	N_2	21/TU
27	Supreme, HCl/NaOCl	N_2	0
28	Supreme, HCl/NaOCl	N_2	21/TU
29	Supreme, HCl/NaOCl, modified coating	N_2	0
30	Supreme, HCl/NaOCl, modified coating	N_2	21/TU
31	Supreme, TWA[d]/Standard	N_2	0
32	Supreme, TWA[d]/Standard	N_2	21/TU
33	Supreme, TWA[d]/Standard, modified coating	N_2	0
34	Supreme, TWA[d]/Standard, modified coating	N_2	21/TU

[a] modified coating...coating on the inner side of the medical gloves (silicon, polymer), [b] For details of the sample preparation compare text (chapter 4.2.1). RT...RT fracture, N_2...freeze fracture, [c] days of ageing/location of ageing, [d] TWA...intermittent washing system

Table 5: Investigated latex samples - other companies

Number	Sample name	Sample preparation[a]	Ageing[b]
35	Peha Soft	RT	0
36	Peha Soft	RT	17/Semperit
37	Flexam	N_2	0
38	Flexam	N_2	17/Semperit
39	Bodyguards	N_2	0
40	Bodyguards	N_2	17/Semperit
41	Sensitex	RT	0
42	Sensitex	N_2	21/TU Graz
43	Supermax	RT	0
44	Ansell	RT	0

[a] For details of the sample preparation compare text (chapter 4.2.1). RT...RT fracture, N_2 ...freeze fracture, [b] days of ageing/location of ageing

Table 6: Investigated, not aged latex samples

Number	Sample name	Sample preparation[a]
45	Sempercare Edition 2008	RT
46	Semperguard 2008	RT
47	Sempercare Edition 2008, rough	RT
48	Sempercare Edition 2008, smooth	RT
49	Sempermed Classic	RT
50	Sempermed Supreme	RT
51	OPH, sterilised	RT

[a] For details of the sample preparation compare text (chapter 4.2.1). RT...RT fracture

4.3 Electroactive composites - Nanocomposite solar cells

4.3.1 Synthesis of precursors for a low bandgap polymer - Poly[Bis(4,4-dihexyl-*4H*-cyclopenta[1,2-*b*:5,4-*b'*]dithiophene)-2-yl-*co*-benzo[*c*][1,2,5]thiadiazole] (pTTTTBT)

In this chapter the synthesis of precursors for a conjugated, semiconducting polymer are described. Parts of this work were carried out in Prof. McCulloch's group during an internship at Imperial College in London. Several routes were investigated to obtain the desired TTTT monomer, but only one route appeared promising. This route is discussed in this chapter.

*Synthesis of 2,5-bis(trimethylstannyl)thieno[3,2-b]thiophene (**1**)* [100-102]

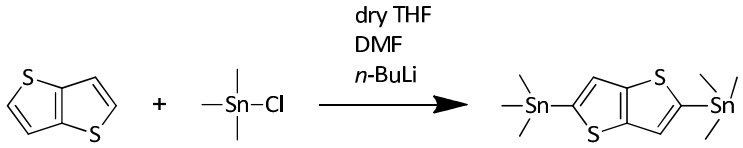

1

Scheme 1: Synthesis of substance 1

Thieno[3,2-*b*]thiophene (7.05 g, 50 mmol, 1 eq) and *N,N,N',N'*-tetramethylethylenediamine (TMEDA) (17 ml, 113 mmol, 2.27 eq) were dissolved in dry THF (140 ml) (clear solution). The reaction mixture was cooled to -78 °C and a 2.5 M solution of *n*-BuLi in hexane (46 ml, 115.5 mmol, 2.3 eq) was added within 15 min. Afterwards the reaction was allowed to warm to room temperature and stirred for 4 h before additional *n*-BuLi (10 ml, 25 mmol, 0.5 eq) was added - an off-white coloured suspension was formed. 1 h later the reaction was cooled to 0 °C and trimethyltin chloride (26 g, 130 mmol, 2.6 eq) was added at once. Subsequently, the cooling bath was removed and the reaction mixture was allowed to warm up to RT and stirred over night. A clear, dark orange solution was formed. The reaction was quenched with water

and extracted with ethyl acetate. The combined organic layers were washed with water and brine, dried over sodium sulphate, and the solvent was removed under reduced pressure to yield a brownish solid. The crude product was recrystallised from hot acetonitrile twice, yielding **1** as a white solid (10.16 g = 43.7 %).

^{1}H-NMR (acetone-d6, ppm): δ 7.40 (s, 2H), 0.39 (s, 18H)

^{13}C-NMR (chloroform-d1, ppm): δ 147.67, 141.43, 126.30, -8.01

^{119}Sn-NMR (chloroform-d1, ppm): δ -25.082

*Synthesis of ethyl 2-bromothiophene-3-carboxylate (**2**)* [46,103]

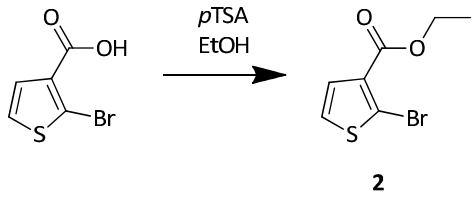

2

Scheme 2: Synthesis of substance 2

2-bromothiophene-3-carboxylic acid (5 g, 24.15 mmol, 1 eq) and *p*-toluenesulfonic acid (*p*TSA) (7 g, 40.6 mmol, 1.68 eq) were dissolved in ethanol (120 ml) and refluxed over night. Ethanol was removed under reduced pressure. The crude product was extracted with dichloromethane (DCM) and saturated sodium hydrogen carbonate. The combined organic layers were washed with brine and dried over sodium sulphate. The solvent was removed under reduced pressure to yield a white solid (compound **2**) (5.59 g = 98 %), which was taken to the next step without further purification.

^{1}H-NMR (chloroform-d1, ppm): δ 7.33 (d, 1H), 7.20 (d, 1H), 4.36-4.29 (q, 2H), 1.39-1.34 (t, 3H)

^{13}C-NMR (chloroform-d1, ppm): δ 162.20, 131.48, 129.59, 125.97, 119.89, 61.19, 14.47

*Synthesis of diethyl 2,2'-(thieno[3,2-b]thiophene-2,5-diyl)bis(thiophene-3-carboxylate) (**3**)* [46,104]

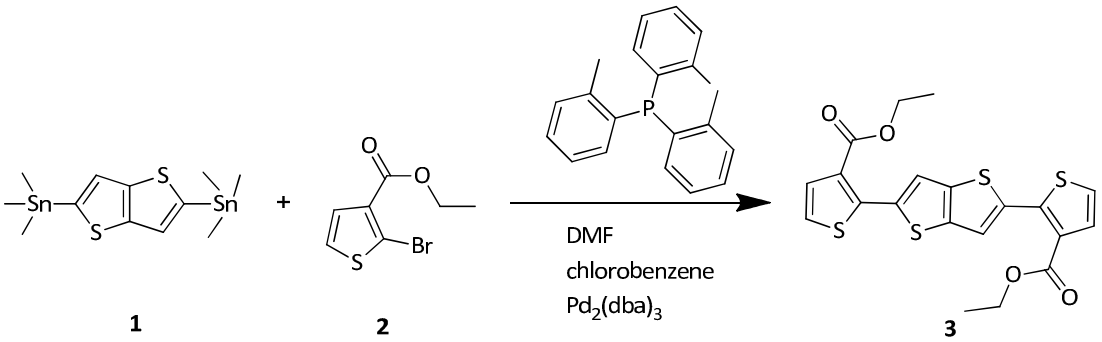

1 **2** **3**

Scheme 3: Synthesis of substance 3

Ethyl 2-bromothiophene-3-carboxylate **2** (4.02 g, 17 mmol, 2.21 eq), 2,5-bis(trimethylstannyl)thieno[3,2-*b*]thiophene **1** (3.618 g, 7.76 mmol, 1 eq), $Pd_2(dba)_3$ (0.156 g, 0.17 mmol, 0.02 eq), tri-*o*-tolylphosphine (0.239 g, 0.785 mmol, 0.1 eq), chlorobenzene (8 ml) and DMF (0.6 ml, 7.76 mmol, 1 eq) were put into a microwave vial with a stir bar under inert atmosphere. The vial was placed in a microwave reactor and heated for 10 min at 200 °C with 1 min prestirring. Subsequently, the reaction mixture was cooled to RT and poured into 100 ml of a methanol/2 M HCl mixture. The precipitate was filtered off and dissolved in hot ethyl acetate. The hot solution was filtered into ethanol and the formed precipitate was filtered off to yield compound **3** as a shiny orange solid (2.96 g = 85 %). The product was used without further purification.

^{1}H-NMR (DCM-d2, ppm): δ 7.69 (s, 2H), 7.50 (d, 2H), 7.29-7.28 (d, 2H), 4.33-4.26 (q, 4H), 1.31 (t, 6H)

^{13}C-NMR (DCM-d2, ppm): δ 163.44, 143.03, 140.96, 136.83, 131.20, 129.23, 125.18, 121.78, 61.43, 14.57

MS (EI, 70 eV): 447.99 Da (molecular ion), 419.96 Da (fragment ion), 391.93 Da (fragment ion)

HRMS: calc 447.9931 Da for $C_{20}H_{16}O_4S_4$, found 447.9922 Da; calc 419.9619 Da for $C_{18}H_{12}O_4S_4$, found 419.9645 Da; calc 391.9305 Da for $C_{16}H_8O_4S_4$, found 391.9337 Da

*Synthesis of 7,7'-(2,2'-(thieno[3,2-b]thiophene-2,5-diyl)bis(thiophene-3,2-diyl)bis(tridecan-7-ol) (**4**)* [46,105]

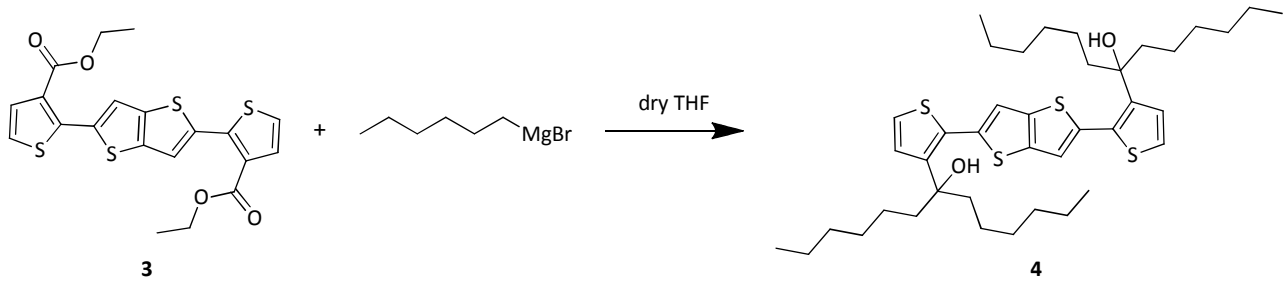

3 **4**

Scheme 4: Synthesis of substance 4

To a solution of compound **3** (2.553 g, 5.69 mmol, 1 eq) in dry THF (20 ml) a 2.0 M solution of hexylmagnesium bromide in ether (13 ml, 26 mmol, 4.6 eq) was added slowly at 0 °C - a brown solution was formed. After 4 h additional hexylmagnesium bromide (8 ml, 16 mmol, 2.8 eq) was added. The reaction mixture was refluxed over night. The reaction was quenched with water (ca. 50 ml) and extracted with ethyl acetate. The combined organic layers were dried over sodium sulphate and the solvent was removed under reduced pressure (3.70 g = 94.6 %). The crude product was taken to the next step without further purification.

*Synthesis of Bis(4,4-dihexyl-4H-cyclopenta[1,2-b:5,4-b']dithiophene) (TTTT) (**5**)* [46,105,106]

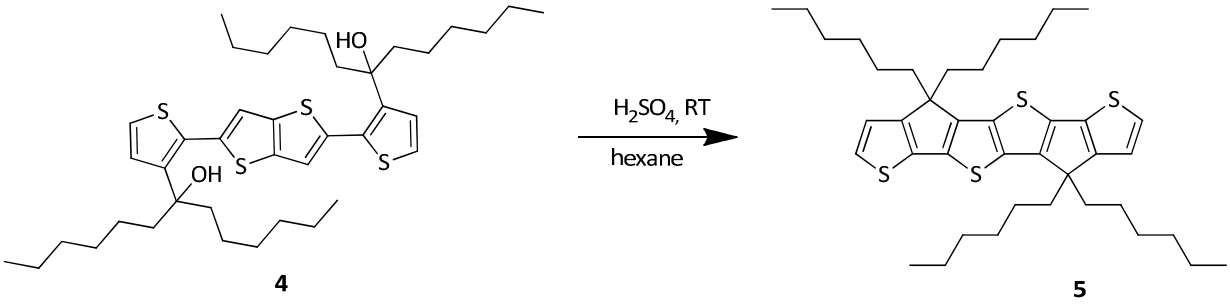

4 **5**

Scheme 5: Synthesis of TTTT 5

Sulphuric acid (8 ml, 150 mmol, 29 eq) was added dropwise to a solution of compound **4** (3.61 g, 5.15 mmol, 1 eq) in hot hexane (70 ml) under vigorous stirring. A black sticky solid precipitated immediately. The mixture was stirred for 16 h at RT before it was quenched with deionised water (ca. 100 ml). The aqueous layer was extracted with DCM (ca. 1000 ml) several times. The organic fractions were washed with saturated sodium hydrogen carbonate and brine, followed by removal of the solvent under reduced pressure. The black solid, which precipitated after adding sulphuric acid, was extracted with hexane in a Soxhlet for 4 d. The obtained solution was evaporated under reduce pressure, and the residual brownish oil purified by column chromatography on alumina (eluent: hexane). The product was obtained as orange oil (50 mg = 1.5 %, mixed fractions).

R_f (on alumina, hexane as eluent): 0.8

MS (EI, 70 eV): 664.33 Da (molecular ion)

HRMS: calc 664.3265 Da for $C_{40}H_{56}S_4$, found 664.3304 Da

FTIR (cm^{-1}): **fractions 1-60** 2925.16 (s), 2854.69 (s), 1460.66 (m), 1377.27 (m), 965.45 (w), 909.11 (w), **mixed fractions** 2925.30 (s), 2854.62 (s), 1464.46 (m), 1377.48 (m)

4.3.2 CIS nanoparticles - Sample preparation for mass spectrometry

First, ITO-coated glass substrates were cleaned according to literature with water and isopropanol in an ultrasonic bath. [107,108] Copper acetate, indium (III) chloride and thiourea in various amounts (1.6, 2.8 and 4 eq) were dissolved in pyridine and stirred until clear precursor solutions were formed. The obtained solutions were sprayed onto dried and cleaned ITO/glass substrates. After drying the substrates were annealed to 200 °C, 300 °C and 450 °C, respectively. After 30 minutes at the selected temperature the samples were cooled to room temperature. The annealing step was carried out under vacuum (p = 20-100 mbar).*

Prior to analyses the obtained CIS films were scraped of the ITO/glass surface and transferred into a glass tube used for direct insertion mass spectrometry (DI-MS). During DI-MS, samples were heated under high vacuum using a ramp from room temperature to 450 °C. [109]

Metal xanthates [110] were dissolved in chloroform. Solutions were directly transferred into glass tubes used for DI-MS.

* The preparation of the samples was carried out by DI Achim Fischereder.

5 Results and Discussion

5.1 Surface characterisation of medical gloves

The influence of several production parameters on the appearance and on the lifetime of medical gloves was investigated. Generally, gloves can be coated on the inner side with silicon oil or a synthetic polymer to facilitate donning. To prevent medical gloves from sticking together, they have either powder on the outer side or are chlorinated. In this chapter the synthetic coating (silicon, polymer) on the inner side is termed modified coating.

5.1.1 Powder coated gloves

Several samples coated with powder were investigated. They differ in the used coagulants, leaching processes and the untreated material, they were made from.

Table 7 gives an overview of these powder-coated (not chlorinated) samples. Some products from other companies were investigated too (compare Table 7).

Table 7: Overview of non-chlorinated latex samples

Number	Sample name[a]	Description[b] [111-117]
13	$CaCl_2$ coagulant	dry powder, washed with water, conventionally sulphur cured, not chlorinated, no silicon oil, RT
14	$CaCl_2$ coagulant, aged	dry powder, washed with water, conventionally sulphur cured, not chlorinated, no silicon oil, 21 days aged, N_2
15	$Ca(NO_3)_2$ coagulant	dry powder, washed with water, conventionally sulphur cured, not chlorinated, no silicon oil, RT
16	$Ca(NO_3)_2$ coagulant, aged	dry powder, washed with water, conventionally sulphur cured, not chlorinated, no silicon oil, 21 days aged, N_2
17	Untreated material	NR-film, OPH Classic, no powder, conventionally sulphur cured, $CaCl_2$-coagulant, not chlorinated, no silicon oil, RT
18	Untreated material, aged	NR-film, OPH Classic, no powder, conventionally sulphur cured, $CaCl_2$-coagulant, not chlorinated, no silicon oil, 21 days aged, N_2
19	Supreme, without leaching	dry powder, sample was wiped dryly, N_2
20	Supreme, without leaching, aged	dry powder, sample was wiped dryly, 21 days aged, N_2
21	Supreme, without leaching, modified coating	dry powder, sample was wiped dryly, N_2
22	Supreme, without leaching, modified coating, aged	dry powder, sample was wiped dryly, 21 days aged, N_2
31	Supreme, TWA[c]/Standard	dry powder, intermittent washing system, without silicon oil, lab dryer, sample was wiped dryly, N_2
32	Supreme, TWA[c]/Standard, aged	dry powder, intermittent washing system, without silicon oil, lab dryer, sample was wiped dryly, 21 days aged, N_2
33	Supreme, TWA[c]/Standard, modified coating	intermittent washing system, without silicon oil, lab dryer, sample was wiped dryly, N_2
34	Supreme, TWA[c]/Standard, modified coating, aged	intermittent washing system, without silicon oil, lab dryer, sample was wiped dryly, 21 days aged, N_2
43	Supermax	powder coated, not chlorinated, smooth surface, washed with water, cracked
44	Ansell	powder coated, not chlorinated, smooth surface, washed with water, RT
45	Sempercare Edition 2008	Smooth surface, not chlorinated, modified coating, powder on outside, cracked
49	Sempermed Classic	OPH sterilised, NR latex, pre-powdered, modified coating, RT
51	OPH[d] sterilised	UV-cross linked latex, smooth surface, not chlorinated, washed with water prior to investigation, RT

[a] modified coating...coating on the inner side of the medical gloves (silicon, polymer), [b] For details of the sample preparation compare text (chapter 4.2.1). RT...RT fracture, N_2...freeze fracture, [c] TWA...intermittent washing system, [d] OPH...surgical glove

Samples with different coagulants (13, 14, 15, 16)

These samples were prepared by dipping into different coagulants, $CaCl_2$ and $Ca(NO_3)_2$ respectively. They were not chlorinated but to facilitate donning they were coated with dry powder. Before investigation in the SEM they were washed with deionised water to remove residual powder from the surface.

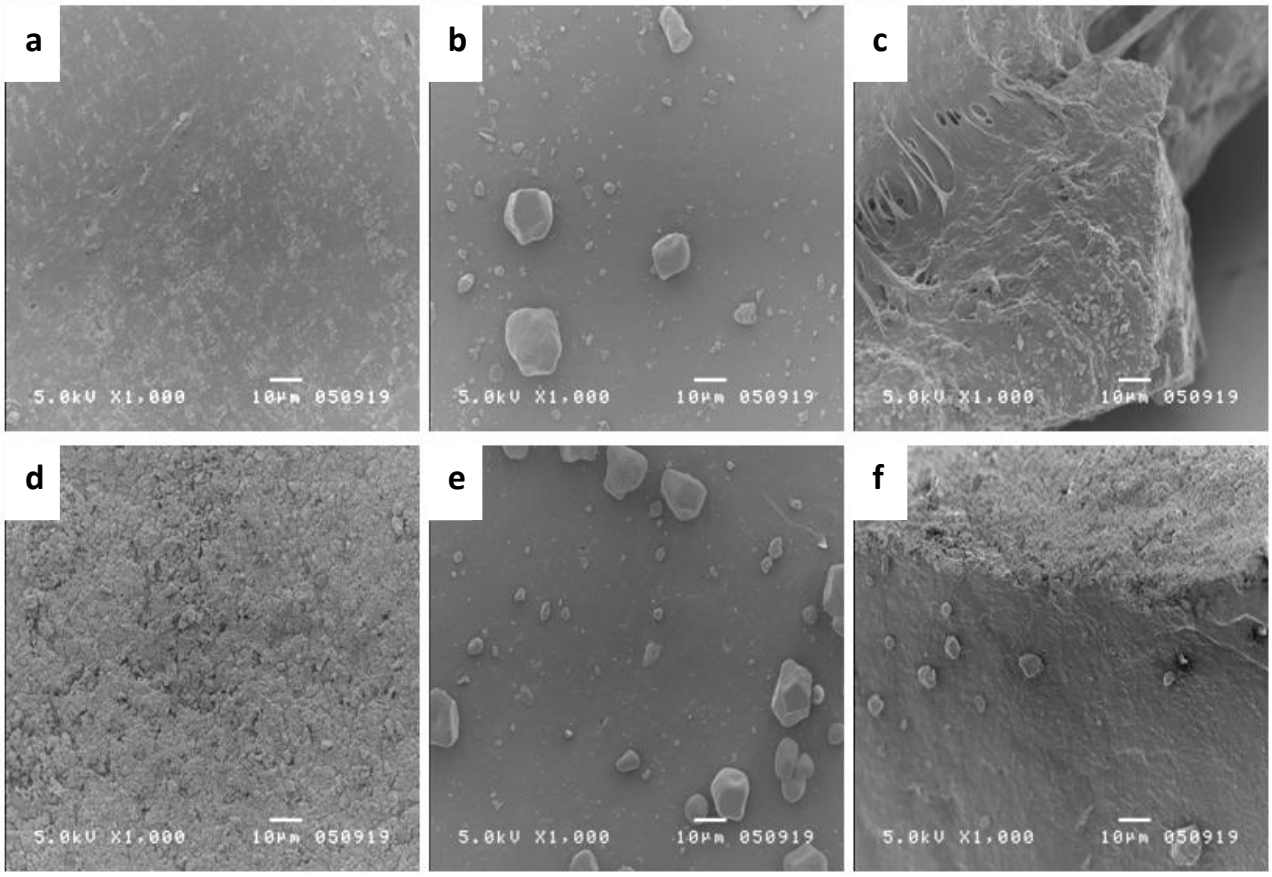

Figure 23: SEM images of samples dipped in $CaCl_2$ coagulant, dry powder coated, not chlorinated (13, 14); top: fresh sample, (a) outer side, (b) inner side, (c) breaking edge (RT fracture); bottom: aged sample (21 days), (d) outer side, (e) inner side, (f) breaking edge (freeze fracture), tilted 10°; 5.0 kV, magnification = 1000 x, wd 10 for outer and inner side, wd 15 for edges

As shown in Figure 23 the outer and inner side (a, b) of the fresh sample were smooth, as well as the inner side of the aged specimen (e). Solely the outer side exhibited small holes which

increased in number during ageing (d). Both breaking edges (c, f) showed globular features, distributed throughout the whole bulk.

The sample dipped into $Ca(NO_3)_2$ coagulant (Figure 24) exhibited only small holes in the aged state (d). Both inner sides (b, e) of the specimen as well as the outer side of the fresh sample (a) possessed a smooth surface. The freeze fractured edge of the aged sample (f) exhibited more globular structures than the breaking edge of the fresh sample (c).This was attributed to different handling conditions (RT and freeze fracture).

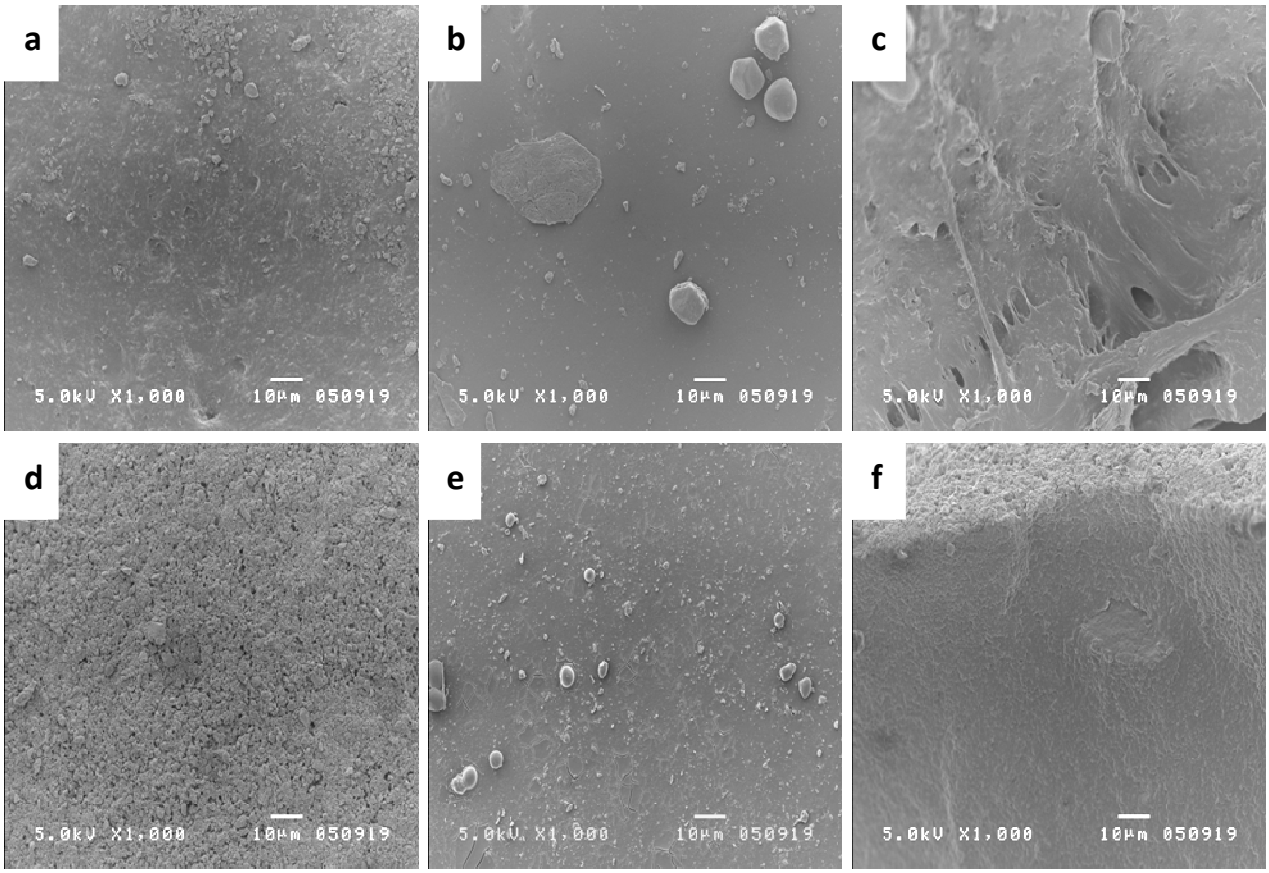

Figure 24: SEM images of samples dipped in $Ca(NO_3)_2$ coagulant, dry powder coated, not chlorinated (15, 16); top: fresh sample, (a) outer side, (b) inner side, (c) breaking edge (RT fracture); bottom: aged sample (21 days), (d) outer side, (e) inner side, (f) breaking edge (freeze fracture), tilted 10°; 5.0 kV, magnification = 1000 x, wd 10 for outer and inner side, wd 15 for edges

In principle there was no significant difference observed between the samples prepared with different coagulants. In both cases holes can be seen on the outer side after ageing. Apart from that, the samples exhibited a smooth surface.

Samples based on the untreated material of surgical gloves (17, 18, 49, 51)

Samples discussed in this part are made from the same untreated material (17). They were not chlorinated and in some cases coated on the inner side with modified coatings (see Table 7 for detailed description of each sample).

In Figure 25 the SEM pictures of the fresh and aged sample of the untreated material (17, 18) are shown.

Already in the fresh sample cracks were present on the outer side (a) which deepened and increased during ageing (d). The inner sides of the fresh and the aged sample (b, e) exhibited a quite smooth surface, although there were some holes present in the fresh state which cannot be found in the aged state. The edges of the untreated material were rather smooth and only few globular structures were found in both samples (c, f).

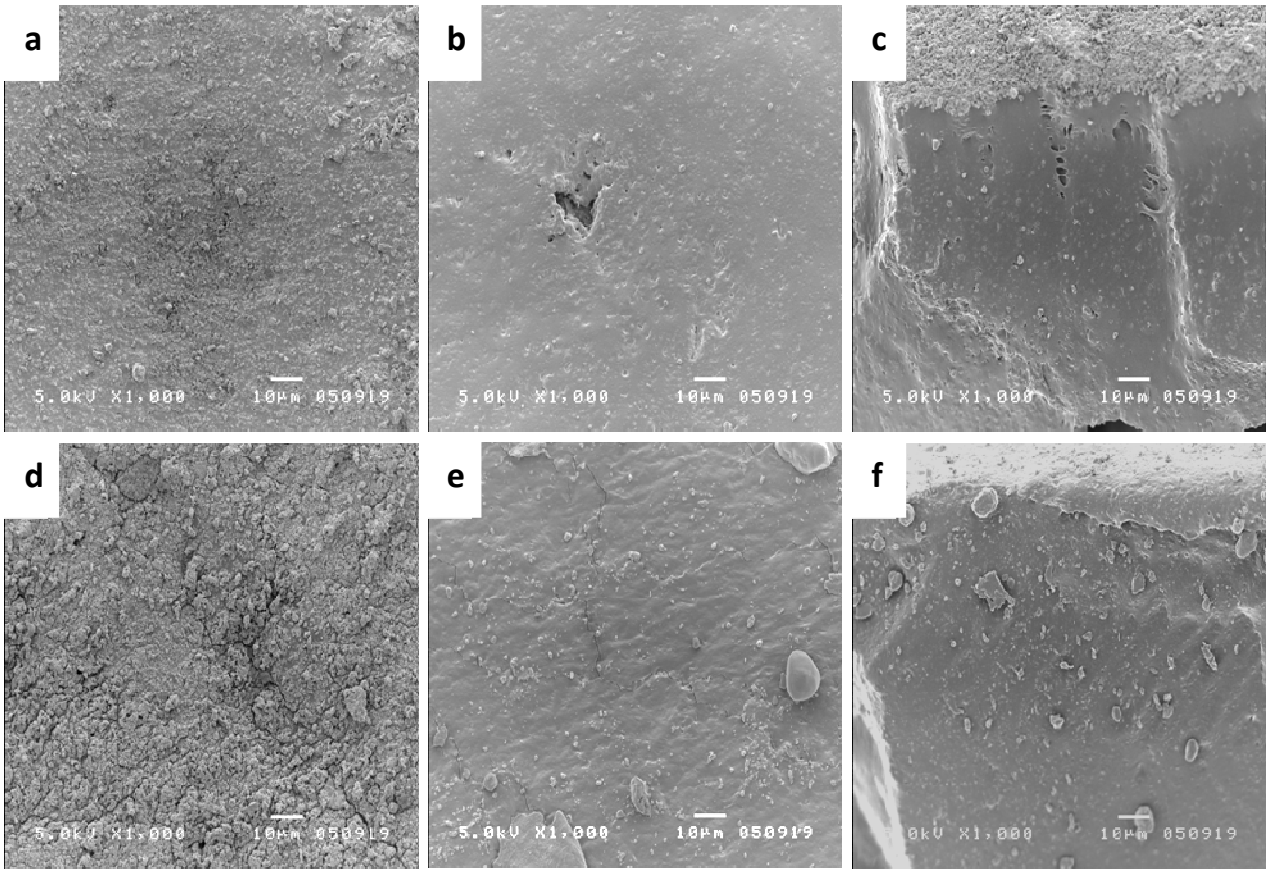

Figure 25: SEM images of the untreated material, not chlorinated (17, 18); top: fresh sample, (a) outer side, (b) inner side, (c) breaking edge (RT fracture); bottom: aged sample (21 days), (d) outer side, (e) inner side, (f) breaking edge (freeze fracture), tilted 10°; 5.0 kV, magnification = 1000 x, wd 10 for outer and inner side, wd 15 for edges

A very smooth surface was observed on the inner side (b) of the sample taken from *Sempermed Classic* (Figure 26), though it was covered with a modified coating. This coating should give a net-like structure to facilitate donning. [116] The outer side of the sample was smooth too, with some residues and also some globular structures visible. Edges exhibited some holes, which are attributed to the RT fracture of the sample, and also some globular features were present in the bulk.

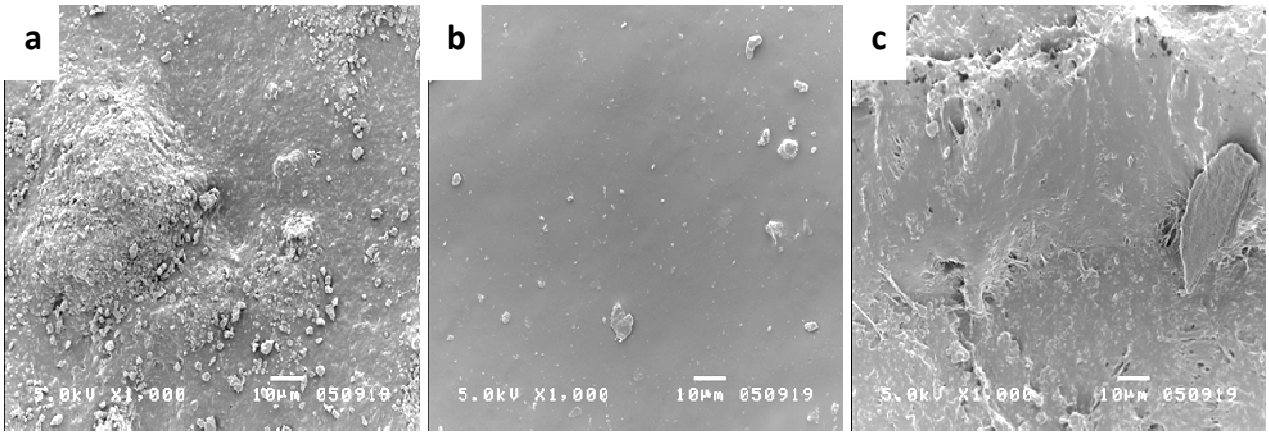

Figure 26: SEM images of Sempermed Classic, not chlorinated, modified coating (49); fresh sample, (a) outer side, (b) inner side, (c) breaking edge (RT fracture); 5.0 kV, magnification = 1000 x, wd 10 for outer and inner side, wd 15 for edges

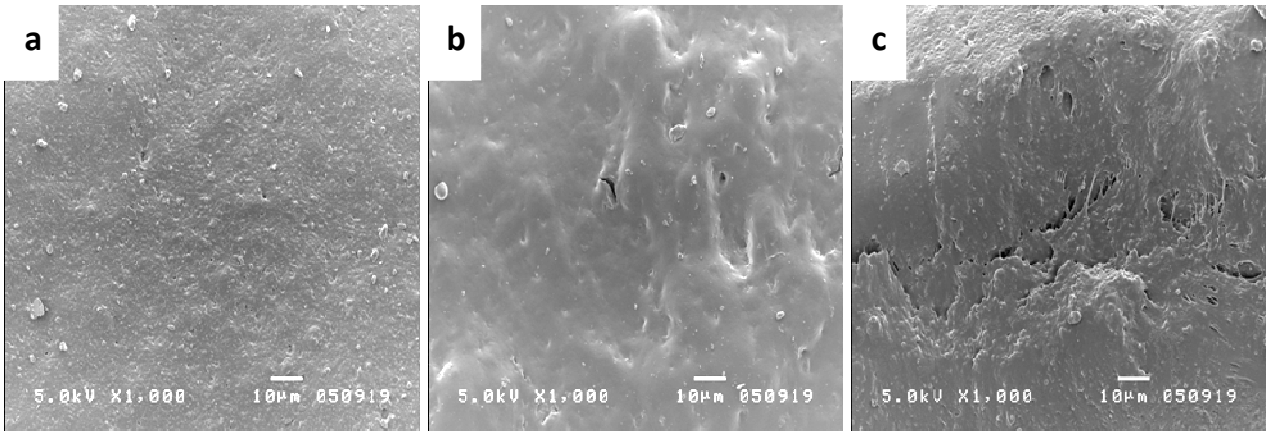

Figure 27: SEM images of OPH sterilised, UV-crosslinked latex, not chlorinated (51); fresh sample, (a) outer side, (b) inner side, (c) breaking edge (RT fracture); 5.0 kV, magnification = 1000 x, wd 10 for outer and inner side, wd 15 for edges

In Figure 27 SEM images of a surgical glove, cross linked with UV are shown. The outer side (a) exhibited a slightly textured surface, with an overall impression of a smooth surface. Equally, the inner side (b) of the specimen showed some textured features, though - compared to the outer side - rather large features (net-like). Globular structures throughout the whole bulk were visible as seen in the picture of the breaking edge (c).

Samples shown in this part were made from the same starting material (untreated material), but were differently processed, *e.g.* with or without modified coating or even powder. The sample shown in Figure 25 is the untreated material itself without any protection from powder or synthetic inner coating. Cracks and holes already visible in the fresh state are interpreted as a result of a missing protective layer, whereas the sample shown in Figure 26 exhibited a smooth surface without cracks. This is assigned to the modified coating of this sample.

Supreme based gloves (19, 20, 21, 22, 31, 32, 33, 34)

Supreme based samples were produced differently on lab scale to investigate the influence of diverse manufacturing parameters. For detailed descriptions of the gloves see Table 7.

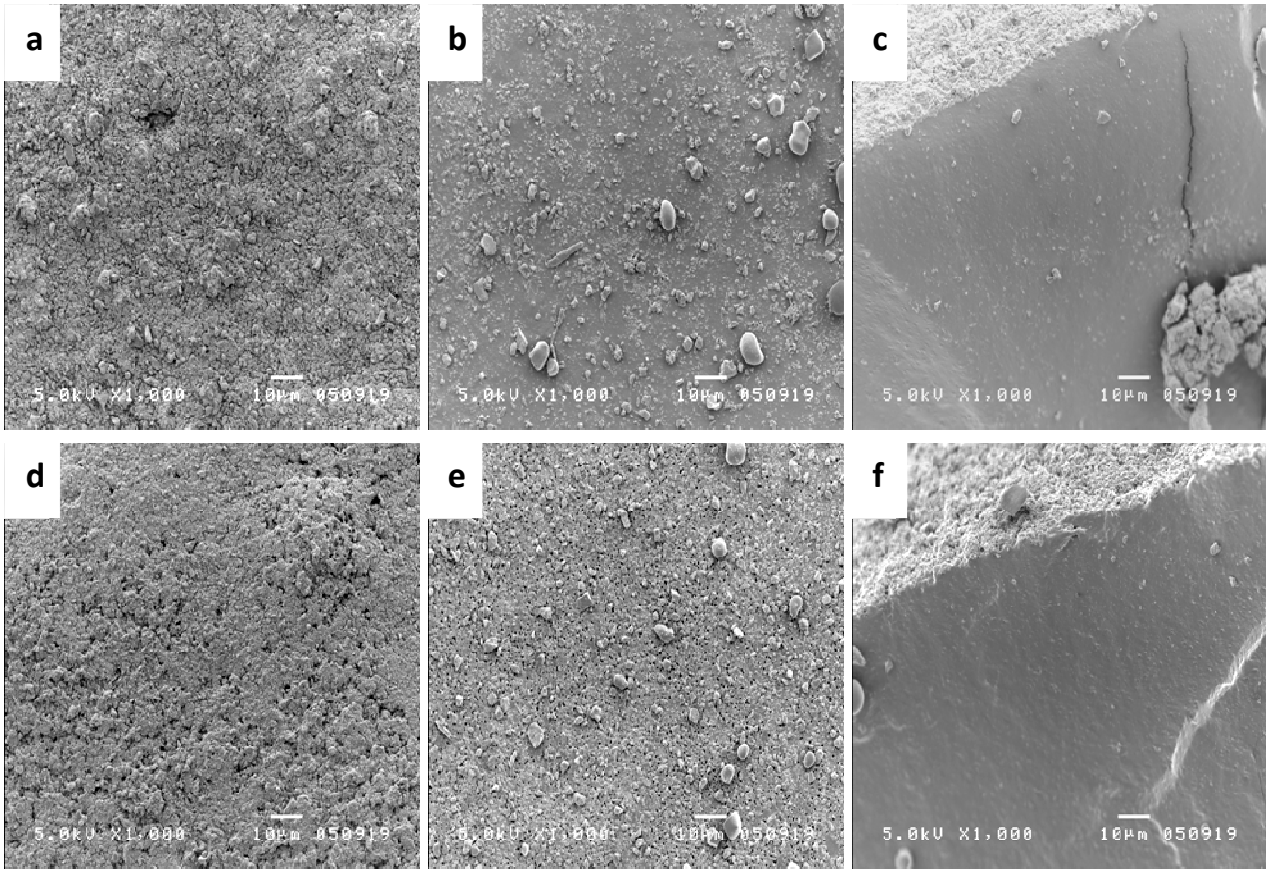

Figure 28: SEM images of Supreme without leaching, not chlorinated (19, 20); top: fresh sample, (a) outer side, (b) inner side, (c) breaking edge (freeze fracture); bottom: aged sample (21 days), (d) outer side, (e) inner side, (f) breaking edge (freeze fracture), tilted 10°; 5.0 kV, magnification = 1000 x, wd 10 for outer and inner side, wd 15 for edges

Although the outer side was covered with powder many small holes were present in the aged sample (d) (Figure 28), while no holes were observed in the fresh sample (a). The same effect was seen at the inner side. The aged sample (e) exhibited small holes all over the sample surface, whereas the fresh sample (b) had a rather smooth surface with no holes. Both edges (c, f) had a rather smooth appearance with no or only few globular structures in the bulk.

Figure 29 shows SEM images of a sample prepared as that in Figure 28, but additionally having a modified coating. Again, small holes were found on the outer side of the aged sample (d) and none in the fresh sample (a). The inner side was coated with a synthetic coating (modified coating), which leads to the net-like structure [116] on the surface of both samples (b, e). The edges of the fresh (c) and aged sample (f), respectively, had a quite smooth appearance with small globular features throughout the bulk.

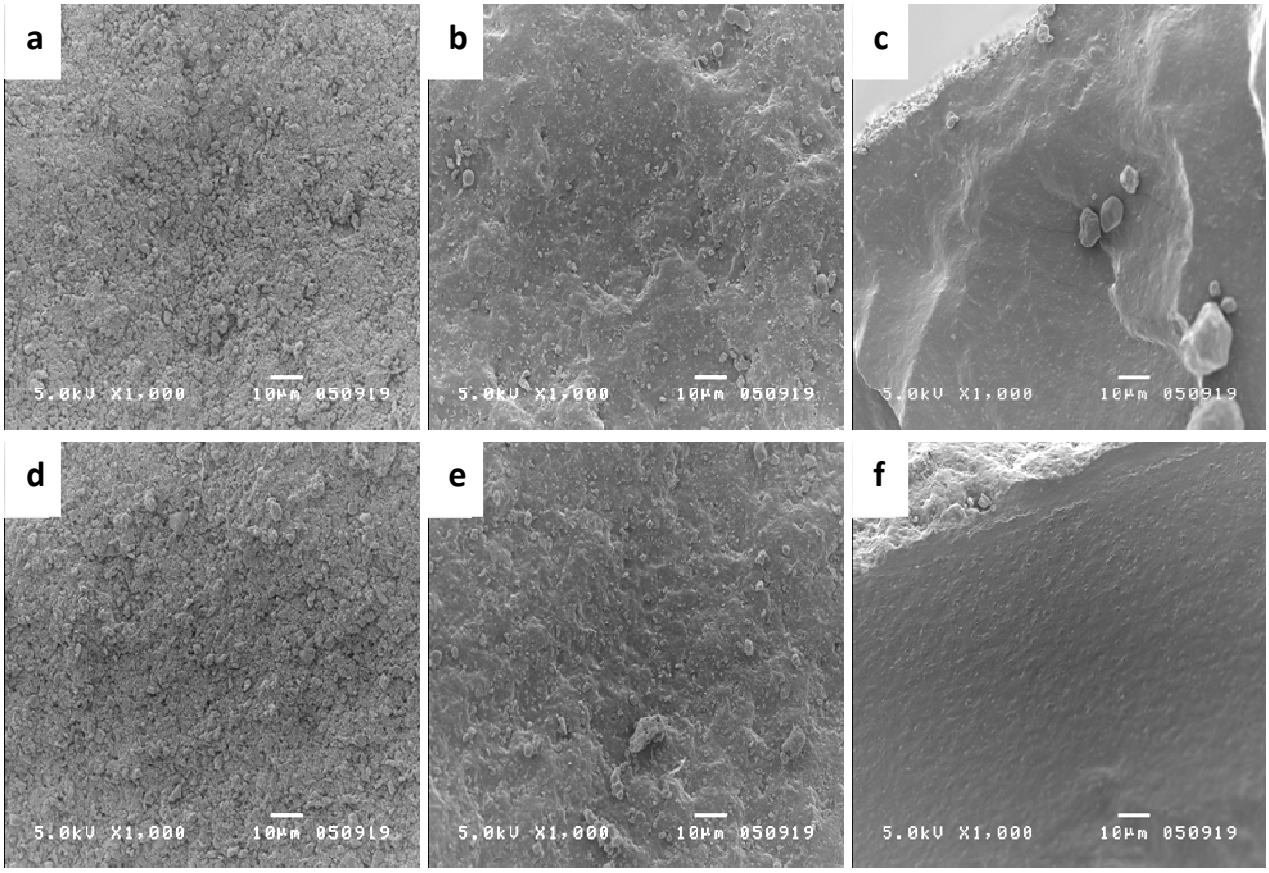

Figure 29: SEM images of Supreme without leaching, not chlorinated, modified coating (21, 22); top: fresh sample, (a) outer side, (b) inner side, (c) breaking edge (freeze fracture), tilted 20°; bottom: aged sample (21 days), (d) outer side, (e) inner side, (f) breaking edge (freeze fracture), tilted 10°; 5.0 kV, magnification = 1000 x, wd 10 for outer and inner side, wd 15 for edges

As shown in Figure 30, the sample washed with the intermittent washing system, exhibited small holes already in the fresh state (a). These small holes turned into large, deep holes after

ageing (d). In both cases the outer side was not smooth as globular structures were observed. Both inner sides (b, e) were quite smooth and exhibited no or only few small holes. Also both edges (c, f) had only few, small holes and globular structures present in the bulk.

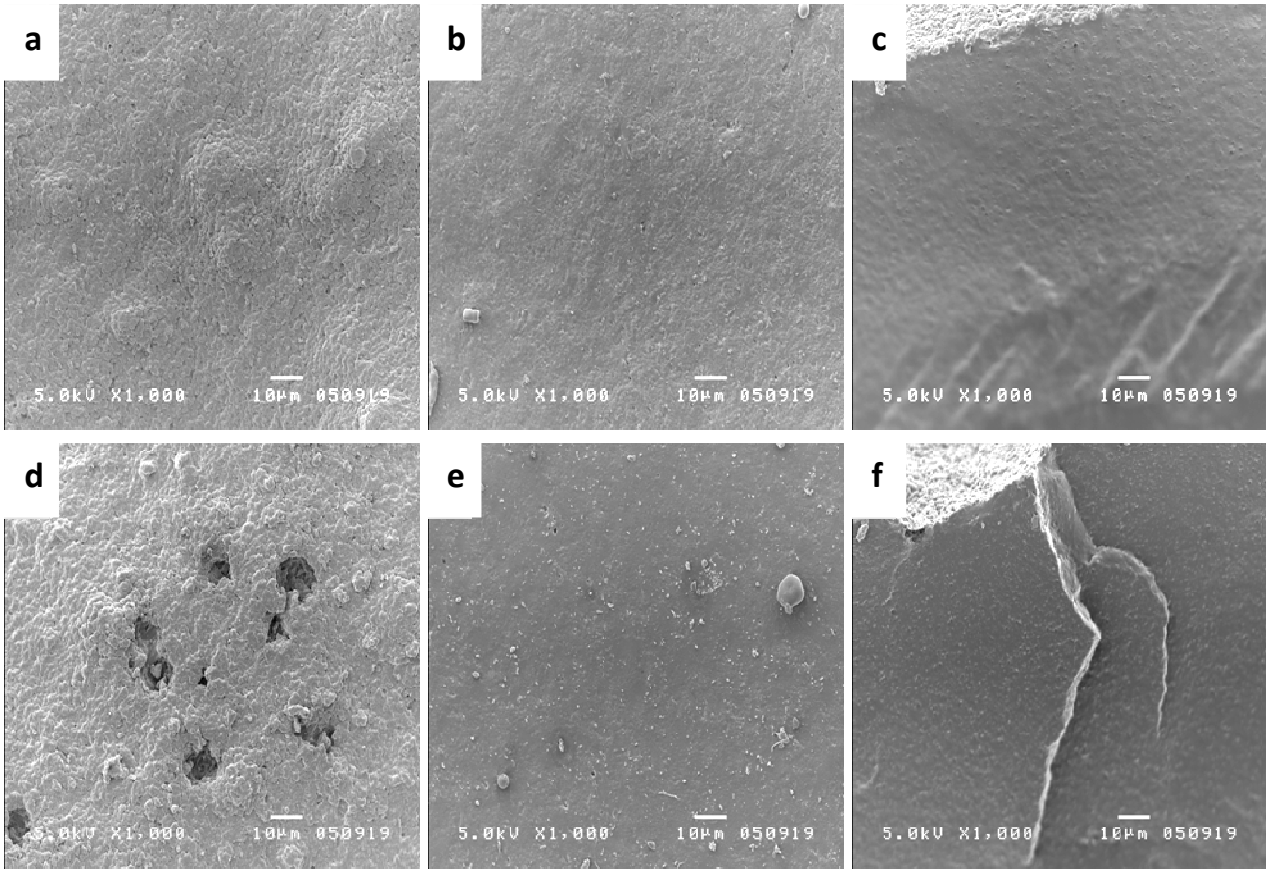

Figure 30: SEM images of Supreme TWA/standard, not chlorinated (31, 32); top: fresh sample, (a) outer side, (b) inner side, (c) breaking edge (freeze fracture); bottom: aged sample (21 days), (d) outer side, (e) inner side, (f) breaking edge (freeze fracture), tilted 10°; 5.0 kV, magnification = 1000 x, wd 10 for outer and inner side, wd 15 for edges

The sample washed with the intermittent washing system and synthetic (modified) coating (Figure 31) had even more holes on the outer side (a, d), but not as deep as in the uncoated sample (Figure 30). The inner sides (b, e) exhibited the typical, net-like structure of the modified coating. [116] Breaking edges in the fresh as well as in the aged state had a smooth appearance with some globular features distributed over the whole bulk.

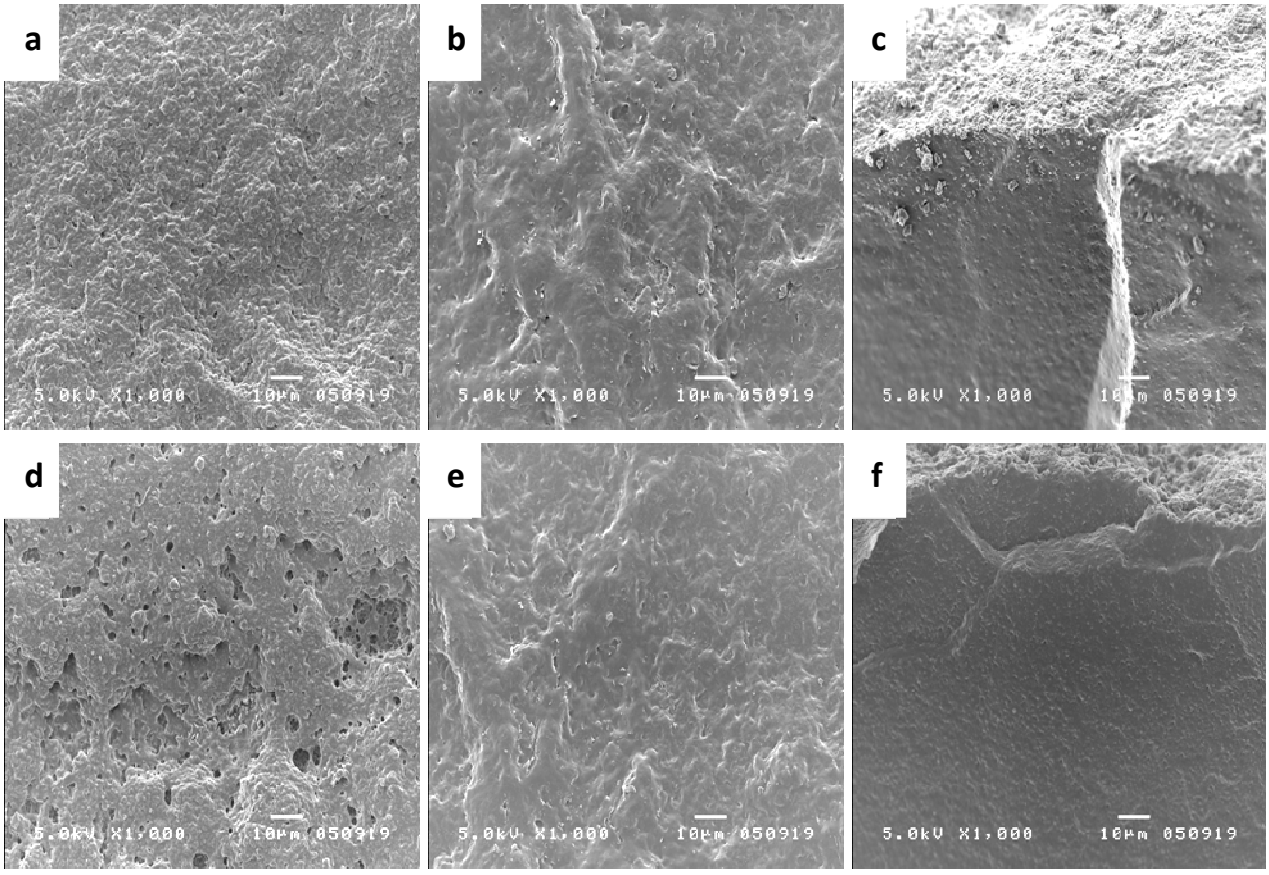

Figure 31: SEM images of Supreme TWA/standard, not chlorinated, modified coating (33, 34); top: fresh sample, (a) outer side, (b) inner side, (c) breaking edge (freeze fracture), tilted 10°; bottom: aged sample (21 days), (d) outer side, (e) inner side, (f) breaking edge (freeze fracture), tilted 10°; 5.0 kV, magnification = 1000 x, wd 10 for outer and inner side, wd 15 for edges

All samples exhibited holes which deepened and widened during ageing. Only the samples with modified coating showed no sign of holes on their inner side. This phenomenon is attributed to this additional layer which can act as protection as well.

Other samples (43, 44, 45)

These samples were prepared by different companies. They were all powder coated and not chlorinated.

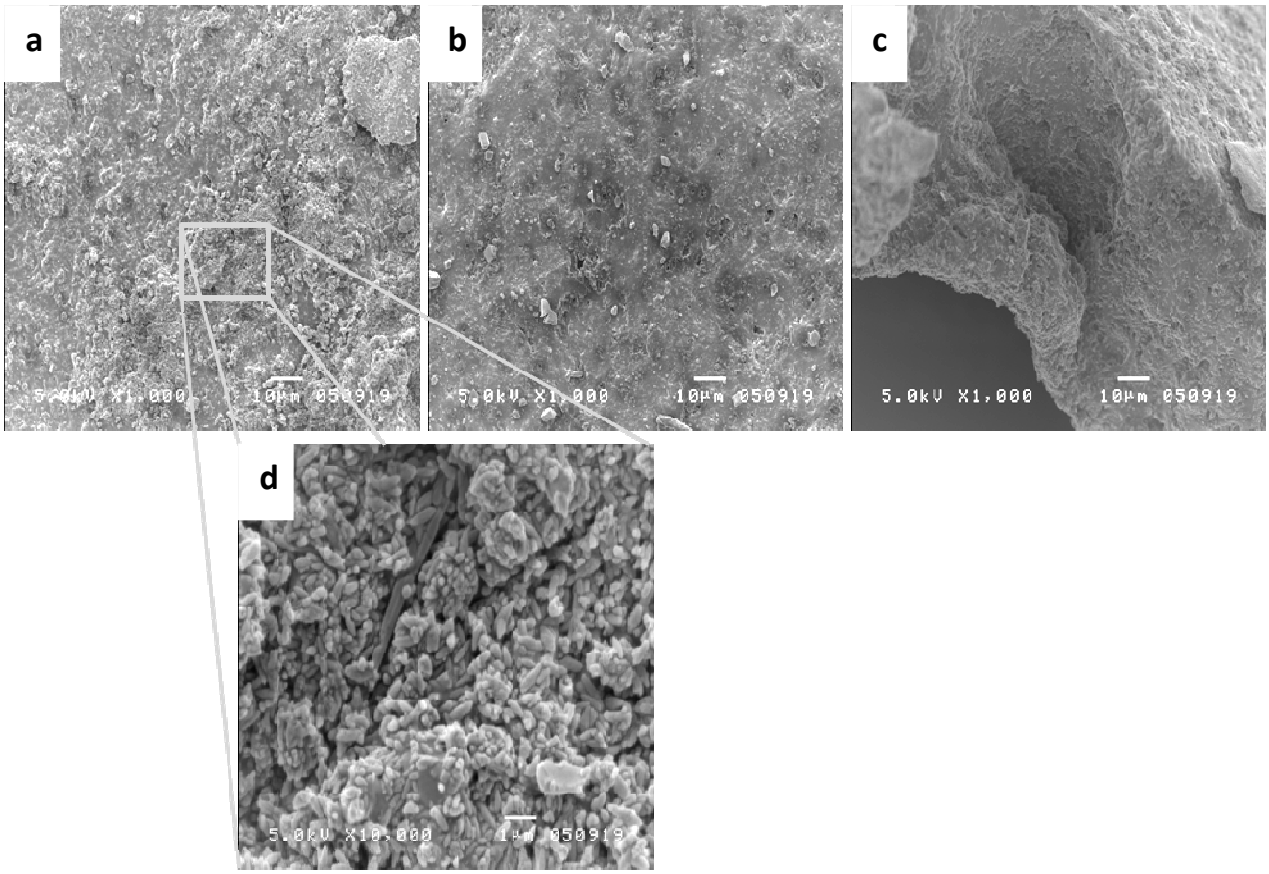

Figure 32: SEM images of Supermax Premium Quality, not chlorinated, powder coated (43); fresh sample, (a) outer side, (b) inner side, (c) breaking edge (RT fracture); 5.0 kV, magnification = 1000 x (d=10000 x), wd 10 for outer and inner side, wd 15 for edges

In Figure 32 SEM images of a fresh sample from *Supermax Premium Quality* (43) are shown. On the outer side (a) residues were visible which turned out to be rod shaped when magnified (d). They are interpreted as remnants from the coagulant bath. The inner side (b) appeared to be smooth with some structures and blackened spots present. When magnifying these black spots

it became obvious that they consisted of the rod shaped remnants too. The edge (c) showed globular features throughout the whole bulk with few holes.

In Figure 33 SEM images of another companies' sample are shown. This sample was powder coated and some residues were found on the outer side (a), as well as on the inner side (b). Again some black spots were visible on both sides which consisted of rod shaped depositions, equally to the product *Supermax*. The breaking edge (c) revealed isolated, but larger holes. They are assigned to fillers, which were quarried out during the RT fracture of the sample. Apart from that, the edge resembled the surface, with residues and black spots present.

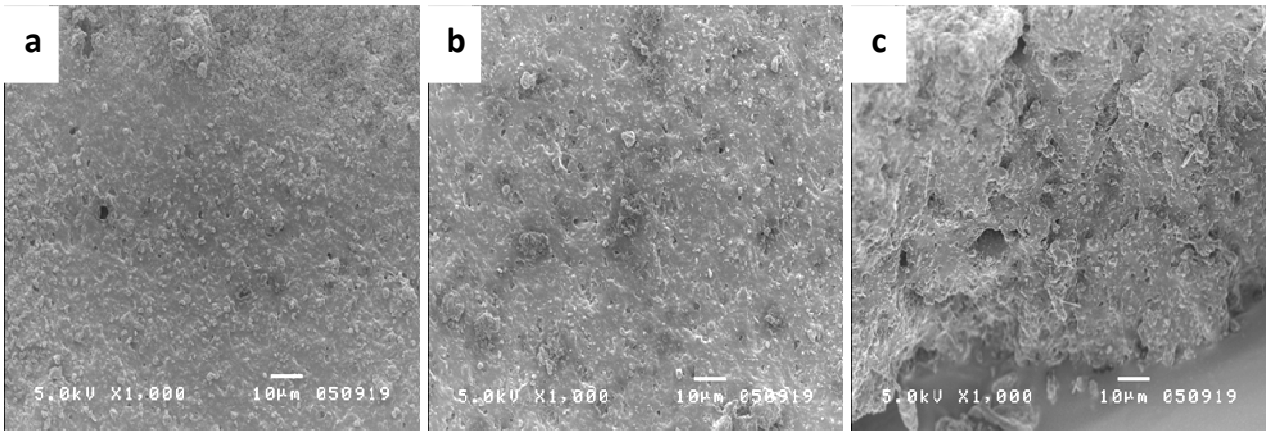

Figure 33: SEM images of Ansell Conform, not chlorinated, powder coated (44); fresh sample, (a) outer side, (b) inner side, (c) breaking edge (RT fracture); 5.0 kV, magnification = 1000 x, wd 10 for outer and inner side, wd 15 for edges

The outer side of *Sempercare Edition 2008* (Figure 34 (a)) was totally covered with residues, which were assigned to originate from the powdering process. The inner side (b) exhibited imbricative structures with many holes. This effect was attributed to come from the coating of the inner side with silicon oil, though this should lead to net-like structures [116]. The edge (c) revealed that some holes were also present in the bulk.

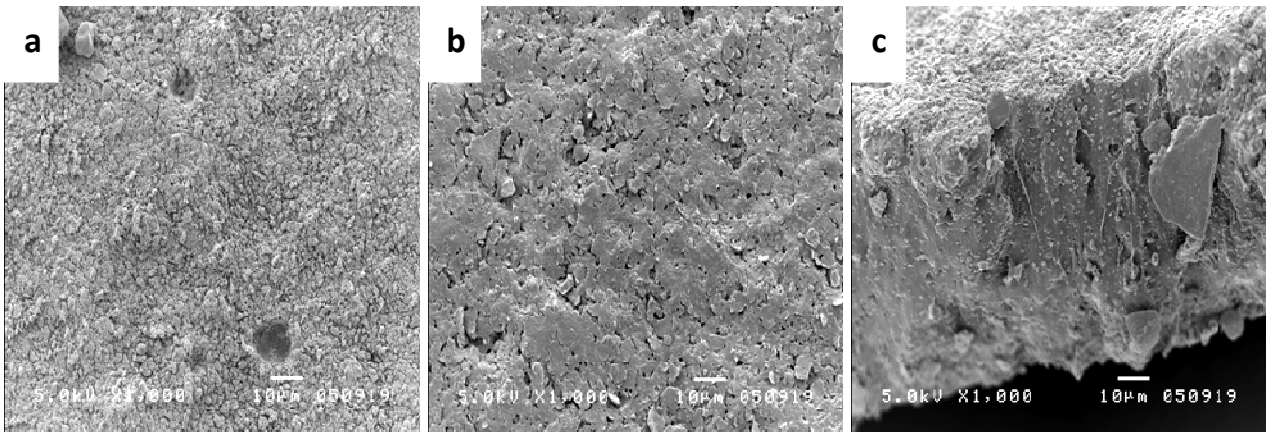

Figure 34: SEM images of Sempercare Edition 2008, modified coating, powder coated (45); fresh sample, (a) outer side, (b) inner side, (c) breaking edge (RT fracture); 5.0 kV, magnification = 1000 x, wd 10 for edge, outer and inner side

The two samples shown in Figure 32 and Figure 33 were very similar although produced by different companies. They showed the same black spots and residues. They were interpreted as coagulants.

SEM images of the sample shown in Figure 34 are somehow different from all other samples regarding the modified coating. This should lead to a net-like structure on the inner side, but in this sample imbricative structures with holes were observed.

5.1.2 Gloves with a low degree of chlorination

Samples discussed in this part have a low degree of chlorination (alkaline) and offer different features (compare description in Table 8).

Table 8: Overview on chlorinated (low degree) samples

Number	Sample name[a]	Description[b]
5	Sempercare IC 2007	rough surface, chlorinated (alkaline), RT
6	Sempercare IC 2007, aged	rough surface, chlorinated (alkaline), 21 days aged, N_2
7	Sempercare IC 2006	rough surface, chlorinated (alkaline), RT
8	Sempercare IC 2006, aged	rough surface, chlorinated (alkaline), 21 days aged, N_2
9	$CaCl_2$ coagulant, modified coating	coated, washed, N_2
10	$CaCl_2$ coagulant, modified coating, aged	coated, washed, 21 days aged, N_2
11	$Ca(NO_3)_2$ coagulant, modified coating	coated, washed, N_2
12	$Ca(NO_3)_2$ coagulant, modified coating, aged	coated, washed, 21 days aged, N_2
23	Supreme, NaOCl	dry powder, NaOCl 50 g/2 l, 2x30 min, sample was wiped dryly, N_2
24	Supreme, NaOCl, aged	dry powder, NaOCl 50 g/2 l, 2x30 min, sample was wiped dryly, 21 days aged, N_2
25	Supreme, NaOCl, modified coating	NaOCl 50 g/2 l, 2x30 min, sample was wiped dryly, N_2
26	Supreme, NaOCl, modified coating, aged	NaOCl 50 g/2 l, 2x30 min, sample was wiped dryly, 21 days aged, N_2
46	Semperguard 2008	rough surface, chlorinated (low degree), RT

[a] modified coating...coating on the inner side of the medical gloves (silicon, polymer), [b] For details of the sample preparation compare text (chapter 4.2.1). RT...RT fracture, N_2...freeze fracture

Sempercare and Semperguard (5, 6, 7, 8, 46)

These latex samples were chlorinated with a low degree of chlorine (alkaline) and had a rough surface (Table 8). To facilitate donning they were coated on the inner side with a fusion-bonded synthetic inner coating (modified coating). [116]

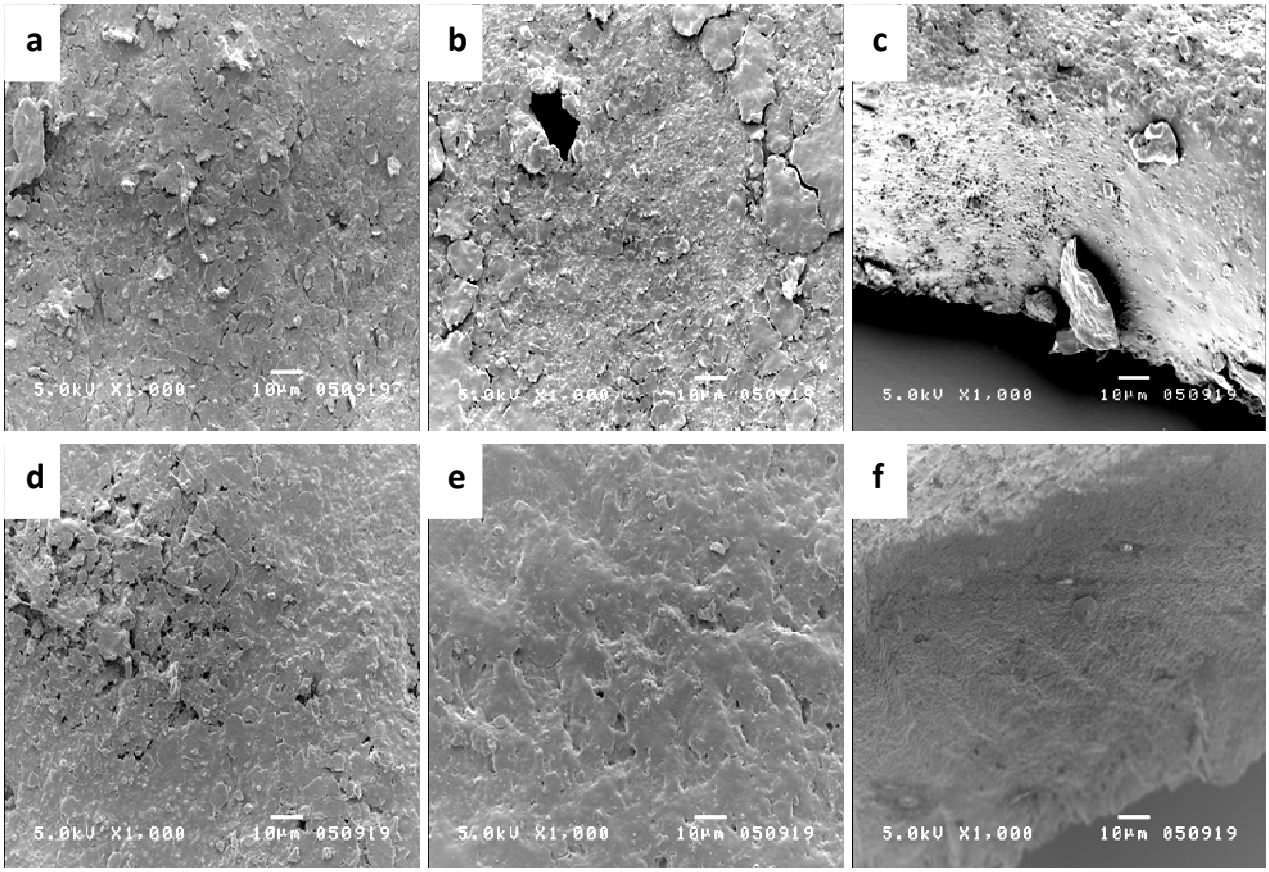

Figure 35: SEM images of Sempercare IC 2007, low degree of chlorination, rough surface (5, 6); top: fresh sample, (a) outer side, (b) inner side, (c) breaking edge (RT fracture); bottom: aged sample (21 days), (d) outer side, (e) inner side, (f) breaking edge (freeze fracture); 5.0 kV, magnification = 1000 x, wd 10 for outer and inner side, wd 15 for edges

In Figure 35 SEM images of *Sempercare IC 2007* are depicted. The outer side of the fresh sample (a) exhibited imbricative structures whereas the surface of the aged sample (d) appeared to break up and showed holes. On the inner side of the fresh specimen (b) some “flakes” and quite big holes were observed. The aged sample (e) exhibited a smooth surface with a net-like

structure, originating from the modified coating, and few small holes. The edge of the fresh sample (c) appeared to be smooth with some holes in the bulk. However, the aged sample (f) did not exhibit holes in the bulk but appeared to be rough.

On the outer side (a) of the sample shown in Figure 36 imbricative structures were present as well as on the inner side (b), but on the outer side the features were more prominent. There were also some holes visible on the outer and inner side as well as in the bulk (c), although the holes in the bulk were smaller.

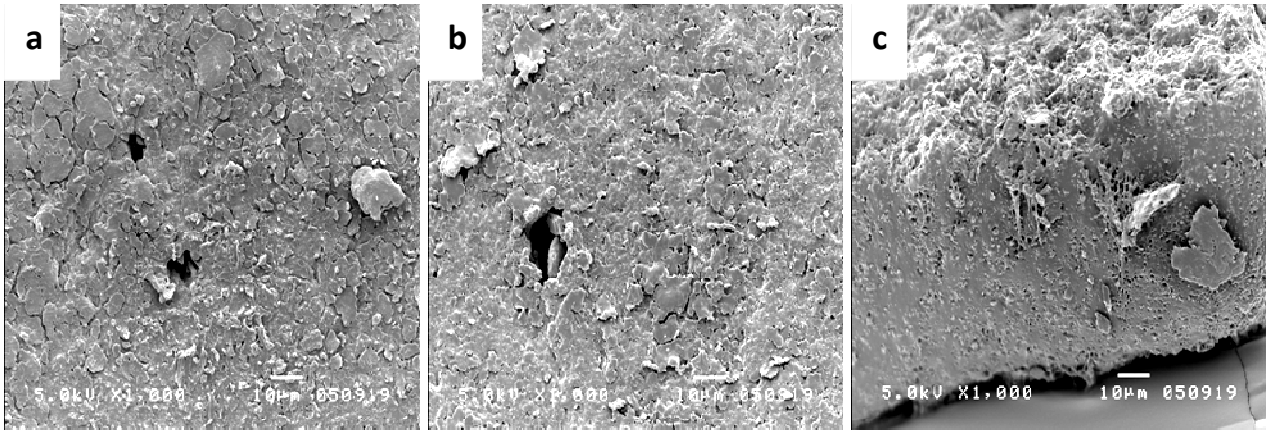

Figure 36: SEM images of Semperguard 2008, low degree of chlorination, rough surface (46); top: fresh sample, (a) outer side, (b) inner side, (c) breaking edge (RT fracture); 5.0 kV, magnification = 1000 x, wd 10 for breaking edge, outer and inner side

The outer side of *Sempercare IC 2006* (Figure 37) exhibited globular structures in the fresh as well as in the aged state. It appeared smooth with only few holes in the surface. The inner side of the aged sample (e) was smooth too and had a net-like structure whereas the fresh sample (b) exhibited more holes. However, the net-like structure was still visible. Both edges (c, f) were smooth and no globular features or many holes were visible. Holes present in the bulk of the fresh sample were attributed to stem from handling (RT fracture).

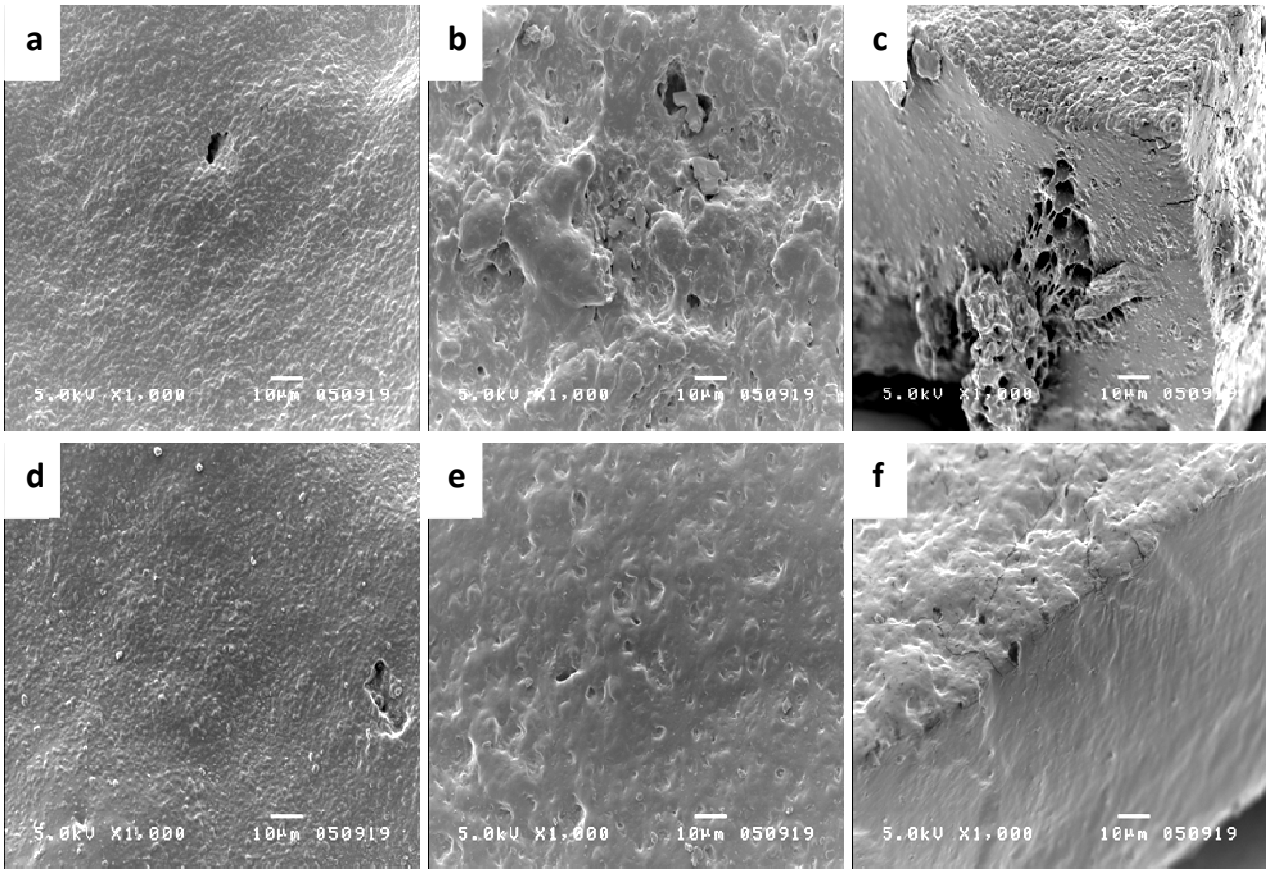

Figure 37: SEM images of Sempercare IC 2006, low degree of chlorination, rough surface (7, 8); top: fresh sample, (a) outer side, (b) inner side, (c) breaking edge (RT fracture), wd 10; bottom: aged sample (21 days), (d) outer side, (e) inner side, (f) breaking edge (freeze fracture), wd 15; 5.0 kV, magnification = 1000 x, wd 10 for outer and inner side

For all of these samples holes, were observed in their fresh as well as in the aged state. In some cases they were even more distinctive in the fresh state than in the aged state.

Samples based on Supreme (23, 24, 25, 26)

Supreme based samples were produced differently on lab scale to investigate the influence of diverse manufacturing parameters. For a detailed description of the gloves see Table 8.

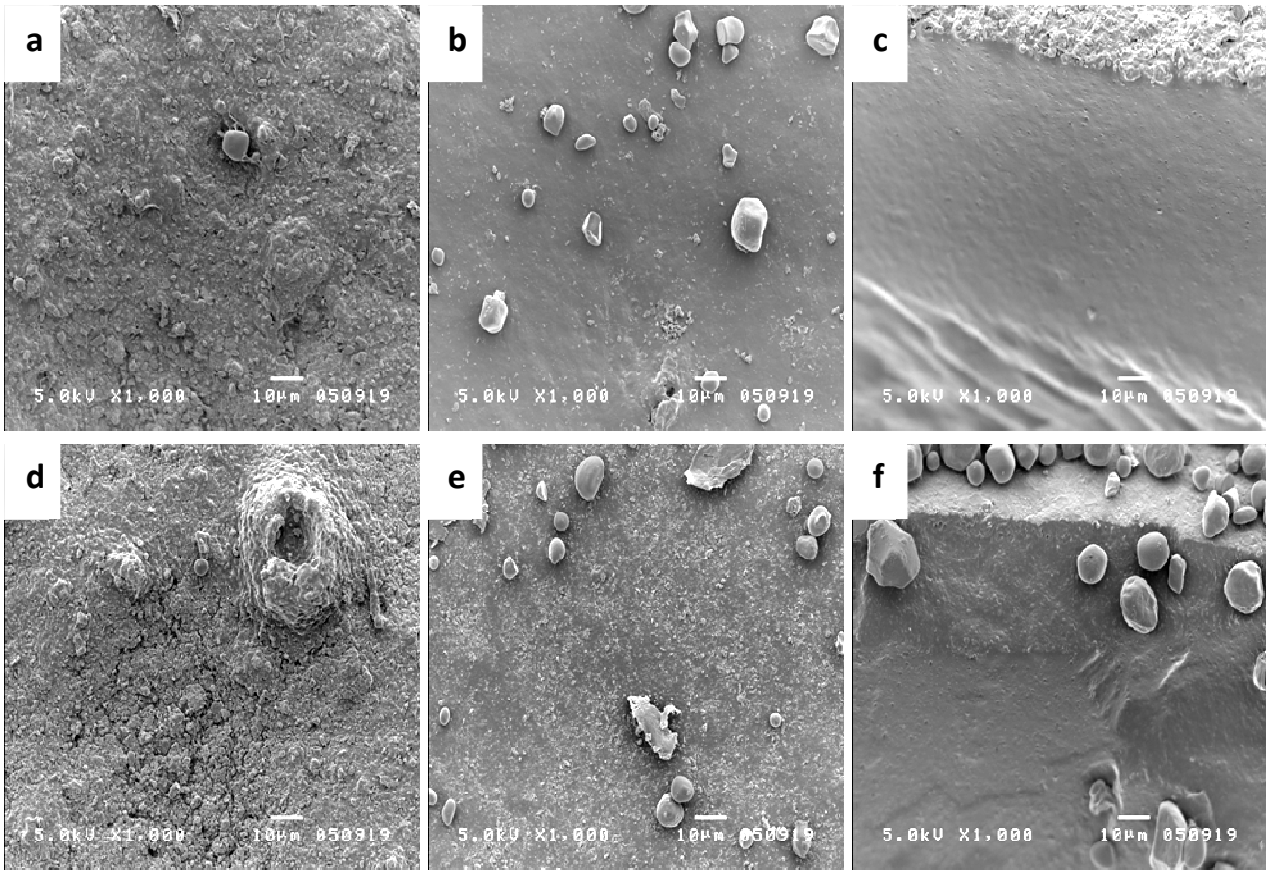

Figure 38: SEM images of Supreme NaOCl, dry powder (23, 24); top: fresh sample, (a) outer side, (b) inner side, (c) breaking edge (freeze fracture); bottom: aged sample (21 days), (d) outer side, (e) inner side, (f) breaking edge (freeze fracture); 5.0 kV, magnification = 1000 x, wd 10 for outer and inner side, wd 15 for edges

As shown in Figure 38 the outer side of the fresh and the aged sample (a, d) were covered with residues, maybe coagulants, and exhibited distinctive structures. Cracks were observed in the aged sample. On the inner side of the fresh sample (b) as well as the aged sample (e) corn starch particles were found, but apart from this the surface was smooth and showed no cracks or holes. The edges (c, f) were smooth and only isolated holes were observed.

The sample taken from *Supreme chlorinated with NaOCl* and modified coating is shown in Figure 39. The fresh and the aged sample resembled each other. The outer sides (a, d) were covered with residues and the inner sides (b, e) exhibited the typical net-like structure from the modified coating. [116] The only difference was on the outer side (d) of the aged sample where cracks were found. The edges were smooth with globular structures and holes distributed over the bulk.

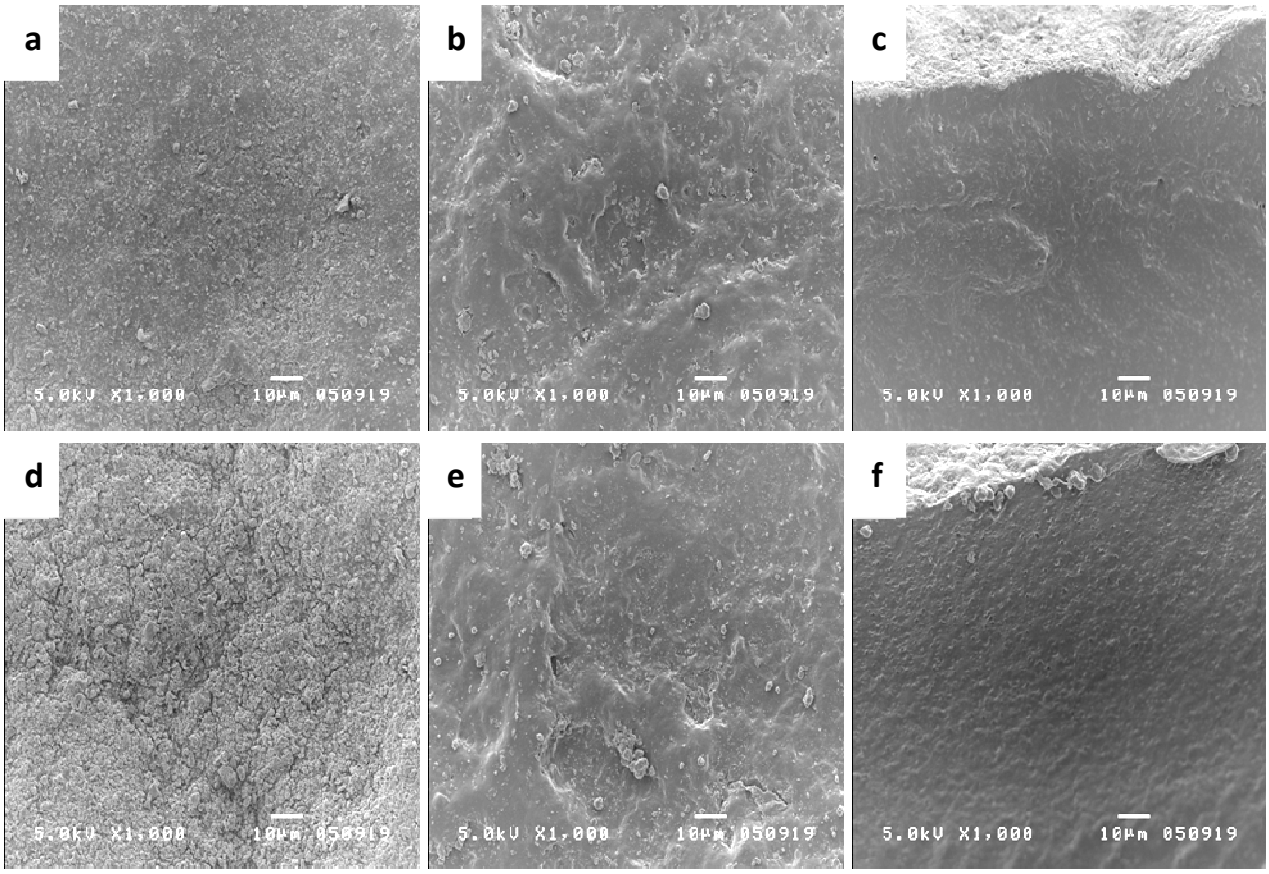

Figure 39: SEM images of Supreme NaOCl, modified coating (25, 26); top: fresh sample, (a) outer side, (b) inner side, (c) breaking edge (freeze fracture); bottom: aged sample (21 days), (d) outer side, (e) inner side, (f) breaking edge (freeze fracture), tilted 10°; 5.0 kV, magnification = 1000 x, wd 10 for outer and inner side, wd 15 for edges

For these two samples (Figure 38 and Figure 39) no significant differences were found. In both samples cracks were present in the aged state.

Samples prepared with different coagulants (9, 10, 11, 12)

These samples were prepared by dipping into different coagulants, $CaCl_2$ and $Ca(NO_3)_2$, respectively, have a low degree of chlorination and were coated with a modified coating (synthetic inner coating) to facilitate donning.

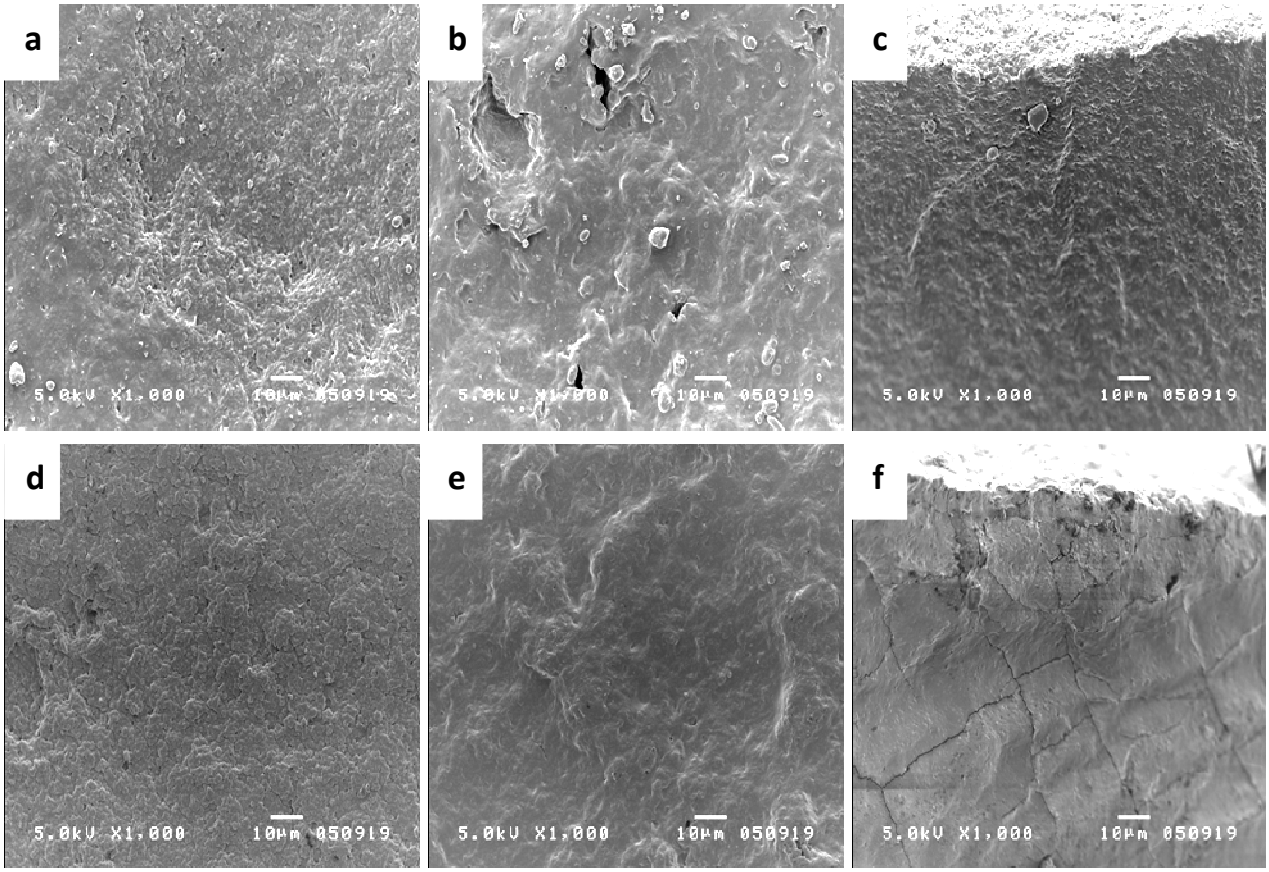

Figure 40: SEM images of samples dipped in $CaCl_2$ coagulant, modified coating (9, 10); top: fresh sample, (a) outer side, (b) inner side, (c) breaking edge (freeze fracture), tilted 10°; bottom: aged sample (21 days), (d) outer side, (e) inner side, (f) breaking edge (freeze fracture), tilted 10°; 5.0 kV, magnification = 1000 x, wd 10 for outer and inner side, wd 15 for edges

As shown in Figure 40 the sample dipped in $CaCl_2$ coagulant bath exhibited globular structures on the outer side of the fresh sample (a). These globular structures appeared to be more prominent in the aged sample (d) and also some cracks were found. The inner sides (b, e) featured the net-like structures of the modified coating and some holes were found in the fresh

sample. The edge of the fresh sample (c) showed globular structures and holes, distributed over the whole area. The aged sample (f) had a smooth edge with no structures and holes. But there were some cracks present which were assigned to come from handling rather than ageing.

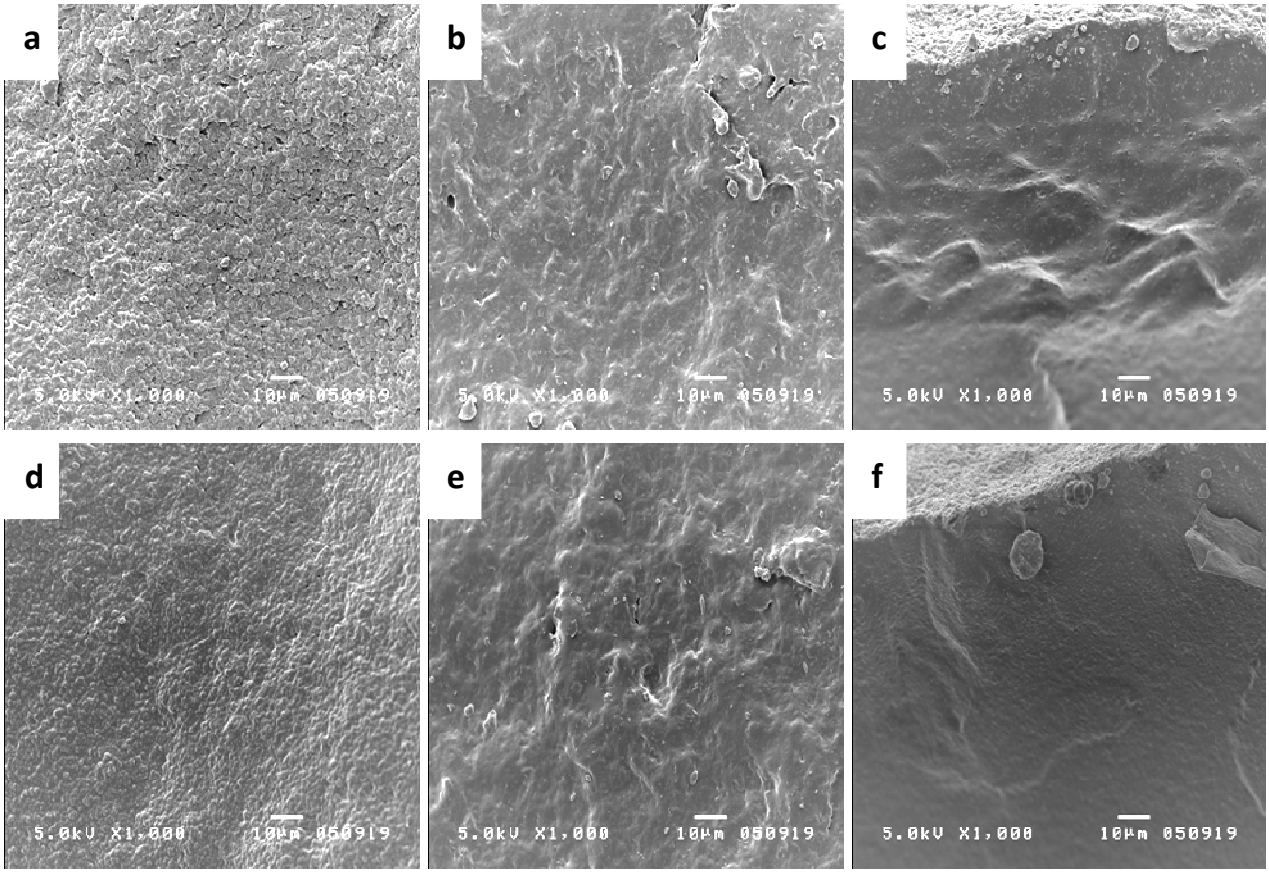

Figure 41: SEM images of samples dipped in $Ca(NO_3)_2$ coagulant, modified coating (11, 12); top: fresh sample, (a) outer side, (b) inner side, (c) breaking edge (freeze fracture), tilted 10°; bottom: aged sample (21 days), (d) outer side, (e) inner side, (f) breaking edge (freeze fracture), tilted 10°; 5.0 kV, magnification = 1000 x, wd 10 for outer and inner side, wd 15 for edges

The sample dipped into the $Ca(NO_3)_2$ coagulant bath (Figure 41) showed globular structures on the outer side of the fresh (a) and the aged sample (d) as well. These structures were more distinctive in the fresh sample and there were also some holes present. The inner sides (b, e) equalled each other well. Both showed the net-like structure of the modified coating. [116] The

edge of the fresh sample (c) was smooth though there were globular structures present. This appearance was the same for the aged sample (f).

Both samples resembled each other. However, the sample with $Ca(NO_3)_2$ as coagulant exhibited holes on the outer side of the sample (fresh and aged) whereas the sample with $CaCl_2$ as coagulant had holes only in the aged state. This sample had holes on the inner side instead, though covered with modified coating.

5.1.3 Gloves with a high degree of chlorination

Samples discussed on the following pages were acidly chlorinated (high degree chlorination) and were prepared with different manufacturing parameters (compare Table 9).

Table 9: Overview on samples with a high degree of chlorination

Number	Sample name[a]	Description[b]
1	Sempercare LF 2007	rough surface, chlorinated (acidic), RT
2	Sempercare LF 2007, aged	rough surface, chlorinated (acidic), 21 days aged, N_2
3	Sempercare LF 2006	rough surface, chlorinated (acidic), RT
4	Sempercare LF 2006, aged	rough surface, chlorinated (acidic), 21 days aged, N_2
27	Supreme, HCl/NaOCl	dry powder, NaOCl/HCl 24 g HCl+28 g NaOCl/2 l, 1x30 min, sample was wiped dryly, N_2
28	Supreme, HCl/NaOCl, aged	dry powder, NaOCl/HCl 24 g HCl+28 g NaOCl/2l, 1x30 min, sample was wiped dryly, 21 days aged, N_2
29	Supreme, HCl/NaOCl, modified coating	NaOCl/HCl 24 g HCl+28 g NaOCl/2 l, 1x30 min, sample was wiped dryly, N_2
30	Supreme, HCl/NaOCl, modified coating, aged	NaOCl/HCl 24 g HCl+28 g NaOCl/2 l, 1x30 min, sample was wiped dryly, 21 days aged, N_2
35	Peha Soft	smooth surface, high degree of chlorination, RT
36	Peha Soft, aged	smooth surface, high degree of chlorination, 17 days aged, RT
47	Sempercare Edition 2008, rough	rough surface, high degree of chlorination, RT
48	Sempercare Edition 2008, smooth	smooth surface, high degree of chlorination, RT
50	Sempermed Supreme	OPH[c] sterilised, NR, powder-free, modified coating, high degree of chlorination, RT

[a] modified coating...coating on the inner side of the medical gloves (silicon, polymer), [b] For details of the sample preparation compare text (chapter 4.2.1). RT...RT fracture, N_2...freeze fracture, [c] OPH…surgical glove

Sempercare, Sempermed and others (1, 2, 3, 4, 47, 48, 50)

These samples were chlorinated with a high degree of chlorine. To reduce tackiness they were coated on the inner side with modified coating. [116] For a detailed description of the samples see Table 9.

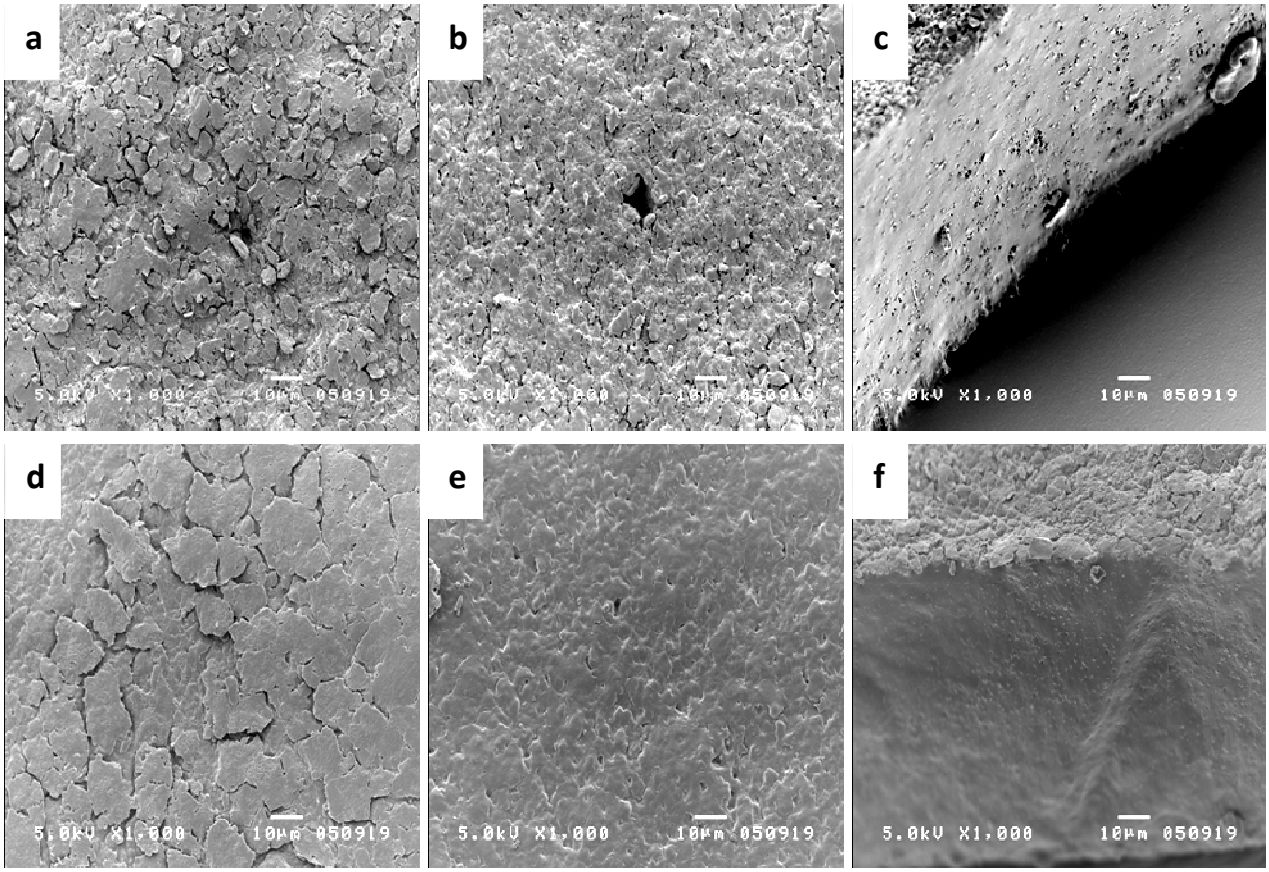

Figure 42: SEM images of Sempercare LF 2007, high degree of chlorination, rough surface (1, 2); top: fresh sample, (a) outer side, (b) inner side, (c) breaking edge (RT fracture); bottom: aged sample (21 days), (d) outer side, (e) inner side, (f) breaking edge (freeze fracture); 5.0 kV, magnification = 1000 x, wd 10 for outer and inner side, wd 15 for edges

SEM images of *Sempercare LF 2007* (Figure 42) exhibited imbricative structures on the outer side of the fresh sample (a) as well as on the aged sample (d). Structures were smaller and more prominent in the fresh sample. In contrast, the aged sample had larger structures and exhibited a smooth surface. The same counts for the inner sides. The inner side of the aged sample (e)

was smooth and showed the net-like structure of the modified coating. [116] The inner side of the fresh sample (b) also had more holes compared to the aged sample. Both edges (c, f) were smooth and had holes in the bulk.

The *Sempercare Edition* sample (47) with the rough surface (Figure 43) exhibited imbricative structures on the outer side (a) as well as on the inner side (b). These structures were bigger on the inner side though and appeared to flake off. On both sides holes were present. The edge (c) appeared to be rough with holes in the bulk.

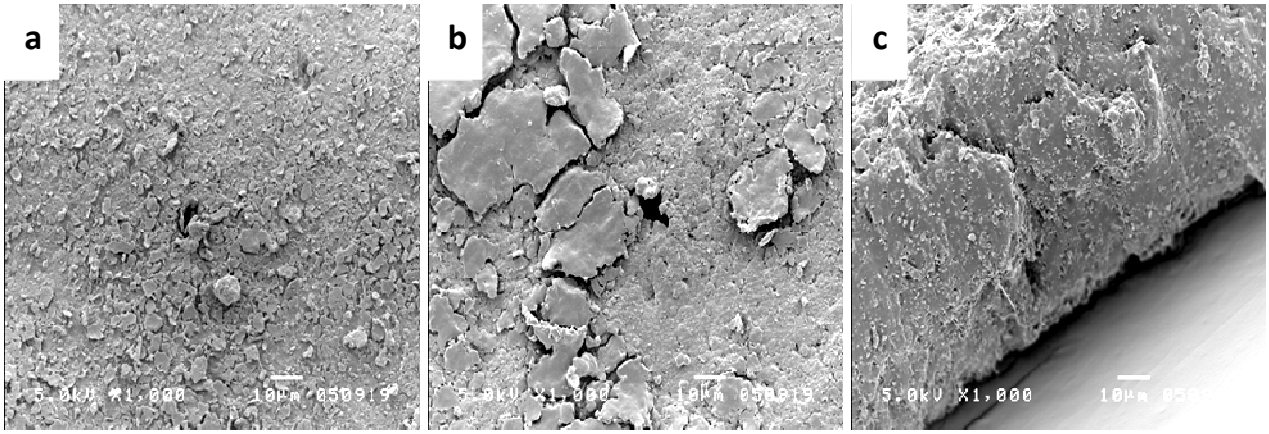

Figure 43: SEM images of Sempercare Edition 2008, high degree of chlorination, rough surface (47); fresh sample, (a) outer side, (b) inner side, (c) breaking edge (RT fracture); 5.0 kV, magnification = 1000 x, wd 10 for breaking edge, outer and inner side

The *Sempercare LF 2006* sample (Figure 44) exhibited distinctive globular structures on the outer side of the fresh sample (a) and also on the inner side (b) structuring was present due to modified coating of the sample. Additionally, holes were found on the inner and outer side of the fresh sample. The aged sample also showed globular structure on the outer side (d) with few holes present. The inner side (e) was smooth compared to the fresh sample and showed few cracks. Both edges (c, f) were smooth and exhibited some holes distributed throughout the bulk.

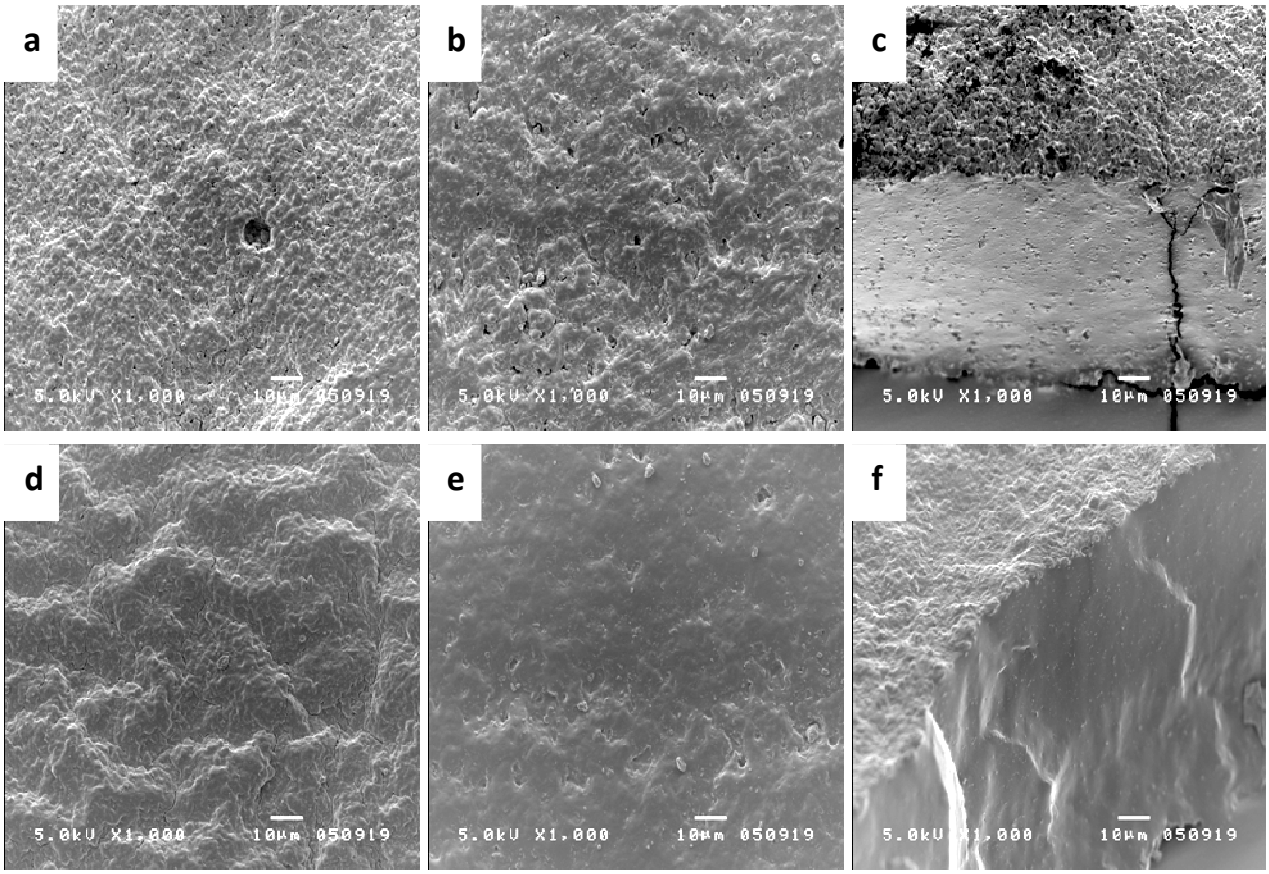

Figure 44: SEM images of Sempercare LF 2006, high degree of chlorination, rough surface (3, 4); top: fresh sample, (a) outer side, (b) inner side, (c) breaking edge (RT fracture), wd 10; bottom: aged sample (21 days), (d) outer side, (e) inner side, (f) breaking edge (freeze fracture), wd 15; 5.0 kV, magnification = 1000 x, wd 10 for outer and inner side

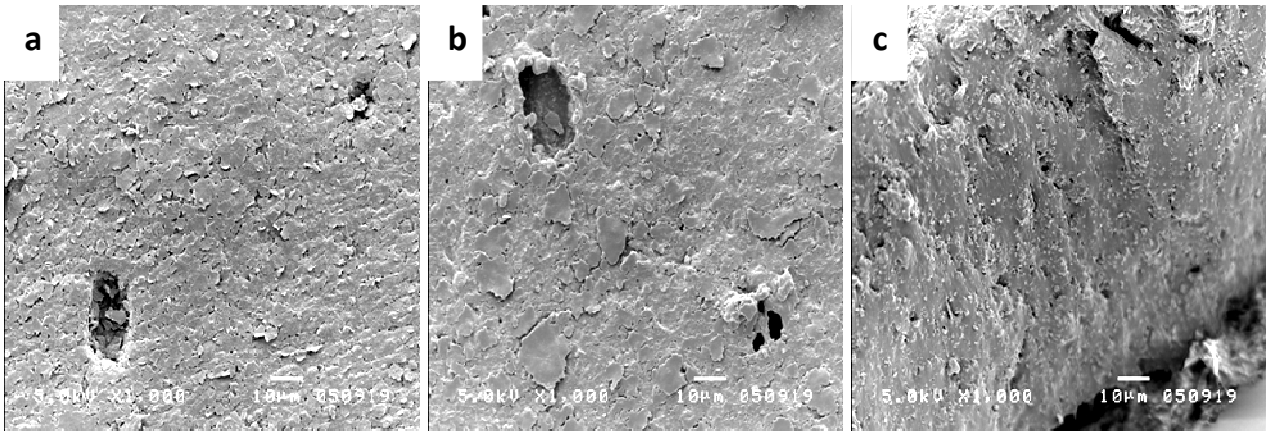

Figure 45: SEM images of Sempercare Edition 2008, high degree of chlorination, smooth surface (48); fresh sample, (a) outer side, (b) inner side, (c) breaking edge (RT fracture); 5.0 kV, magnification = 1000 x, wd 10 for breaking edge, outer and inner side

The outer side (a) and the inner side (b) of the other *Sempercare Edition* sample (smooth surface) (Figure 45) also exhibited imbricative structures with holes in the surface, but was smooth compared to the sample shown in Figure 43. The edge (c) was rough and holes were present in the bulk as well.

In Figure 46 SEM images of a product from another company (*Hartmann Peha Soft*) were shown. The outer side of the fresh sample (a) showed a crazing effect and the cracks and holes deepened throughout ageing (d). The inner side of the fresh (b) and the aged sample (e) also showed this crazing effect with deepened features in the aged sample. The edge of the fresh sample (RT fracture, c) was rough and had holes all over the area. The aged sample (freeze fractured, f) on the other hand was smooth, but had also holes in the bulk. This difference in appearance is attributed to the difference in handling of the samples.

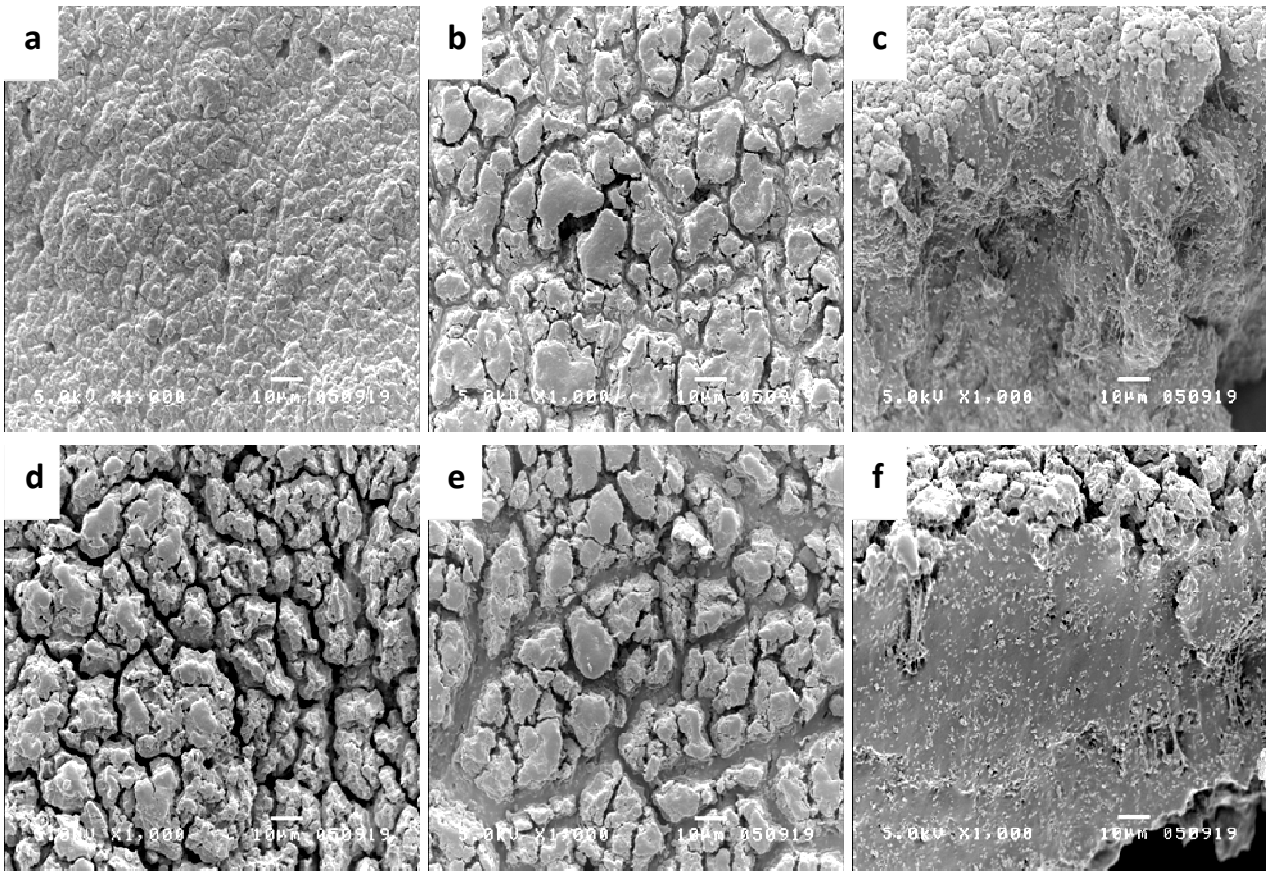

Figure 46: SEM images of Hartmann's Peha Soft, high degree of chlorination, smooth surface (35, 36); top: fresh sample, (a) outer side, (b) inner side, (c) breaking edge (RT fracture); bottom: aged sample (17 days), (d) outer side, (e) inner side, (f) breaking edge (RT fracture); 5.0 kV, magnification = 1000 x, wd 10 for outer and inner side, wd 15 for breaking edges

The samples herein exhibited not only holes on their outer and on their inner side, but also showed imbricative structures, which in some cases were more distinctive. These damages were caused by the acidic chlorination process, which is quite aggressive to the material.

The sample shown in Figure 46 was somehow different as it showed a severe crazing effect already present in the fresh sample. [18,19,118] This effect, resembling an elephant's skin, leads in most cases to early fracture of the material. Crazing is caused by light-catalysed oxidation and leads to an interpenetrating network of cracks.

Samples based on Supreme (27, 28, 29, 30)

To investigate the influence of different manufacturing parameters, *Supreme* based samples were produced on lab scale. For a detailed description of the gloves see Table 9.

SEM images of *Sempermed Supreme* (Figure 47) exhibited distinctive globular structures on its outer side (a). The inner side (b) of the sample was smooth, showed the characteristic net-like structure of the modified coating and had few holes. The edge (c) was smooth as well and showed only isolated holes.

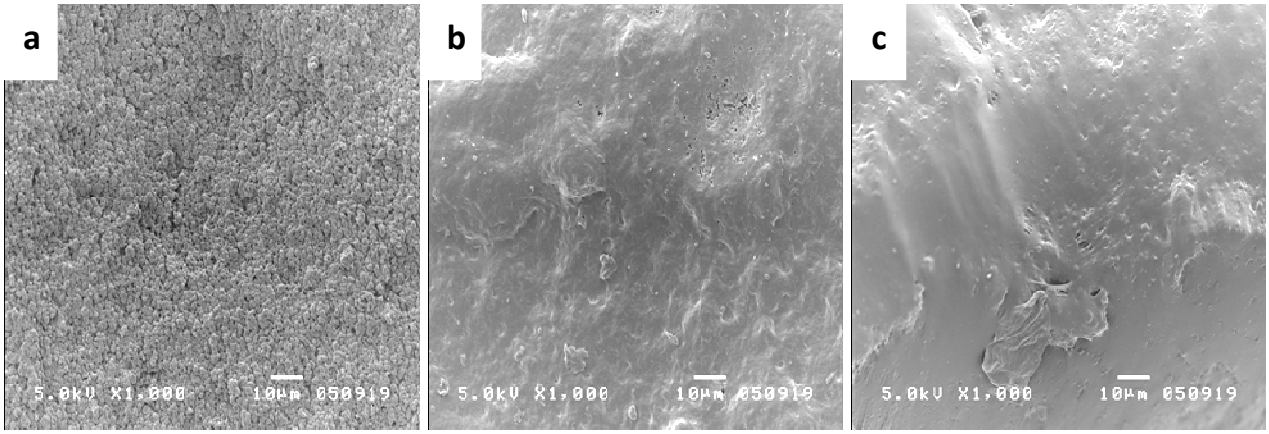

Figure 47: SEM images of Sempermed Supreme, high degree of chlorination, modified coating (50); fresh sample, (a) outer side, (b) inner side, (c) breaking edge (RT fracture); 5.0 kV, magnification = 1000 x, wd 10 outer and inner side, wd 15 for breaking edge

The samples taken from *Supreme HCl/NaOCl* (see Figure 48) showed a severe crazing effect. The outer (a) and inner side (b) of the fresh sample had cracks all over the surface area with holes present. The edge (c) was quite smooth but revealed the effect of acidic chlorination, *i.e*. a line just below the surface. The crazing effect was intensified during ageing. The cracks were deepened on the outer side (d) and on the inner side (e) as well. The ageing effect was clearly visible at the edge (f): the surface appeared to be stripped off the bulk material and underneath the surface holes became visible.

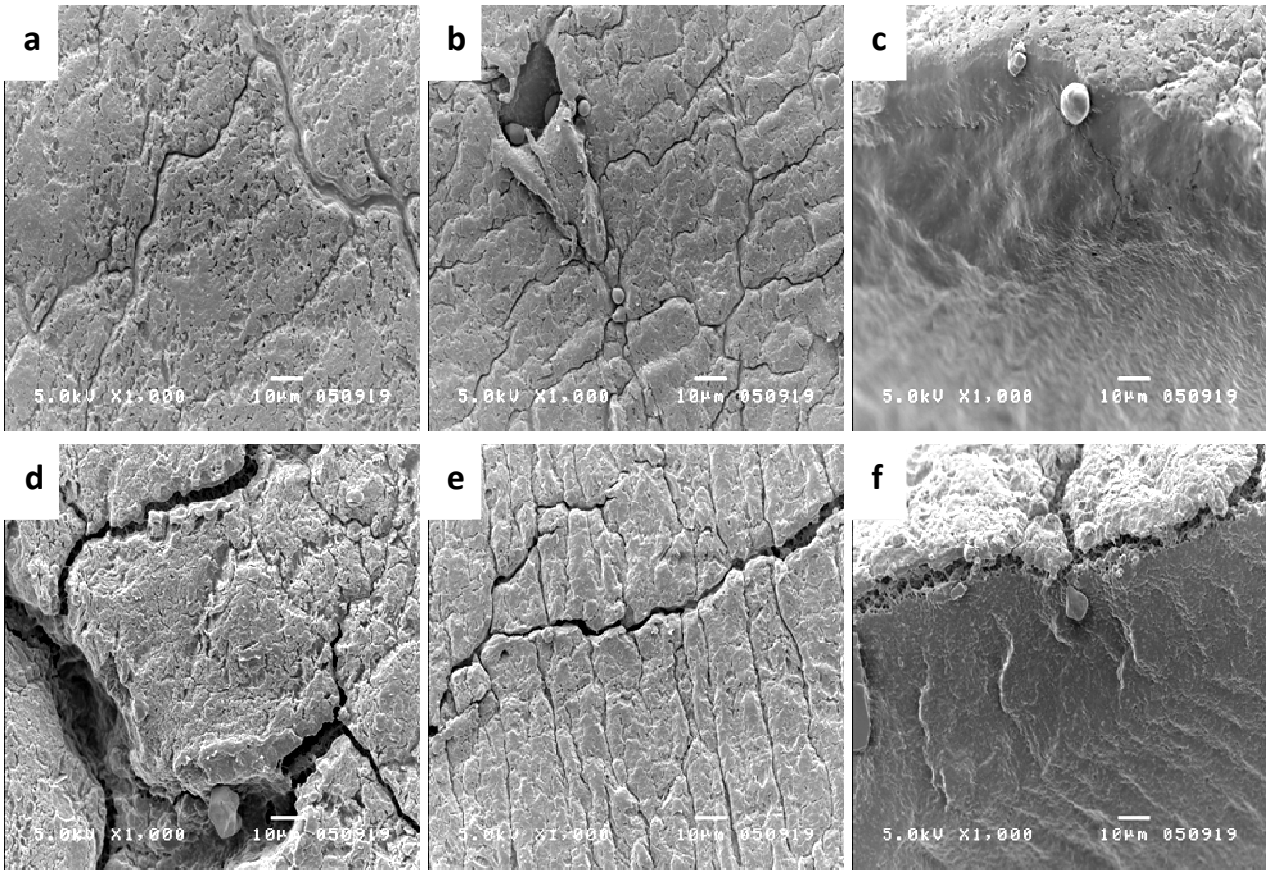

Figure 48: SEM images of Supreme HCl/NaOCl, dry powder (27, 28); top: fresh sample, (a) outer side, (b) inner side, (c) breaking edge (freeze fracture); bottom: aged sample (21 days), (d) outer side, (e) inner side, (f) breaking edge (freeze fracture), tilted 10°; 5.0 kV, magnification = 1000 x, wd 10 for outer and inner side, wd 15 for edges

Approximately the same effects were observed in the sample with modified inner coating (Figure 49). The only difference was that the ageing effect was not as distinctive as in the sample without modified coating.

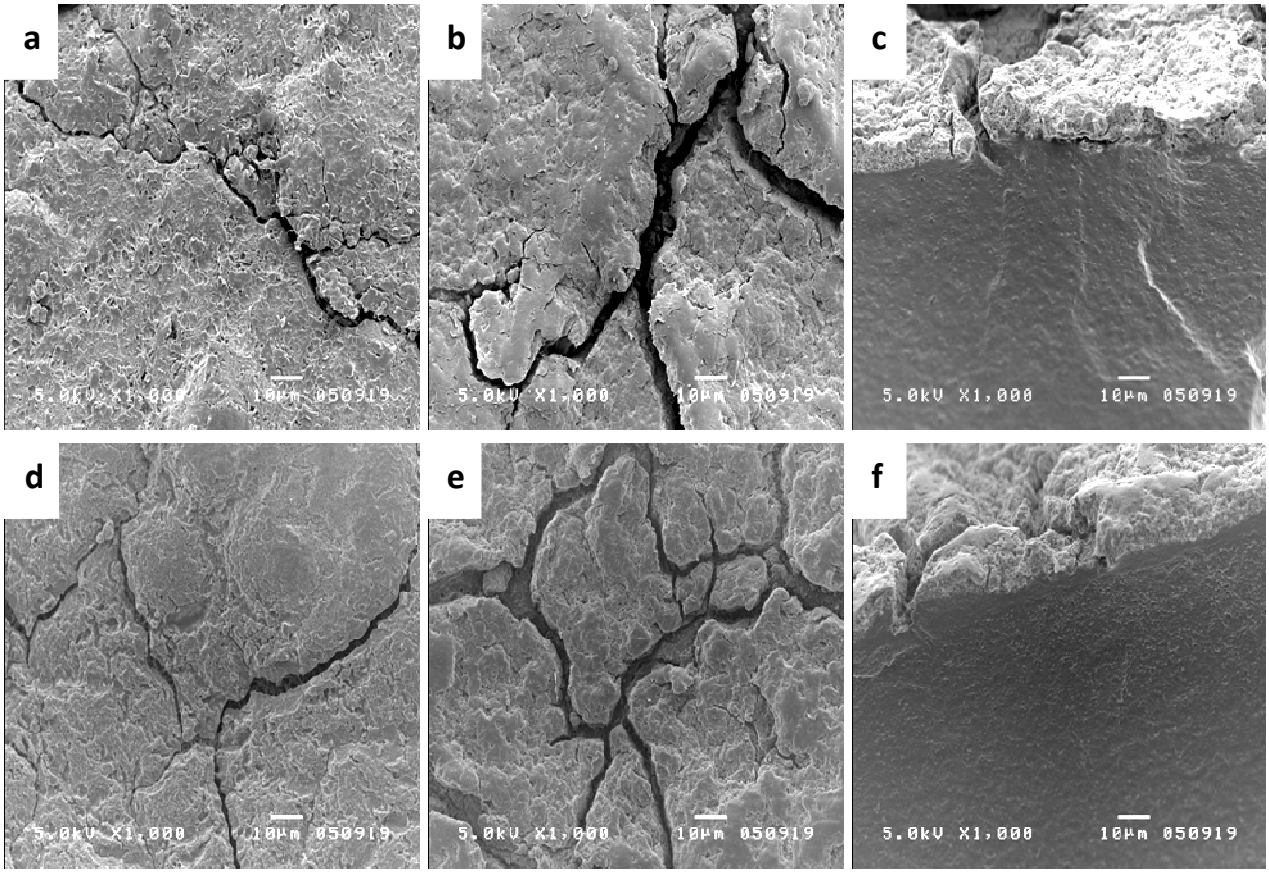

Figure 49: SEM images of Supreme HCl/NaOCl, modified coating (29, 30); top: fresh sample, (a) outer side, (b) inner side, (c) breaking edge (freeze fracture), tilted 10°; bottom: aged sample (21 days), (d) outer side, (e) inner side, (f) breaking edge (freeze fracture), tilted 10°; 5.0 kV, magnification = 1000 x, wd 10 for outer and inner side, wd 15 for edges

As described earlier, the chlorination process had a strong impact on the surface. In Figure 48 and Figure 49 the same crazing effect as in Figure 46 was observed. Additionally, it can be seen which damaging effect the chlorination had regarding the edges. The bulk material appeared to be stripped off the surface below and holes became visible underneath.

5.2 Contributions to improved nanocomposite solar cells

5.2.1 Synthesis of precursors for a low bandgap polymer

In chapter 4.3.1 the synthesis of a thieno[3,2-*b*]thiophene containing monomer was described. Following reasons were considered for the synthesis of a monomer and its use as polymer in hybrid solar cells.

The monomers already offers an extended π-π*-system, which can be further increased by polymerisation. It should have high planarity, due to the bridging of the outer thiophene rings to the thienothiophene moiety, and twisting should be avoided. The planarity also enforces charge transport between polymer chains leading to high charge carrier mobilities. The LUMO and thus the bandgap can be further decreased by copolymerising this monomer with an electron poor monomer, *e.g.* benzothiadiazole or bithiazole. For better solubility alkyl chains are introduced leading to a highly regioregular polymer. Irregularities in the molecule would disturb the conjugation thus leading to lowered carrier mobility. All these parameters do not only affect the bandgap but also the charge carrier mobility in the molecule and other important factors such as air stability. [46,119,120]

Scheme 6 shows the pathway leading to TTTT (compound **5**).

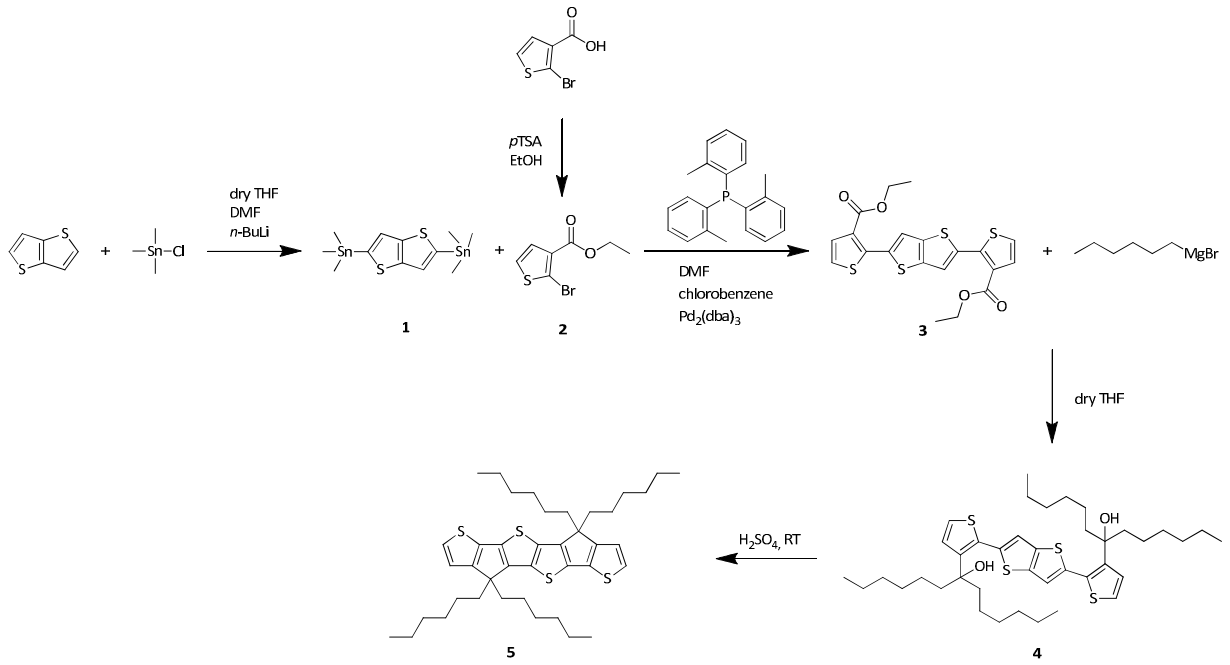

Scheme 6: Reaction pathway leading to TTTT

Stannylation of thieno[3,2-b]thiophene

Stannylation of thieno[3,2-*b*]thiophene was performed according to the instructions given by Dr. Martin Heeney (Imperial College London). [102,121]

Thieno[3,2-*b*]thiophene and TMEDA in dry THF were stirred with *n*-BuLi at -78 °C. After warming up to RT and cooling to 0 °C afterwards, trimethyltin chloride was added quickly. Stirring over night resulted in a dark orange solution. To quench excess trimethyltin chloride, water was added. Subsequently, the solution was subjected to a standard work up procedure. Recrystallisation in acetonitrile gave a white solid in good yield, as described in literature.

This was proved by ^{1}H-NMR spectroscopy (Figure 50) which showed typical peaks at 7.40 ppm (s, 2H) for the aromatic protons and 0.39 ppm (s, 18H) for the methyl groups attached to the tin. Also the ^{13}C-NMR spectrum (Figure 51) confirmed the presence of the stannylated thieno[3,2-*b*]thiophene mainly due to the peak at around -8 ppm. But also the other peaks at 147.67,

141.43 and 126.30 ppm fit perfectly. ^{119}Sn-NMR spectroscopy revealed a single peak at -25.082 ppm indicating that the substance is almost pure.

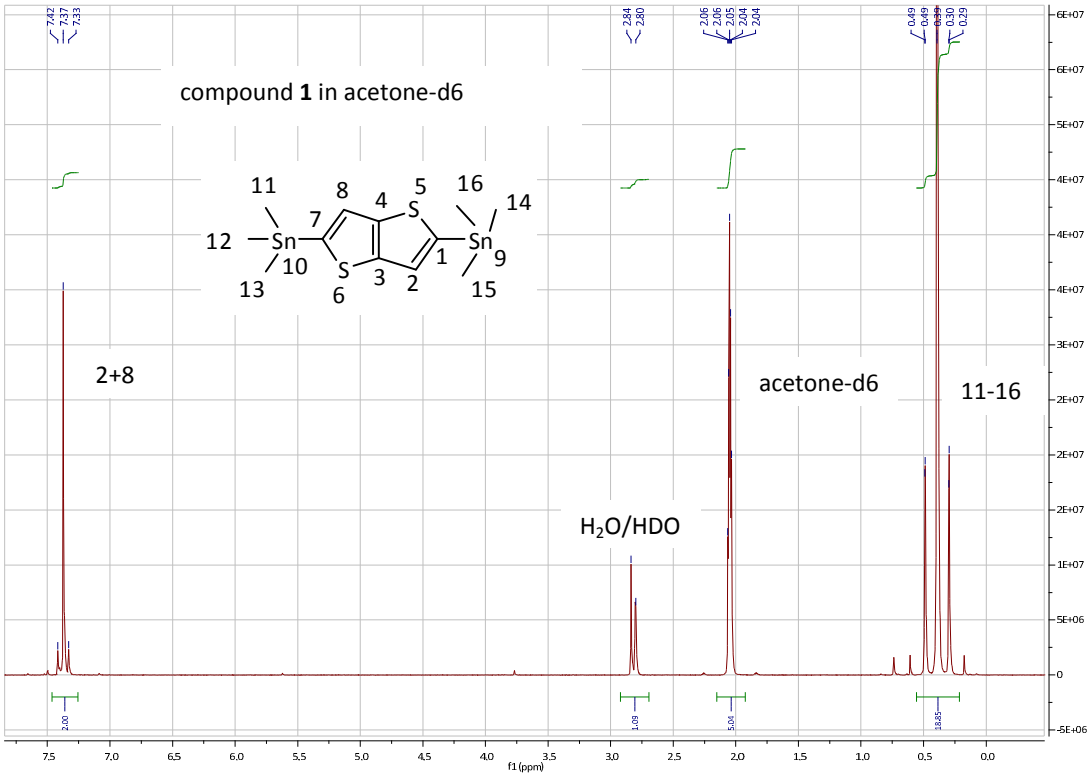

Figure 50: ^{1}H-NMR spectrum of substance 1

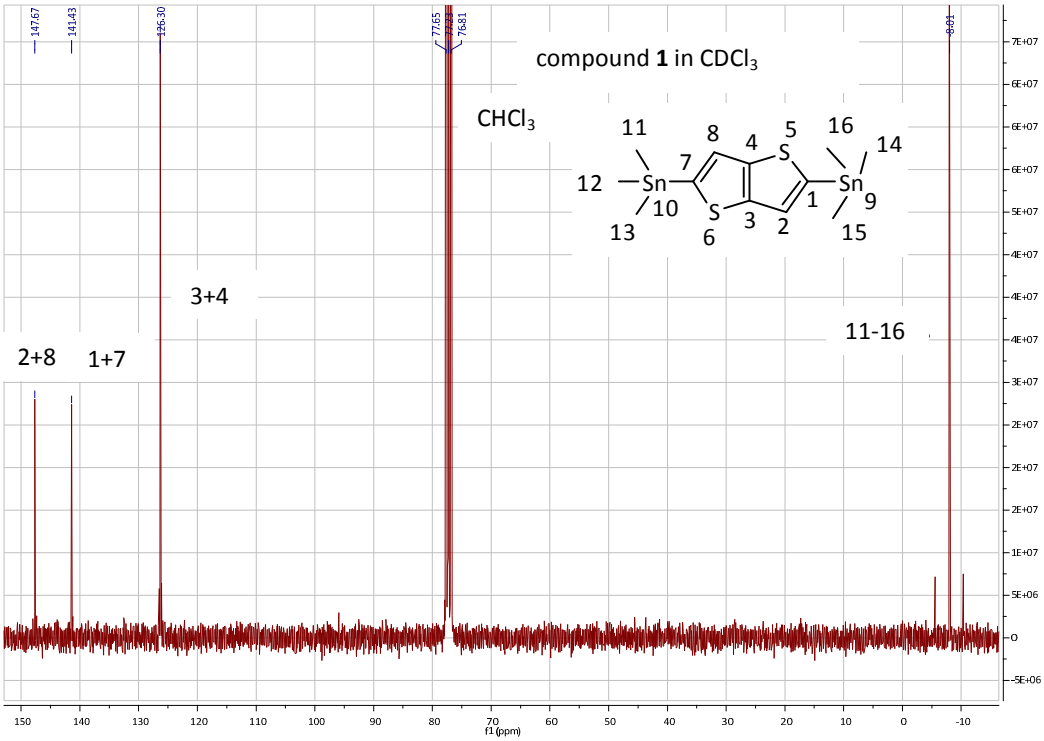

Figure 51: ^{13}C-NMR spectrum of substance 1

Esterification of 2-bromo-3-carboxylic acid

Esterification of the carboxylic acid was carried out according to literature procedures with an acidic catalyst and an alcohol.[46,103] Therefore 2-bromothiophene-3-carboxylic acid and *p*TSA were dissolved in ethanol and refluxed over night. Both, ethanol and *p*TSA were used in excess to ensure complete conversion of the acid. The solvent was removed under reduced pressure and the oily residue was extracted with DCM, washed with saturated sodium hydrogen carbonate and brine and dried over sodium sulphate. Again the solvent was removed under reduced pressure yielding compound **2** as a white solid in very good yield (98 %). This product was taken to the next step without further purification.

Purity of substance **2** was shown by NMR spectroscopy. Only a small amount of DCM was present in the proton NMR (Figure 52). The ethyl ester was identified by the presence of a quartett at around 4.3 ppm representing the methylene group next to the oxygen and a triplett

at 1.39-1.34 ppm (methyl group). Also the ^{13}C-NMR spectrum (Figure 53) indicated that substance **2** was obtained because peaks at 61.19 and 14.47 ppm appeared. These peaks corresponded with the methylene and the methyl group now present in the molecule.

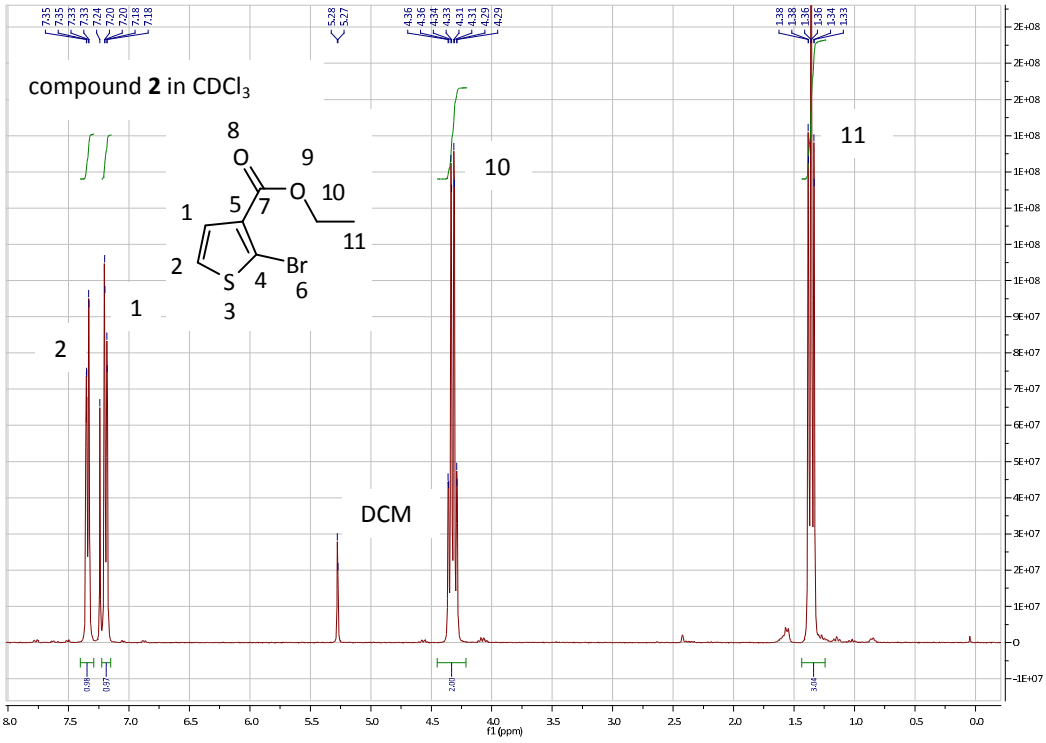

Figure 52: ^{1}H-NMR spectrum of substance 2

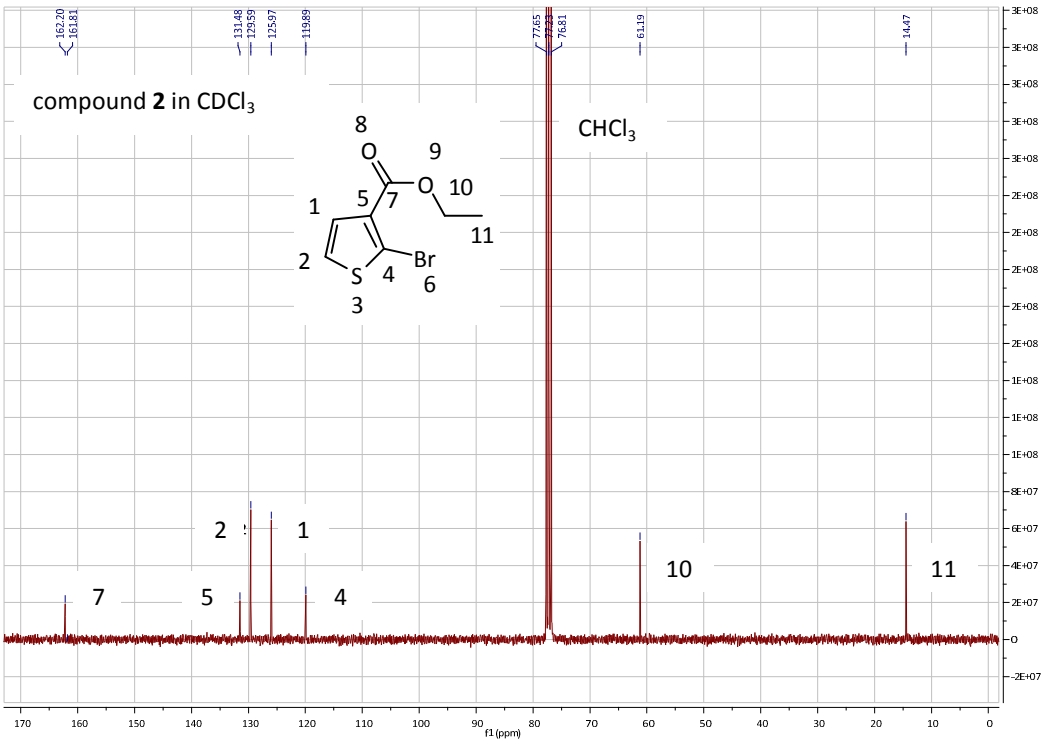

Figure 53: ^{13}C-NMR spectrum of substance 2

*Microwave Stille coupling of compounds **1** and **2*** [46,101,104]

Microwave syntheses for organic reactions have gained interest over the last years. [104,122,123] A Stille microwave coupling was employed for coupling of the stannylated thieno[3,2-*b*]thiophene **1** and the ethyl ester **2** according to a procedure reported by Tierney et al..[104] This microwave route was chosen due to a reduction of the reaction time and the resulting high yields.

A microwave vial was charged with compounds **1** and **2**, tri-*o*-tolylphosphine, chlorobenzene, DMF and $Pd_2(dba)_3$. DMF was used instead of LiCl, which was used in literature reports. It was observed, that DMF is able to solubilise not only the starting material but also the product. Its use also leads to improved reaction conditions and higher yields.

The vial was purged with argon and sealed. The reaction was stirred at 200 °C for 10 min in the microwave reactor. The reaction mixture was poured into a mixture of methanol and 2 M HCl

and the formed precipitate was filtered off and washed. The resulting solution was filtered into ethanol and filtered to give a shiny orange solid in good yield (85 %). The peaks in both, proton- and carbon-NMR spectra were in good agreement with theoretical calculations (Figure 54 and Figure 55).

Additionally, an EI mass spectrum (Figure 56) was recorded. The observed peaks corresponded with the calculated masses verifying the NMR results and leading to the conclusion that substance **3** was obtained in high purity.

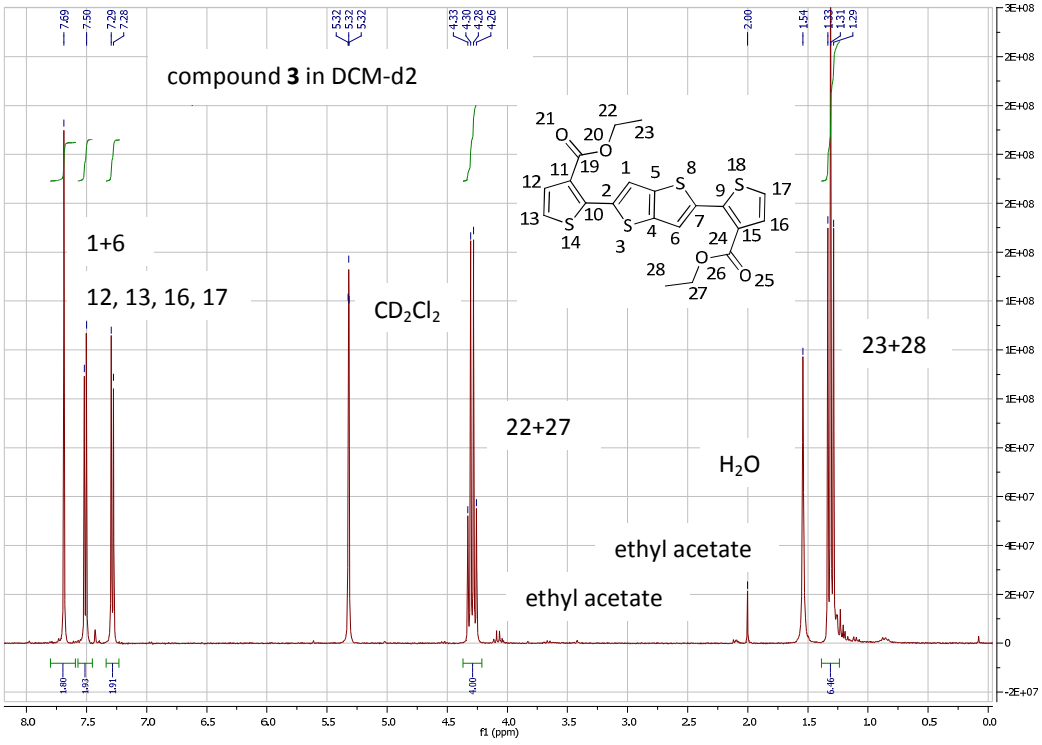

Figure 54: ^{1}H-NMR spectrum of substance 3

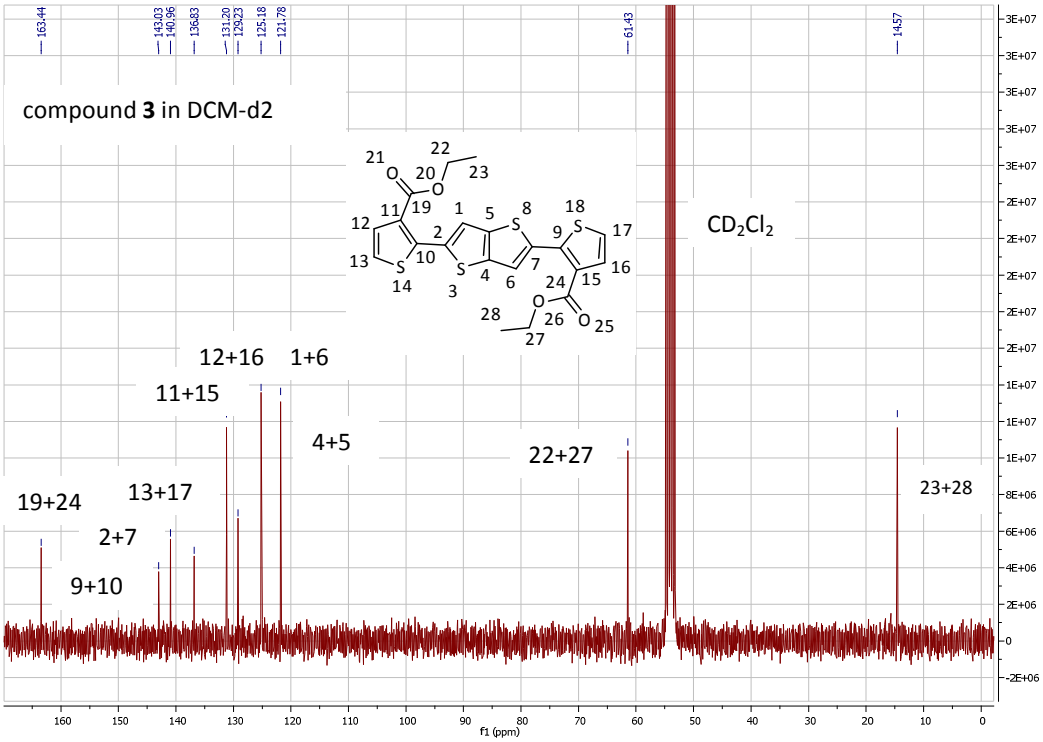

Figure 55: ^{13}C-NMR spectrum of substance 3

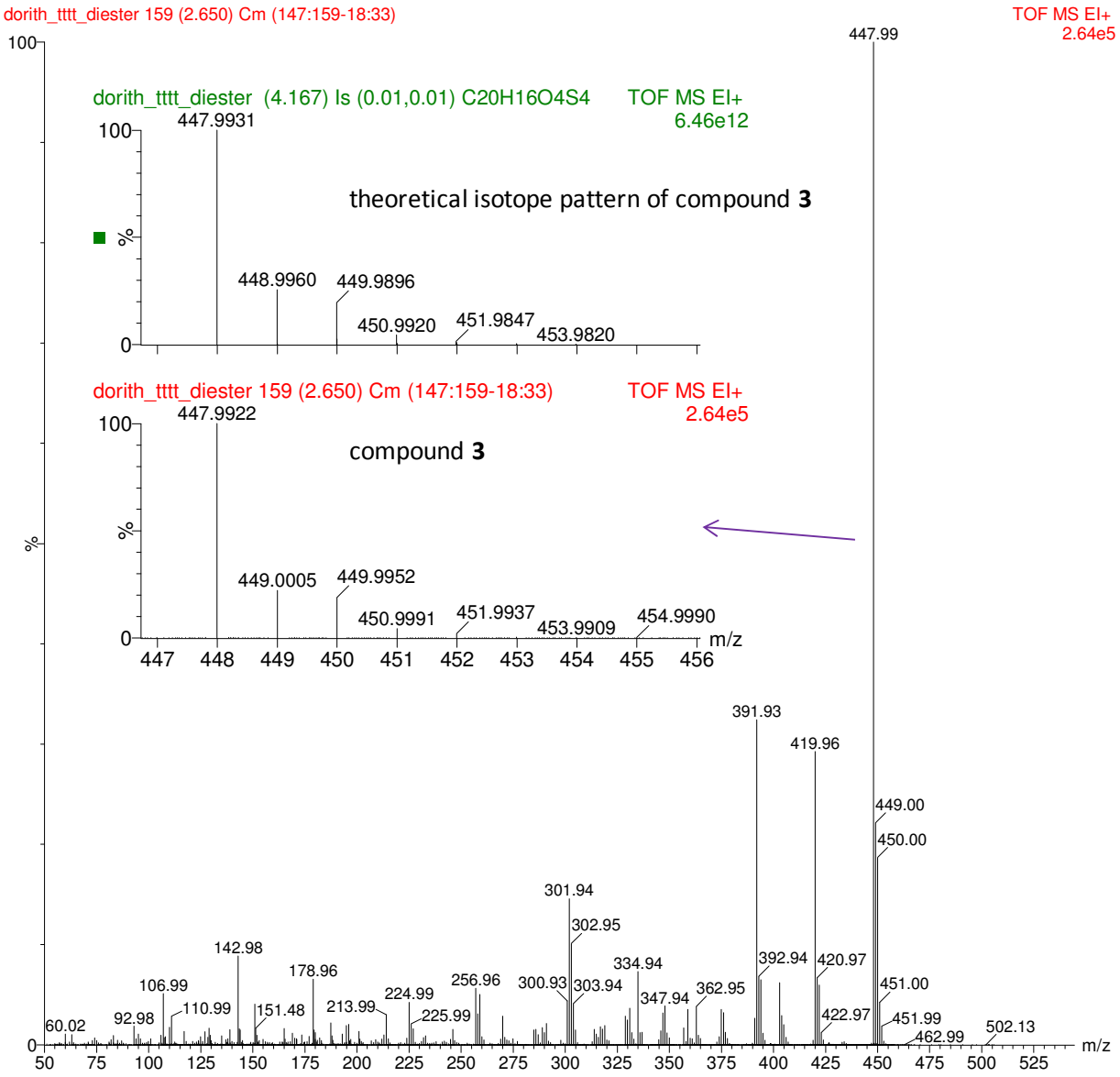

Figure 56: EI-MS spectrum of substance 3

Introduction of side chains through Grignard reaction [46,105,124]

The introduction of side chains should lead to a better solubility of the final molecule. [119,125] In this case, this was achieved by the introduction of alkyl chains, through Grignard reaction of an alkyl magnesium bromide with ester **3**.

Linear hexyl side chains were chosen regarding possible side reactions in the following synthetic step. Branched alkyl chains (*e.g.* 2-ethyl hexyl) could favour eliminations during the following ring closure, leading to "dead" alkenes. In literature aromatic side chains were reported [105] to work fine on thiophene-phenylene-thiophene units. One of the side chains reported therein was already employed in the synthesis of TTTT during the internship. Hence, it was decided to use the linear hexyl side chains.

Hexylmagnesium bromide was added to a solution of **3** in dry THF at 0 °C. An excess of Grignard reagent was used to ensure full alkylation of the starting material. After refluxing over night the reaction was subjected to a standard work up procedure. The remaining solvent was removed under reduced pressure resulting in a brownish oil in acceptable yield (94.6 %). The crude product was used without further purification in the next step.

NMR spectra were recorded, but due to the multitude of side products (mono-, di-, and trialkylated compounds), interpretation was not successful.

*Ringclosure step to obtain TTTT **5*** [46,105,106]

The ring closure step is a crucial point in the whole synthesis. Several different chemicals, including DCM, hexane, HCl and sulphuric acid were used in test reactions to see whether a ring closure takes place. Literature reports stated that Lewis acids do not work and favour the formation of alkenes. It is also known, that suphuric acid in hexane works well with thiophene-phenylene-thiophene units or thiophene-cyclopenta-thiophene moieties. [105,106] Combining the results from the test reactions and the literature reports, it was decided to use sulphuric acid in hexane in this work. Although the synthesis of 4*H*-cyclopenta[2,1-*b*:3,4-*b'*]dithiophenes is

literature known, the yield in the double ring closure in the synthesis of TTTT was not comparable.

In this work compound **4** was dissolved in hot hexane and the sulphuric acid was added dropwise under vigorous stirring resulting immediately in a sticky black solid. After stirring over night at RT, the reaction mixture was quenched with water and subjected to a standard work up procedure. The formed black solid was extracted for 4 d with hexane in a Soxhlet yielding a brownish oil. The obtained crude product was purified by column chromatography on alumina with hexane as eluent (yield = 1.5 %).

To verify the structure of **5**, ^{1}H- and ^{13}C-NMR were recorded. Because peaks were too broad to give unambiguous results, FTIR spectra (Figure 57) were recorded too. The FTIR spectra showed typical peaks for aliphatic and aromatic fragments (Table 10) but these results combined with the NMR results did not necessarily lead to the conclusion that the desired molecule **5** was isolated successfully.

Table 10: Assignment of absorptions observed in the FTIR spectra of compound 5

	wavenumber/cm^{-1}	intensity	assignment
1	2925.30, 2925.16	s	aliphatic out of plane stretching
2	2854.69, 2854.69	s	aliphatic in plane stretching
3	1460.66, 1460.66	m	aliphatic out of plane deformation C-H scissor vibration
4	1377.27, 1377.27	m	CH_3 in plane deformation C=C stretching (aromatic ringssystem) C=C in plane vibration
5	965.45	w	C-H deformation (substituted aromatics) C-C skeleton vibration (5-membered ring) CH out of plane deformation (substituted thiophene) CH in plane deformation (substituted thiophene)
6	909.11	w	C-H deformation (substituted aromatics)

An EI mass spectrum (Figure 58) was recorded to verify that the desired molecule **5** was obtained. Results showed that **5** was formed unambiguously, although only as side product among enriched long alkyl chains and tin compounds.

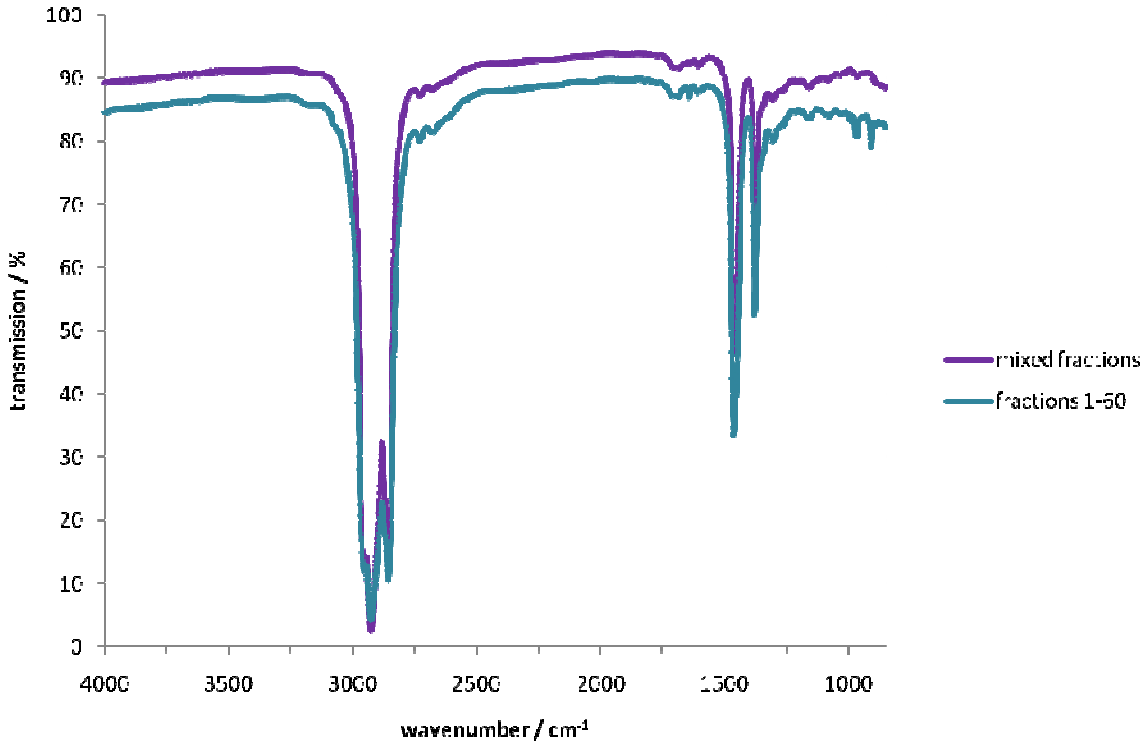

Figure 57: FTIR spectra of substance 5

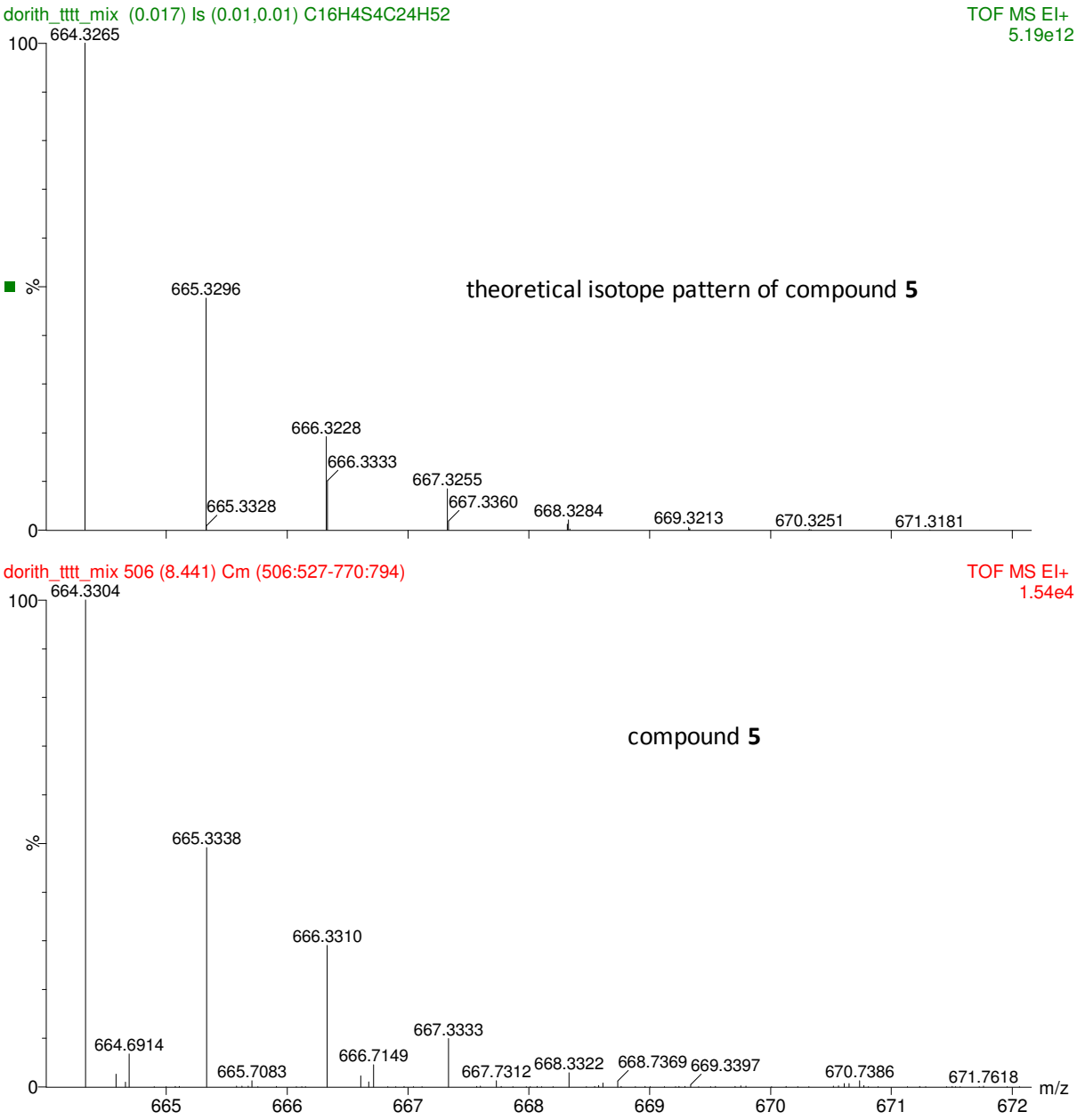

Figure 58: HRMS data of the "mixed fractions" of substance 5

5.2.2 Characterisation of CIS nanoparticles

In this work the influences of different amounts of thiourea and different annealing temperatures on the formation of side products were investigated by means of mass spectrometry (EI-MS). Therefor precursor solutions with copper acetate, indium (III) chloride and thiourea (1.6, 2.8 and 4 eq) in pyridine were prepared, spray-coated onto ITO/glass substrates and annealed at different temperatures (200 °C, 300 °C and 450 °C). In all these samples a constant Cu/In ratio of 1.5 was kept.

Mass spectra revealed the presence of a volatile compound evaporating above approximately 150 °C, which can be seen in the total ion chromatogram (Figure 59). This volatile compound has a molecular mass of 126.0653 Da. The mass corresponds well to the molecular formula $C_3H_6N_6$ which has a calculated accurate mass of 126.0654 Da. Consequently, the signal was interpreted as the molecular ion of melamine.

To verify the result, typical fragment ions of the compound were detected, *e.g.* $C_2H_5N_4$ with a mass of 85.0517 Da (calculated accurate mass: 85.0514 Da). Additionally, the structure was confirmed by comparison with an EI database (Wiley NIST) spectrum.

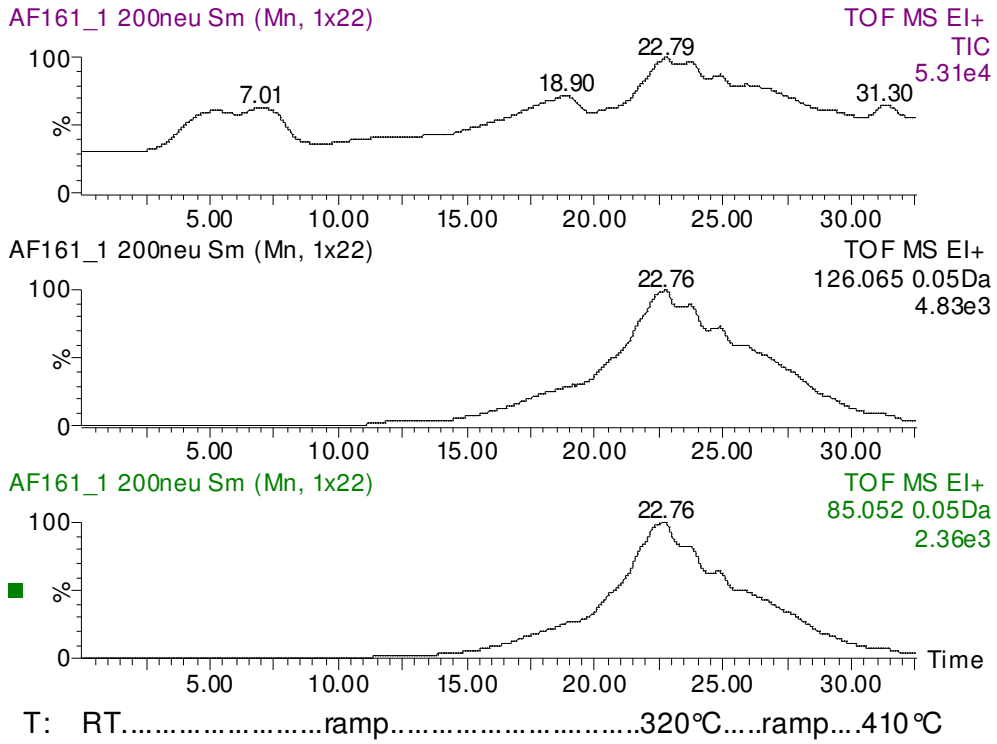

Figure 59: EI-MS total ion chromatogram and selected ion traces of melamine in $CuInS_2$ thin films prepared at 200°C (4 eq thiourea) (top: total ion current, middle: ion trace molecular ion, bottom: ion trace fragment ion ($C_2H_5N_4$))

Melamine was observed in the samples with 1.6 and 2.8 eq too, but with lower intensity.

In literature, several reports can be found mentioning the presence of impurities formed during the formation of CIS films prepared from thiourea as sulphur source. [126-128] It has to be mentioned, that other groups also found melamine, more or less at the same time, when the experiments described in this work were carried out. [107] Melamine (2,4,6-Triamino-1,3,5-triazine) can be formed through trimerisation of dicyandiamide. Thus, the formation of melamine during the annealing step can be easily explained, though it was not expected here. [129,130]

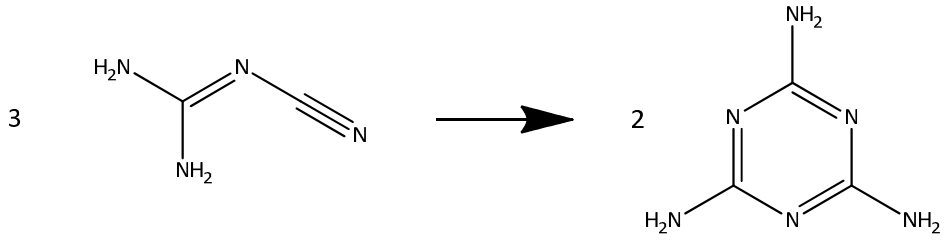

Scheme 7: Trimerisation of dicyandiamide

However, the presence of melamine in the films for photovoltaic applications is a crucial point, because melamine has a rather high melting point (350°C, decomposition point). [130,131] Therefore, it has to be assumed, that it stays within the nanocomposite layer and influences the properties of the solar cell. [107]

Consequently, an alternative to thiourea as sulphur source was investigated. Metal-xanthates with different metals (Cu, In, Ga, Zn, Sn, Cd) were synthesised and characterised by EI mass spectrometry. [110]

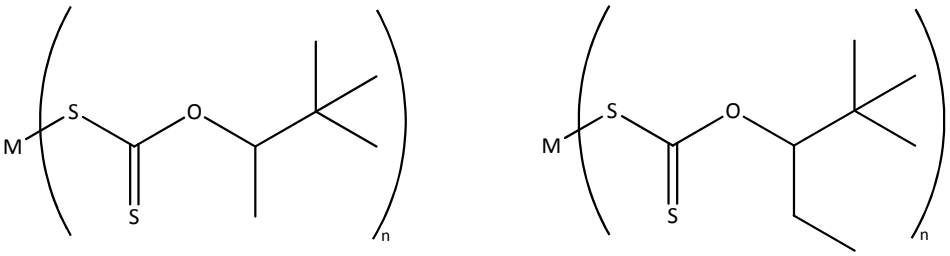

M = Cu, In, Ga, Zn, Sn, Cd

Scheme 8: Structures of novel metal-xanthates

These novel metal-xanthates form metal sulphides via the Chugaev rearrangement. In this rearrangement only side products with low boiling points are formed, hence no impurities should remain in nanocomposite layers. [132] To get more insight into the thermal decomposition behaviour, selected xanthates were investigated by means of EI-MS (Figure 60 and Figure 61).

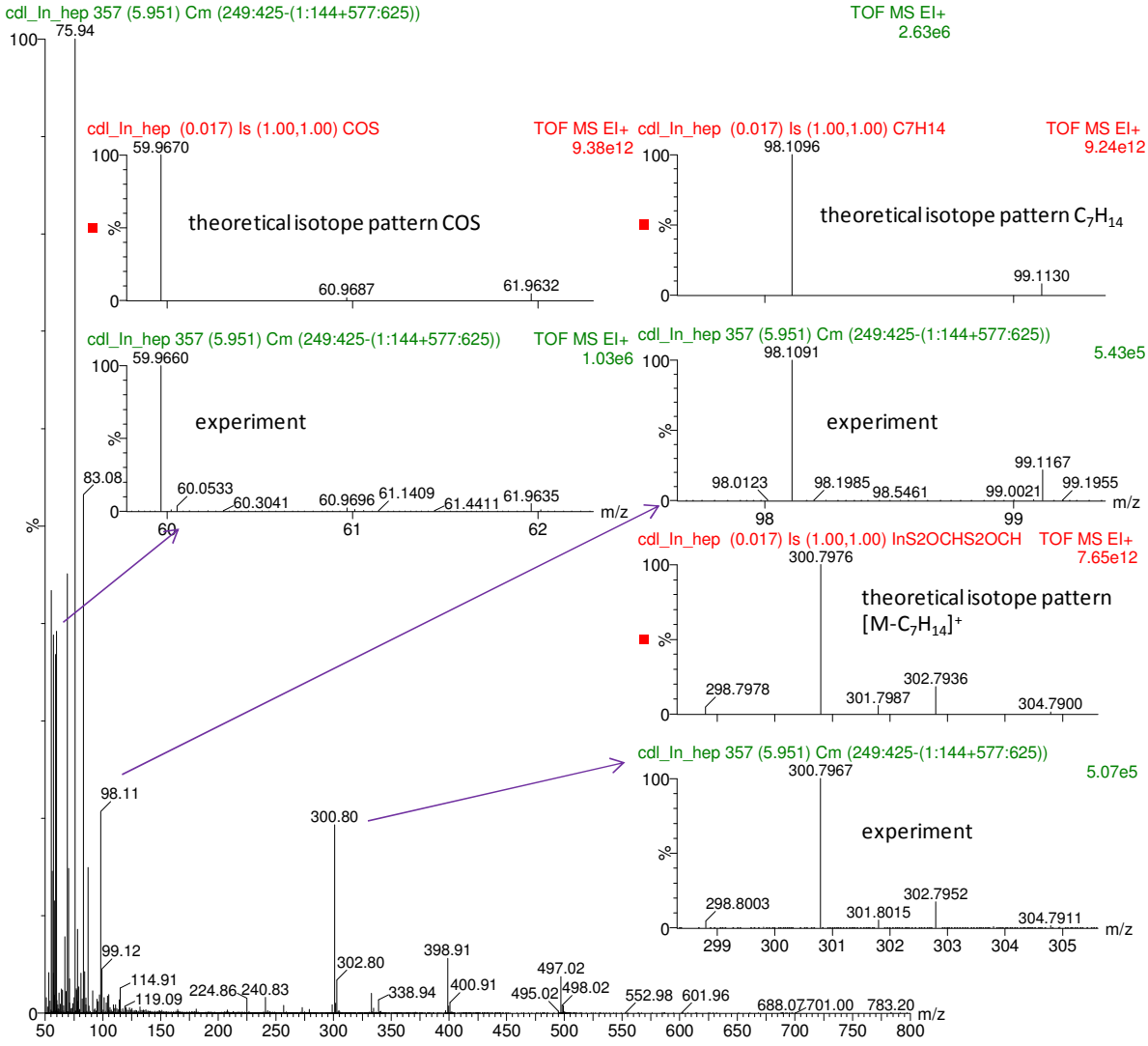

Figure 60: EI-MS spectrum of indium *O*-2,2-dimethylpentan-3-yl dithiocarbonate

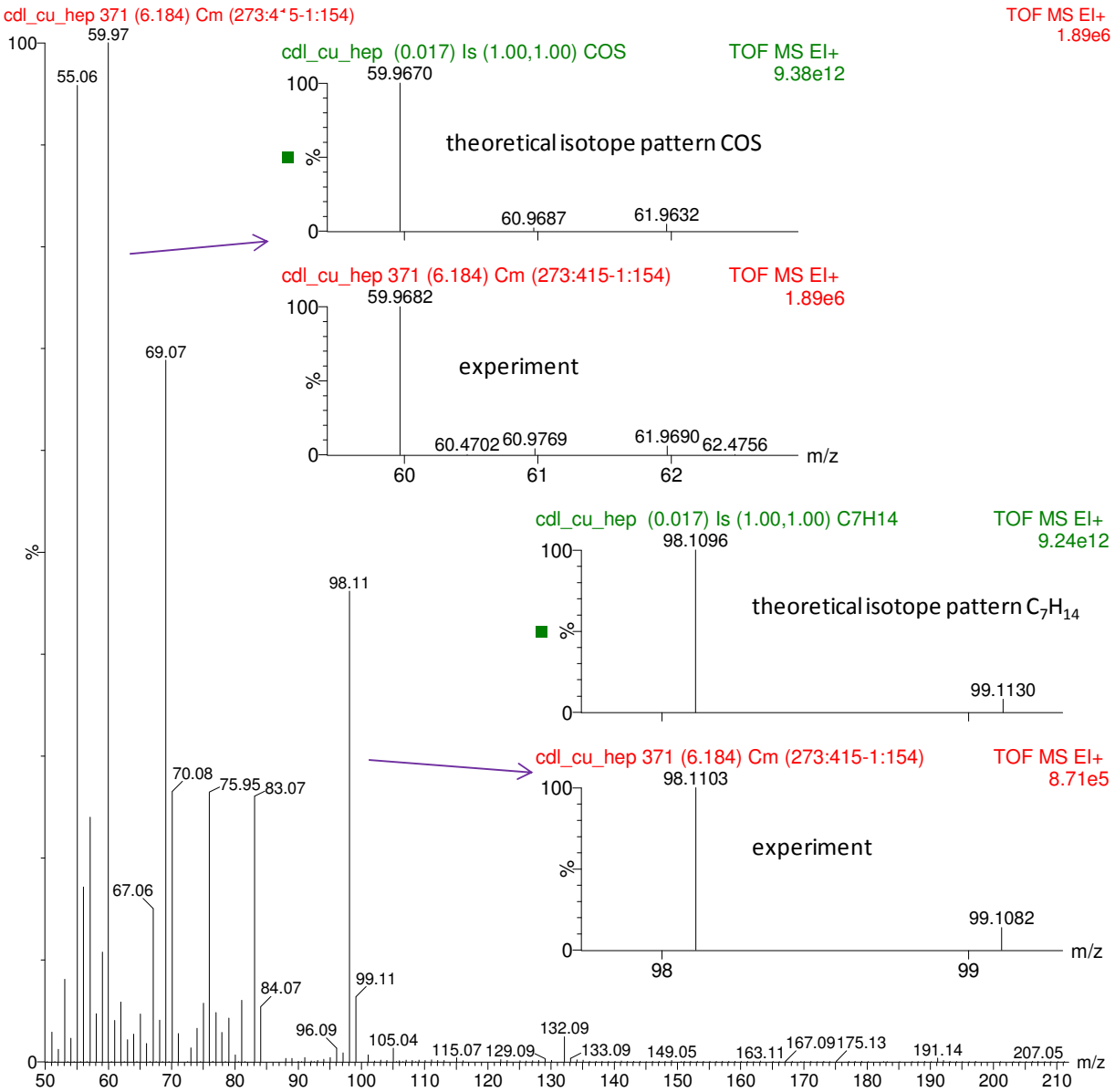

Figure 61: EI-MS spectrum of copper *O*-2,2-dimethylpentan-3-yl dithiocarbonate

During the investigation of copper-xanthates and indium-xanthates it was observed that the indium compound (Figure 60) evaporated in high vacuum above approx. 140 °C. The molecular ion peak was observed as well as some typical fragment ions. Simultaneously a decomposition reaction was observed. In contrast to this behaviour, no evaporation of the copper-xanthate

was found. This compound immediately decomposes and the EI mass spectrum showed only organic fragments (Figure 61). Only low mass side products, such as COS, CS_2 and the alkyl residue, evaporated.

Due to the evaporation of indium-xanthate during film formation of $CuInS_2$ high amounts are needed, when the aim is a stoichiometric CIS film. Thus, substitution of the vacuum annealing step by annealing under inert conditions and under atmospheric pressure seems promising for CIS films with defined stoichiometry.

6 Summary and Conclusion

6.1 Surface characterisation of medical gloves

Within this work, various latex gloves were investigated by means of scanning electron microscopy. Samples, produced under varied processing conditions, were compared.

Summing up, it became obvious that the processing parameters had a crucial impact on the ageing behaviour of latex and on the appearance of sample surfaces as well as on the lifetime of such products.

Highest influences on the ageing behaviour have the degree of chlorination and the coating system, respectively.

Chlorination of medical gloves is carried out to reduce tackiness of the material, but problems occur depending on the degree of chlorination. Regarding the SEM images of the investigated samples, it was obvious that acidic chlorination (NaOCl/HCl) was stronger and affected the material even more compared to alkaline chlorination (NaOCl). Ageing damages were more severe and the so called crazing effect could be seen very clearly as the surface resembled an elephant's skin. This effect led to an interpenetrating network of cracks caused by light-catalysed oxidation of the material. [18,19,118]

Instead of chlorination, other coatings are often used to reduce tackiness of medical gloves. Either powder or a modified coating can be applied. Powder is often replaced by modified coatings (*e.g.* silicon oil or a synthetic polymer coating) to reduce the allergens present on the surface of medical gloves. Non chlorinated (powder-coated) gloves had holes as well, but they were small and less abundant compared to the ones in chlorinated gloves.

With respect to the SEM images shown in this work, modified coatings are assigned to act as a protective layer during ageing. However, as this modified coating was only applied to the inner side of the glove, holes and cracks still appeared on the outer side of the sample.

To complete the characterisation of latex samples, it was investigated whether the coagulant bath influenced the ageing behaviour. Two different coagulants, $Ca(NO_3)_2$ and $CaCl_2$ respectively, used during production of gloves were compared. No significant differences were found.

6.2 Contributions to improved nanocomposite solar cells

The concept of hybrid solar cells should combine advantages of inorganic and organic solar cells. In hybrid solar cells both components, the semiconducting inorganic nanoparticles and the semiconducting organic polymer, harvest sunlight and therefore higher power conversion efficiencies can be obtained. Within this work both components have been investigated separately. Additionally, syntheses of precursors for a low bandgap polymer were carried out. [56,133]

Several requirements, regarding the polymer, have to be considered. It has to be air stable and insensitive to ambient conditions, but has to match the optical bandgap of the nanoparticles as well as the spectrum of the sun.

For this reason precursors for a low bandgap polymer with a thieno[3,2-*b*]thiophene moiety bridged to thiophene were synthesised. Elongation of the π-system leads to lower bandgaps, in addition to several other factors. Synthesis of diethyl 2,2'-(thieno[3,2-*b*]thiophene-2,5-diyl)bis(thiophene-3-carboxylate) (compound **3**) was successfully achieved (Figure 62), although it was carried out over several steps. Each step afforded products in good yield and high purity.

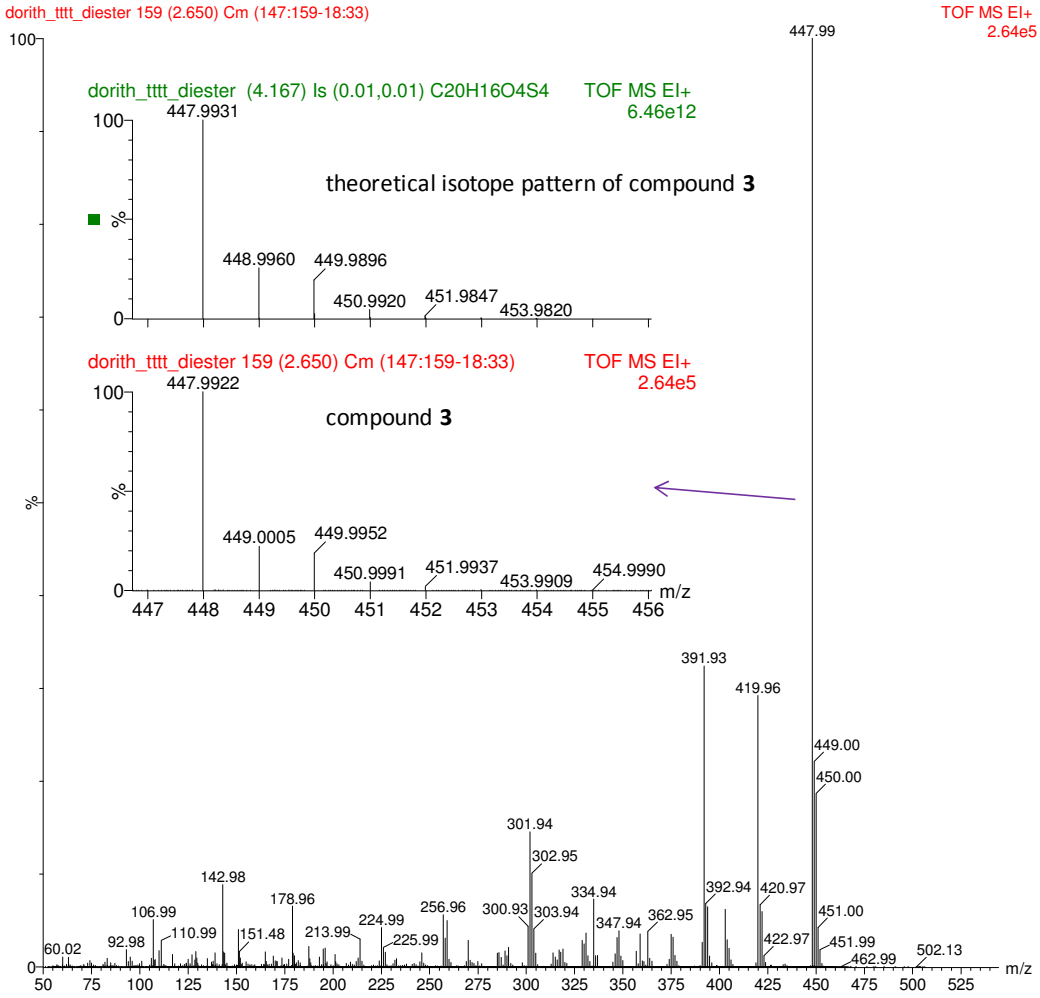

Figure 62: EI mass spectrum of 2,2'-(thieno[3,2-*b*]thiophene-2,5-diyl)bis(thiophene-3-carboxylate)

Problems occurred during introduction of alkyl chains to the ester functionality of compound **3**. According to NMR, a mixture of mono-, di-, tri-, and tetra alkylated products was obtained. The crude product was used in the next step without further purification, because separation was not successful within this work.

The next step - ring closure - turned out to be the most difficult step in this route. Although the reaction is known in literature, dehydration and ring closing was problematic. [105,106] Several acid

solvent mixtures and reaction temperatures were investigated. The most promising was sulphuric acid in hexane. After addition of the acid, a black solid precipitated immediately. Soxhlet extraction was used to purify the product. Further purification of TTTT by column chromatography on alumina still gave not a really pure product. Therefore, mass spectrometry was successfully used to identify the desired molecule within the mixture (Figure 63).

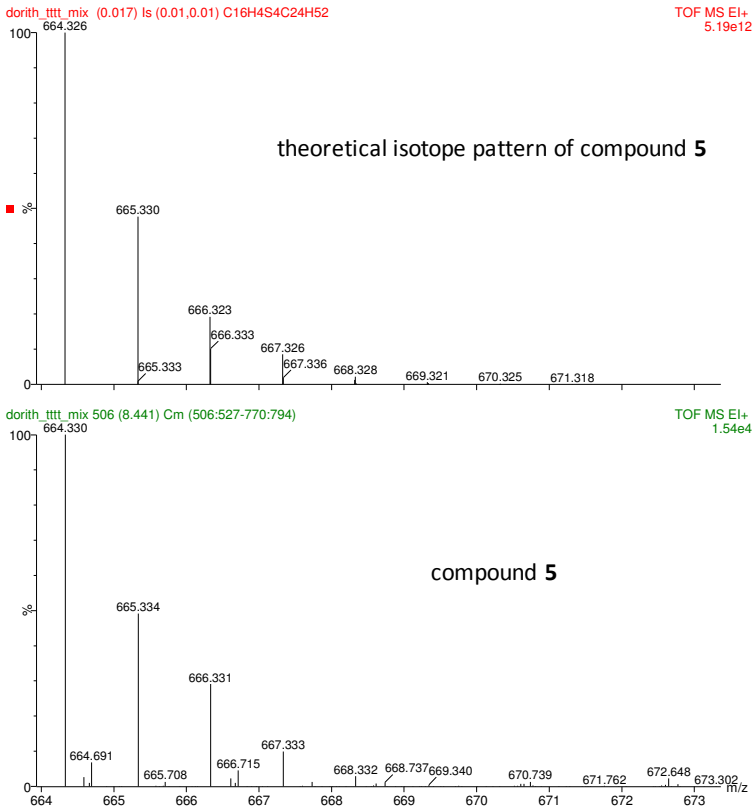

Figure 63: HRMS of TTTT (compound 5)

Future attempts will focus on improvement of the ring closing step, the purification of TTTT and its polymerisation.

Concerning the inorganic part of nanocomposite solar cells, many semiconducting materials can be considered. Mostly, metal sulphides are used. [68,69,72,73,75,76,134,135] This work deals with the characterisation of $CuInS_2$ prepared via different methods.

Firstly, CIS prepared from metal salts and thiourea was investigated by means of mass spectrometry. It was shown that the use of excess thiourea leads to an undesired side product. During the annealing step thiourea undergoes decomposition followed by trimerisation of cyanamide. The substance was identified as melamine (2,4,6-Triamino-1,3,5-triazine). Melamine, remains in the active layer of solar cells and strongly influences the electronic properties (*e.g.* traps for charge carriers), hence lowers the performance of solar cells.

To circumvent the problem of undesired side-products, novel metal-xanthates were investigated as precursors for metal sulphides. Decomposition of metal-xanthates leads to metal sulphides via Chuagev rearrangement. During this rearrangement only volatile compounds, as side products, are formed, which can be evaporated from the active layer. [110,132]

Metal-xanthates can be volatile, depending on the metal used. When comparing copper and indium-xanthates during mass spectrometric analysis, it was found, that the indium compound evaporates at approximately 140°C (Figure 64). This is an important observation, since evaporation of indium means, that the stoichiometry of the obtained CIS films is influenced, which again has an impact on the performance of hybrid solar cells.

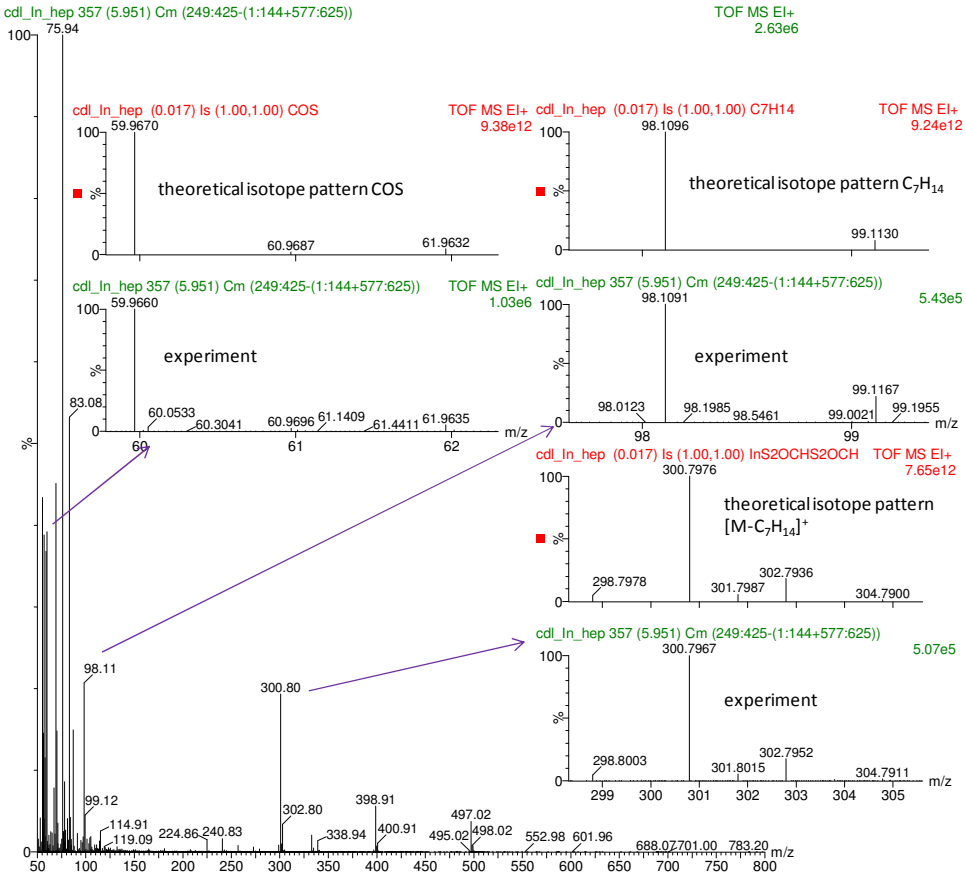

Figure 64: EI mass spectrum of indium *O*-2,2-dimethylpentan-3-yl dithiocarbonate

Contrary to this, the investigated copper-xanthates showed a completely different behaviour. Only small organic molecules were formed during the thermal decomposition, such as COS, CS_2 and alkyl residues, but no indication for the evaporation of copper was found in mass analysis.

These differences lead to an imbalance in stoichiometry. Indium-xanthates are needed in excess to obtain stoichiometric CIS films, because it partially evaporates under vacuum conditions. Annealing steps under atmospheric pressure could solve this problem.

7 Bibliography

(1) Ilschner, B.; Lees, J. K.; Dhingra, A. K.; McCullough, R. L. Composite materials. *Ullmann's Encyclopedia of Industrial Chemistry;* Wiley-VCH Verlag GmbH & Co. KGaA: Weinheim **2005**.

(2) Ehrenstein, G. W.; Kabelka, J. Reinforced Plastics. *Ullmann's Encyclopedia of Industrial Chemistry;* Wiley-VCH Verlag GmbH & Co. KGaA: Weinheim **2005**.

(3) Jeong, W. ROMP-based polymer composites and biorenewable rubbers, Iowa State University, PhD thesis, **2009**.

(4) Work, W. J.; Horie, K.; Hess, M.; Stepto, R. F. T. *Pure and Applied Chemistry* **2004**, *76*, 1985-2007.

(5) Greve, H.-H.; Threadingham, D. Rubber, 1. Survey *Ullmann's Encyclopedia of Industrial Chemistry*; Wiley-VCH Verlag GmbH&Co. KGaA: Weinheim, **2000**.

(6) Greve, H.-H. Rubber, 2. Natural *Ullmann's Encyclopedia of Industrial Chemistry*; Wiley-VCH Verlag GmbH&Co. KGaA: Weinheim, **2000**.

(7) Tanaka, Y.; Sakdapipanich, J. T. *Biopolymers Online*; Wiley-VCH Verlag GmbH&Co. KGaA, **2005**.

(8) Yip, E.; Cacioli, P. *Journal of Allergy and Clinical Immunology* **2002**, *110*, S3-S14.

(9) Resing, W. *Natuurrubber* **2000**, *17*.

(10) Röthemeyer, F.; Sommer, F. *Kautschuktechnologie: Werkstoffe, Verarbeitung, Produkte*; 2nd ed.; Carl Hanser Verlag: München, Wien, **2006**.

(11) Naus, H.; Collard, F.; Winkel, H. te *Natuurrubber* **2000**, *17*.

(12) Ingles, D. *Natuurrubber* **2000**, *17*.

(13) Osmann, M. O.; Jensen, S. L. *World Journal of Surgery* **1999**, *23*, 630-637.

(14) Schlögl, S. Photochemische Techniken zur Vernetzung von Naturkautschuk- und Isopren-Latex für die Herstellung von allergiefreien Latexartikeln, TU Graz, Doktorarbeit, **2008**.

(15) Eckhart, W. U.; Gradmann, C. *Ärzte Lexikon*; 3rd ed.; Springer Verlag: Heidelberg, **2006**.

(16) Ansell Europe, date accessed: 05.01.2011, http://www.anselleurope.com/medical/index.cfm?page=manu_ppf_procs&lang=de.

(17) Mark, J. E.; Erman, B.; Eirich, F. R. *Science and Technology of Rubber*; 3rd ed.; Elsevier Academic Press, **2005**.

(18) Engels, H.-W. In *Ullmann's Encyclopedia of Industrial Chemistry*; Wiley-VCH Verlag GmbH&Co. KGaA: Weinheim, **2007**.

(19) Mausser, R. F. *The Vanderbilt Latex Handbook*; 3rd ed.; R.T. Vanderbilt Company Inc.: Norwalk, **1987**.

(20) Blackley, D. C. *Polymer Latices: Science and Technology Volume 3*; 2nd ed.; Springer Verlag, **1998**.

(21) Pro2Solutions, date accessed: 12.1.2011, http://www.pro2s.com/faq_process.htm.

(22) Calvert, K. O. *Polymer Latices and their Applications*; Macmillan Publishing Co., **1982**.

(23) Blackley, D. C. *Polymer Latices: Types of Latices*; 2nd ed.; Chapman & Hall: London, **1997**.

(24) Kubik, S. Ozonisierung. *Römpp Online*, date accessed: 31.5.2011, http://www.roempp.com/prod/.

(25) Shafiee, S.; Topal, E. *Energy Policy* **2009**, *37*, 181-189.

(26) Razykov, T. M.; Ferekides, C. S.; Morel, D.; Stefanakos, E.; Ullal, H. S.; Upadhyaya, H. M. *Solar Energy* **2011**.

(27) International Energy Agency *Renewables in Global Energy Supply*, **2007**.

(28) Grätzel, M. *Nature* **2001**, *414*, 338-344.

(29) Fradler, C. Investigations on the Layer Formation in Nanocomposite Solar Cells, TU Graz, Diplomarbeit, **2010**.

(30) Günes, S.; Sariciftci, N. S. *Inorganica Chimica Acta* **2008**, *361*, 581-588.

(31) Shirakawa, H.; Louis, E. J.; MacDiarmid, A. G.; Chiang, C. K.; Heeger, A. J. *Journal of the Chemical Society, Chemical Communications* **1977**, 578-580.

(32) Chiang, C. K.; Fincher, C. R. J.; Park, Y. W.; Heeger, A. J.; Shirakawa, H.; Louis, E. J.; Gau, S. C.; McDiarmid, A. G. *Physical Review Letters* **1977**, *39*, 1098-1101.

(33) McCullough, R. D.; Lowe, R. D.; Jayaraman, M.; Anderson, D. L. *The Journal of Organic Chemistry* **1993**, *58*, 904-912.

(34) McCullough, R. D.; Lowe, R. D. *Journal of the Chemical Society, Chemical Communications* **1992**, 70-72.

(35) Peet, J.; Kim, J. Y.; Coates, N. E.; Ma, W. L.; Moses, D.; Heeger, A J.; Bazan, G. C. *Nature Materials* **2007**, *6*, 497-500.

(36) Neef, C. J.; Ferraris, J. P. *Macromolecules* **2000**, *33*, 2311-2314.

(37) Burroughes, J. H.; Bradley, D. D. C.; Brown, A. R.; Marks, R. N.; Mackay, K.; Friend, R. H.; Burns, P. L.; Holmes, A. B. *Nature* **1990**, *347*, 539-541.

(38) Tang, W.; Ke, L.; Tan, L.; Lin, T.; Kietzke, T.; Chen, Z.-Kuan *Macromolecules* **2007**, *40*, 6164-6171.

(39) Leclerc, M. *Journal of Polymer Science Part A: Polymer Chemistry* **2001**, *39*, 2867-2873.

(40) Cheng, Y.-J.; Yang, S.-H.; Hsu, C.-S. *Chemical Reviews* **2009**, *109*, 5868-5923.

(41) Blouin, N.; Michaud, A; Leclerc, M. *Advanced Materials* **2007**, *19*, 2295-2300.

(42) Wakima, S.; Aiumlcha, B.-R.; Taob, Y.; Leclerc, M. *Polymer Reviews* **2008**, *48*, 432-462.

(43) Dierschke, F.; Grimsdale, A. C.; Müllen, K. *Synthesis* **2003**, *16*, 2470-2472.

(44) Rath, T. Synthesis and Characterization of Nanocrystalline Semiconducting Materials for Nanocomposite Solar Cells, TU Graz, Dissertation, **2008**.

(45) *Handbook of Conducting Polymers: Conjugated Polymers*; Skotheim, T. A.; Reynolds, J. R., Eds.; 3rd ed.; CRC Press, Taylor & Francis Group: Boca Raton, FL, **2007**.

(46) James, D. Towards the Synthesis of low band band-gap polymers for organic photovoltaics, Imperial College London, Master thesis, **2010**.

(47) Shockley, W.; Queisser, H. J. *Journal of Applied Physics* **1961**, *32*, 510.

(48) Kroon, R.; Lenes, M.; Hummelen, J.; Blom, P.; Boer, B. de *Polymer Reviews* **2008**, *48*, 531-582.

(49) McCulloch, I.; Heeney, M.; Chabinyc, M. L.; DeLongchamp, D.; Kline, R. J.; Cölle, M.; Duffy, W.; Fischer, D.; Gundlach, D.; Hamadani, B.; Hamilton, R.; Richter, L.; Salleo, A.; Shkunov, M.; Sparrowe, D.; Tierney, S.; Zhang, W. *Advanced Materials* **2009**, *21*, 1091-1109.

(50) Boudreault, P.-L. T.; Najari, A.; Leclerc, M. *Chemistry of Materials* **2010**, 456-469.

(51) McCulloch, I.; Heeney, M.; Bailey, C.; Genevicius, K.; Macdonald, I.; Shkunov, M.; Sparrowe, D.; Tierney, S.; Wagner, R.; Zhang, W.; Chabinyc, M. L.; Kline, R. J.; McGehee, M. D.; Toney, M. F. *Nature Materials* **2006**, *5*, 328-333.

(52) McCulloch, I.; Salleo, A. In *MRS Tutorial: Materials Science & Charge Transport in Organic Electronics*; San Francisco, **2010**.

(53) Brabec, C. J.; Heeney, M.; McCulloch, I.; Nelson, J. *Chemical Society Reviews* **2011**, *40*, 1185-1199.

(54) Günes, S.; Neugebauer, H.; Sariciftci, N. S. *Chemical Reviews* **2007**, *107*, 1324-38.

(55) Saunders, B. R.; Turner, M. L. *Advances in Colloid and Interface Science* **2008**, *138*, 1 - 23.

(56) Pagliaro, M.; Palmisano, G.; Cirimina, R. *Flexible Solar Cells*; Wiley-VCH Verlag GmbH&Co. KGaA: Weinheim, **2008**.

(57) Krebs, F. C.; Jørgensen, M.; Norrman, K.; Hagemann, O.; Alstrup, J.; Nielsen, T. D.; Fyenbo, J.; Larsen, K.; Kristensen, J. *Solar Energy Materials and Solar Cells* **2009**, *93*, 422-441.

(58) Krebs, F. C. *Solar Energy Materials and Solar Cells* **2009**, *93*, 1636-1641.

(59) Nunzi, J.-M. *C.R. Physique* **2002**, *3*, 523-542.

(60) Skompska, M. *Synthetic Metals* **2010**, *160*, 1-15.

(61) Günes, S.; Neugebauer, H.; Sariciftci, N. S. *Chemical Reviews* **2007**, *107*, 1324-38.

(62) Weller, H. *Angewandte Chemie International Edition* **1993**, *32*, 41 -53.

(63) Shaheen, S. E.; Brabec, C. J.; Sariciftci, N. S.; Padinger, F.; Fromherz, T.; Hummelen, J. C. *Applied Physics Letters* **2001**, *78*, 841.

(64) Sariciftci, N. S.; Braun, D.; Zhang, C.; Srdanov, V. I.; Heeger, A. J.; Stucky, G.; Wudl, F. *Applied Physics Letters* **1993**, *62*, 585.

(65) Yang, X.; Loos, J.; Veenstra, S. C.; Verhees, W. J. H.; Wienk, M. M.; Kroon, J. M.; Michels, M. A. J.; Janssen, R. A. J. *Nano Letters* **2005**, *5*, 579-583.

(66) Arici, E.; Meissner, D.; Schäffler, F.; Sariciftci, N. S. *International Journal of Photoenergy* **2003**, *5*, 199-208.

(67) Huynh, W. U.; Dittmer, J. J.; Alivisatos, A. P. *Science* **2002**, *295*, 2425-2427.

(68) Greenham, N.; Peng, X.; Alivisatos, A. *Physical Review B: Condensed Matter* **1996**, *54*, 17628-17637.

(69) Wang, L.; Liu, Y.; Jiang, X.; Qin, D.; Cao, Y. *Journal of Physical Chemistry C* **2007**, *111*, 9538-9542.

(70) Arici, E.; Hoppe, H.; Schäffler, F.; Meissner, D.; Malik, M. A.; Sariciftci, N. S. *Thin Solid Films* **2004**, *451-452*, 612-618.

(71) Arici, E.; Hoppe, H.; Schäffler, F.; Meissner, D.; Malik, M. A; Sariciftci, N. S. *Applied Physics A: Materials Science & Processing* **2004**, *79*, 59-64.

(72) Arici, E.; Sariciftci, N. S.; Meissner, D. *Advanced Functional Materials* **2003**, *13*, 165-171.

(73) Piber, M.; Rath, T.; Grießer, T.; Trimmel, G.; Stelzer, F.; Meissner, D. In *World Conference on Photovoltaic Energy Conversion, Conference Record of the 2006 IEEE 4th*; Hawaii, **2006**; pp. 247-248.

(74) Watt, A. A. R.; Blake, D.; Warner, J. H.; Thomsen, E. A; Tavenner, E. L.; Rubinsztein-Dunlop, H.; Meredith, P. *Journal of Physics D: Applied Physics* **2005**, *38*, 2006-2012.

(75) McDonald, S. A; Konstantatos, G.; Zhang, S.; Cyr, P. W.; Klem, E. J. D.; Levina, L.; Sargent, E. H. *Nature Materials* **2005**, *4*, 138-42.

(76) Günes, S.; Fritz, K. P.; Neugebauer, H.; Sariciftci, N. S.; Kumar, S.; Scholes, G. D. *Solar Energy Materials and Solar Cells* **2007**, *91*, 420-423.

(77) Salafsky, J. S. *Physical Review B* **1999**, *59*, 885-894.

(78) Zeng, T.-W.; Lin, Y.-Y.; Lo, H.-H.; Chen, C.-W.; Chen, C.-H.; Liou, S.-C.; Huang, H.-Y.; Su, W.-F. *Nanotechnology* **2006**, *17*, 5387-5392.

(79) Hal, P. A. van; Wienk, M. M.; Kroon, J. M.; Verhees, J. H.; Sloof, L. H.; Gennip, W. J. H. van; Jonkheijm, P.; Janssen, R. A. J. *Advanced Materials* **2003**, *15*, 118-121.

(80) Beek, W. J. E.; Wienk, M. M.; Janssen, R. A. J. *Advanced Materials* **2004**, *16*, 1009-1013.

(81) Ravirajan, P.; Peiró, A. M.; Nazeeruddin, M. K.; Graetzel, M.; Bradley, D. D. C.; Durrant, J. R.; Nelson, J. *The Journal of Physical Chemistry B* **2006**, *110*, 7635-7639.

(82) Quist, P. A. C.; Beek, W. J. E.; Wienk, M. M.; Janssen, R. A. J.; Savenije, T. J.; Siebbeles, L. D. A. *The Journal of Physical Chemistry B* **2006**, *110*, 10315-10321.

(83) Arici, E.; Sariciftci, N.; Meissner, D. *Advanced Functional Materials* **2003**, *13*, 165-171.

(84) Saunders, B. R.; Turner, M. L. *Advances in Colloid and Interface Science* **2008**, *138*, 1-23.

(85) Goetzberger, A. *Solar Energy Materials and Solar Cells* **2000**, *62*, 1-19.

(86) WikiCommons, SEM electrons photons, date accessed: 22.5.2011, http://commons.wikimedia.org/wiki/File:Sem_electrons_photons.svg.

(87) Reingruber, H. *Rasterelektronenmikroskopie-Praktikum für Fortgeschrittene*; TU Graz, **2010**.

(88) Flegler, S. L.; Heckmann, J. W.; Klomparens, K. L. *Elektronenmikroskopie: Grundlagen-Methoden-Anwendungen*; Spektrum Akademischer Verlag: Heidelberg, **1995**.

(89) Goldstein, J.; Newbury, D.; Joy, D.; Lyman, C.; Echlin, P.; Lifshin, E.; Michae, J.; I, C. *Scanning Electron Microscopy and X-Ray Microanalysis*; 3rd ed.; Kluwer Academic/Plenum Publishers: New York, **2003**.

(90) Egerton, R. F. *Physical Principles of Electron Microscopy*; Springer Science + Business Media Inc.: New York, 2005.

(91) Amelinckx, S.; Dyck, D. van; Landuyt, J. van; Tendeloo, G. van *Electron Microscopy: Principles and Fundamentals*; Wiley-VCH Verlag GmbH&Co. KGaA: Weinheim, **1997**.

(92) Smith College, Scanning Electron Microscopy (SEM) Machine Variables, date accessed: 20.1.2011, http://131.229.114.77/microscopy/semvar.html.

(93) Institut für Umweltbiotechnologie, TU Graz, *Praktikum Mikroskopie,* **2006**.

(94) Montaudo, G.; Lattimer, R. *Mass Spectrometry of Polymers*; CRC Press, Taylor & Francis Group, **2002**.

(95) Linscheid, M. Mass spectrometry. *Ullmann's Encyclopedia of Industrial Chemistry,* Wiley-VCH Verlag GmbH & Co. KGaA: Weinheim **2005**.

(96) Hesse, M.; Meier, H.; Zeeh, B. *Spektroskopische Methoden in der organischen Chemie*; 7th ed.; Thieme: Stuttgart, **2005**.

(97) Wikipedia, EI source date accessed: 31.3.2011, http://en.wikipedia.org/wiki/File:Schematic_diagram_of_an_EI_ion_source.jpg.

(98) Burgoyne, T. W.; Hieftje, G. M. *Mass Spectrometry Reviews* **1996**, *15*, 241-259.

(99) Gottlieb, H. E.; Kotlyar, V.; Nudelman, A. *Journal of Organic Chemistry* **1997**, *3263*, 7512-7515.

(100) Heeney, M. Stannylation of Thienothiophene, working paper.

(101) Stille, J. K. *Angewandte Chemie International Edition* **1986**, *25*, 508-524.

(102) Heeney, M.; Bailey, C.; Genevicius, K.; Shkunov, M.; Sparrowe, D.; Tierney, S.; McCulloch, I. *Journal of the American Chemical Society* **2005**, *127*, 1078-1079.

(103) Fischer, E.; Speier, A. *Berichte der Deutschen Chemischen Gesellschaft* **1895**, 3252-3258.

(104) Tierney, S.; Heeney, M.; Mcculloch, I. *Synthetic Metals* **2005**, *148*, 195-198.

(105) Chan, S.-Hua; Chen, C.-Ping; Chao, T.-Chih; Ting, C.; Lin, C.-Sheng; Ko, B.-Tsan *Macromolecules* **2008**, *41*, 5519-5526.

(106) Van Mierloo, S.; Adriaensens, P. J.; Maes, W.; Lutsen, L.; Cleij, T. J.; Botek, E.; Champagne, B.; Vanderzande, D. J. *The Journal of Organic Chemistry* **2010**.

(107) Maier, E.; Rath, T.; Haas, W.; Werzer, O.; Saf, R.; Hofer, F.; Meissner, D.; Volobujeva, O.; Bereznev, S.; Mellikov, E. *Solar Energy Materials and Solar Cells* **2011**, *95*, 1354-1361.

(108) Fischereder, A.; Rath, T.; Haas, W.; Amenitsch, H.; Albering, J.; Meischler, D.; Larissegger, S.; Edler, M.; Saf, R.; Hofer, F.; Trimmel, G. *Chemistry of Materials* **2010**, *22*, 3399–3406.

(109) Fischereder, A.; Rath, T.; Haas, W.; Amenitsch, H.; Meischler, D.; Zankel, A.; Saf, R.; Hofer, F.; Trimmel, G. *in work*.

(110) Schenk, A. Novel metal-xanthates for preparation of metal sulphides for photovoltaic applications, TU Graz, Master thesis, **2011**.

(111) Ansell, date accessed: 3.2.2009, www.ansell.eu.

(112) Cardinal Health, date accessed: 3.2.2009, www.cardinalhealth.com.

(113) Hartmann, date accessed: 3.2.2009, http://produktkatalog.hartmann.info.

(114) LCH Medical, date accessed: 3.2.2009, www.lch-medical.com.

(115) Medisavers, date accessed: 3.2.2009, www.medisavers.co.uk.

(116) Semperit Technische Produkte GmbH, Sempermed, date accessed: 3.2.2009, http://www.sempermed.com/de/medizinische_handschuhe/downloads/deutsch.html.

(117) Supergloves, Supermax, date accessed 11.2.2011, www.supergloves.com.

(118) Elias, H. G. Plastics , General Survey. *Ullmann's Encyclopedia of Industrial Chemistry,* Wiley-VCH Verlag GmbH & Co. KGaA: Weinheim **2005**.

(119) Reiss, P.; Couderc, E.; De Girolamo, J.; Pron, A. *Nanoscale* **2010**, *3*, 446-489.

(120) Kingsborough, R.; Waller, D.; Gaudiana, R.; Muhlbacher, D.; Morana, M.; Scharber, M.; Zhu, Z. *Journal of Macromolecular Science: Part A* **2010**, *47*, 478-483.

(121) Heeney, M.; Bailey, C.; Genevicius, K.; Shkunov, M.; Sparrowe, D.; Tierney, S.; McCulloch, I. *Journal of the American Chemical Society* **2005**, *127*, 1078-9.

(122) Kappe, C. O.; Dallinger, D.; Murphree, S. *Practical Microwave Synthesis for Organic Chemists*; 1st ed.; Wiley-VCH Verlag GmbH&Co. KGaA: Weinheim, **2008**.

(123) Nehls, B. S.; Asawapirom, U.; Füldner, S.; Preis, E.; Farrell, T.; Scherf, U. *Advanced Functional Materials* **2004**, *14*, 352-356.

(124) Grignard, V. *Comptes rendus hebdomadaires des séances de l'Académie des sciences* **1900**, *130*, 1322.

(125) Kingsborough, R.; Waller, D.; Gaudiana, R.; Muhlbacher, D.; Morana, M.; Scharber, M.; Zhu, Z. *Journal of Macromolecular Science: Part A* **2010**, *47*, 478-483.

(126) Krunks, M.; Mikli, V.; Bijakina, O.; Rebane, H.; Mere, A.; Varema, T.; Mellikov, E. *Thin Solid Films* **2000**, *361*, 61-64.

(127) Krunks, M. *Thin Solid Films* **2002**, *403-404*, 71-75.

(128) Krunks, M.; Leskelä, T.; Niinistö, L. *Japanese Journal of Applied Physics* **2000**, *39*, 181-186.

(129) Schaber, P. *Thermochimica Acta* **2004**, *424*, 131-142.

(130) Crews, G. M.; Ripperger, W.; Burkhard, D.; Güthner, T.; Mertschenk, B. Melamine and Guanamines. *Ullmann's Encyclopedia of Industrial Chemistry,* Wiley-VCH Verlag GmbH & Co. KGaA: Weinheim **2006**.

(131) Melamin. *Römpp Online,* date accessed: 30.4.2011, http://www.roempp.com/prod/.

(132) Tschugaeff, L. *Berichte der Deutschen Chemischen Gesellschaft* **1899**, *32*, 3332-3335.

(133) Saunders, B. R.; Turner, M. L. *Advances in Colloid and Interface Science* **2008**, *138*, 1-23.

(134) Arici, E.; Meissner, D.; Schäffler, F.; Sariciftci, N. S. *International Journal of Photoenergy* **2003**, *5*, 199-208.

(135) Watt, A. A. R.; Blake, D.; Warner, J. H.; Thomsen, E. aA. Tavenner, E. L.; Rubinsztein-Dunlop, H.; Meredith, P. *Journal of Physics D: Applied Physics* **2005**, *38*, 2006-2012.

8 Appendix

8.1 Abbreviations

SEM	scanning electron microscope/scanning electron microscopy
RT	room temperature
ppt	precipitate
eq	equivalents
M	molar
DCM	dichloromethane
DMF	dimethyl formamide
TU	thiourea
CIS	$CuInS_2$
mmol	millimol
ml	milliliter
mg	milligrams
EI-MS	electron impact mass spectrometry
TOF	time-of-flight
MALDI	matrix assisted laser desorption ionisation
*p*TSA	*p*-toluene sulphonic acid
HRMS	high resolution mass spectrometry
n-BuLi	*n*-butyl lithium

8.2 Used Chemicals

All chemicals were obtained from Sigma Aldrich, Alfa Aesar, Fluka, Merck and Roth and used without further purification unless otherwise stated (Table 3).

8.3 List of Figures

Figure 1: Production of powder coated latex gloves [8,14,16] 16

Figure 2: Production of powder-free latex gloves. [8,14,16] The highlighted area (blue rectangle) shows the differences to powder-coated medical gloves. 21

Figure 3: World primary energy supplies [27] 25

Figure 4: Influence of the conjugation length on the bandgap. [53] LUMO (lowest unoccupied molecular orbital), HOMO (highest occupied molecular orbital) 27

Figure 5: Effects leading to a low bandgap polymer. [40] LUMO (lowest unoccupied molecular orbital), HOMO (highest occupied molecular orbital), D (donor), A (acceptor), BLA (bond length alternation) 28

Figure 6: The bandgap can be lowered through the interaction of donor and acceptor units. [40,53] LUMO (lowest unoccupied molecular orbital), HOMO (highest occupied molecular orbital), D (donor), A (acceptor) 29

Figure 7: Schematic drawing of a nanocomposite solar cell 30

Figure 8: Transport of charges within a solar cell. [55] HOMO (highest occupied molecular orbital), LUMO (lowest unoccupied molecular orbital), VB (valence band), CB (conduction band), h^+ (hole), e^- (electron), IP (ionisation potential), E_g (bandgap), hv (incident light), acceptor (inorganic nanoparticles), donor (organic polymer) 32

Figure 9: Schematic drawing of a bilayer heterojunction (left) and a bulk heterojunction (right). [55] h^+ (hole), e^- (electron), L_{pol} (mean domain size of the polymer), L_{ex} (exciton diffusion length) 32

Figure 10: Schematic drawing for the production of CIS/polymer nanocomposite solar cells. ITO (indium tin oxide), TU (thiourea) 33

Figure 11: Interactions of primary electrons and specimen. [86] a: secondary electrons (SE); b: backscattered electrons (BSE); c: Auger electrons; d: characteristic X-rays 34

Figure 12: Interactions of the electron beam with the specimen [87] 35

Figure 13: Dependence of atomic number (Z) and acceleration voltage (E_0) on the interaction volume [90] 36

Figure 14: Edge effect in SEM. More electrons escape from morphological surface features. [92] 37

Figure 15: Schematic diagram of a scanning electron microscope (SEM) [87] 39

Figure 16: Schematic drawing of a Wehnelt cylinder (left) and a tungsten filament (right) [87] 40

Figure 17: Scanning principle in a SEM [90] 43

Figure 18: Everhart-Thornley detector [90] 43
Figure 19: Resolution and magnification areas in microscopy [93] 45
Figure 20: Schematic drawing of a mass spectrometer 48
Figure 21: Schematic drawing of an EI source. [97] e^-: electron; $M^{+\bullet}$: molecular ion 49
Figure 22: Micro channel plate (top) and signal amplification in a channel (bottom) [94] 51
Figure 23: SEM images of samples dipped in $CaCl_2$ coagulant, dry powder coated, not chlorinated (13, 14); top: fresh sample, (a) outer side, (b) inner side, (c) breaking edge (RT fracture); bottom: aged sample (21 days), (d) outer side, (e) inner side, (f) breaking edge (freeze fracture), tilted 10°; 5.0 kV, magnification = 1000 x, wd 10 for outer and inner side, wd 15 for edges 67
Figure 24: SEM images of samples dipped in $Ca(NO_3)_2$ coagulant, dry powder coated, not chlorinated (15, 16); top: fresh sample, (a) outer side, (b) inner side, (c) breaking edge (RT fracture); bottom: aged sample (21 days), (d) outer side, (e) inner side, (f) breaking edge (freeze fracture), tilted 10°; 5.0 kV, magnification = 1000 x, wd 10 for outer and inner side, wd 15 for edges 68
Figure 25: SEM images of the untreated material, not chlorinated (17, 18); top: fresh sample, (a) outer side, (b) inner side, (c) breaking edge (RT fracture); bottom: aged sample (21 days), (d) outer side, (e) inner side, (f) breaking edge (freeze fracture), tilted 10°; 5.0 kV, magnification = 1000 x, wd 10 for outer and inner side, wd 15 for edges 70
Figure 26: SEM images of Sempermed Classic, not chlorinated, modified coating (49); fresh sample, (a) outer side, (b) inner side, (c) breaking edge (RT fracture); 5.0 kV, magnification = 1000 x, wd 10 for outer and inner side, wd 15 for edges 71
Figure 27: SEM images of OPH sterilised, UV-crosslinked latex, not chlorinated (51); fresh sample, (a) outer side, (b) inner side, (c) breaking edge (RT fracture); 5.0 kV, magnification = 1000 x, wd 10 for outer and inner side, wd 15 for edges 72
Figure 28: SEM images of Supreme without leaching, not chlorinated (19, 20); top: fresh sample, (a) outer side, (b) inner side, (c) breaking edge (freeze fracture); bottom: aged sample (21 days), (d) outer side, (e) inner side, (f) breaking edge (freeze fracture), tilted 10°; 5.0 kV, magnification = 1000 x, wd 10 for outer and inner side, wd 15 for edges 73
Figure 29: SEM images of Supreme without leaching, not chlorinated, modified coating (21, 22); top: fresh sample, (a) outer side, (b) inner side, (c) breaking edge (freeze fracture), tilted 20°; bottom: aged sample (21 days), (d) outer side, (e) inner side, (f) breaking edge (freeze fracture), tilted 10°; 5.0 kV, magnification = 1000 x, wd 10 for outer and inner side, wd 15 for edges 74
Figure 30: SEM images of Supreme TWA/standard, not chlorinated (31, 32); top: fresh sample, (a) outer side, (b) inner side, (c) breaking edge (freeze fracture); bottom: aged sample (21 days), (d) outer side, (e) inner side, (f) breaking edge (freeze fracture), tilted 10°; 5.0 kV, magnification = 1000 x, wd 10 for outer and inner side, wd 15 for edges 75

Figure 31: SEM images of Supreme TWA/standard, not chlorinated, modified coating (33, 34); top: fresh sample, (a) outer side, (b) inner side, (c) breaking edge (freeze fracture), tilted 10°; bottom: aged sample (21 days), (d) outer side, (e) inner side, (f) breaking edge (freeze fracture), tilted 10°; 5.0 kV, magnification = 1000 x, wd 10 for outer and inner side, wd 15 for edges 76

Figure 32: SEM images of Supermax Premium Quality, not chlorinated, powder coated (43); fresh sample, (a) outer side, (b) inner side, (c) breaking edge (RT fracture); 5.0 kV, magnification = 1000 x (d=10000 x), wd 10 for outer and inner side, wd 15 for edges 77

Figure 33: SEM images of Ansell Conform, not chlorinated, powder coated (44); fresh sample, (a) outer side, (b) inner side, (c) breaking edge (RT fracture); 5.0 kV, magnification = 1000 x, wd 10 for outer and inner side, wd 15 for edges 78

Figure 34: SEM images of Sempercare Edition 2008, modified coating, powder coated (45); fresh sample, (a) outer side, (b) inner side, (c) breaking edge (RT fracture); 5.0 kV, magnification = 1000 x, wd 10 for edge, outer and inner side 79

Figure 35: SEM images of Sempercare IC 2007, low degree of chlorination, rough surface (5, 6); top: fresh sample, (a) outer side, (b) inner side, (c) breaking edge (RT fracture); bottom: aged sample (21 days), (d) outer side, (e) inner side, (f) breaking edge (freeze fracture); 5.0 kV, magnification = 1000 x, wd 10 for outer and inner side, wd 15 for edges 81

Figure 36: SEM images of Semperguard 2008, low degree of chlorination, rough surface (46); top: fresh sample, (a) outer side, (b) inner side, (c) breaking edge (RT fracture); 5.0 kV, magnification = 1000 x, wd 10 for breaking edge, outer and inner side 82

Figure 37: SEM images of Sempercare IC 2006, low degree of chlorination, rough surface (7, 8); top: fresh sample, (a) outer side, (b) inner side, (c) breaking edge (RT fracture), wd 10; bottom: aged sample (21 days), (d) outer side, (e) inner side, (f) breaking edge (freeze fracture), wd 15; 5.0 kV, magnification = 1000 x, wd 10 for outer and inner side 83

Figure 38: SEM images of Supreme NaOCl, dry powder (23, 24); top: fresh sample, (a) outer side, (b) inner side, (c) breaking edge (freeze fracture); bottom: aged sample (21 days), (d) outer side, (e) inner side, (f) breaking edge (freeze fracture); 5.0 kV, magnification = 1000 x, wd 10 for outer and inner side, wd 15 for edges 84

Figure 39: SEM images of Supreme NaOCl, modified coating (25, 26); top: fresh sample, (a) outer side, (b) inner side, (c) breaking edge (freeze fracture); bottom: aged sample (21 days), (d) outer side, (e) inner side, (f) breaking edge (freeze fracture), tilted 10°; 5.0 kV, magnification = 1000 x, wd 10 for outer and inner side, wd 15 for edges 85

Figure 40: SEM images of samples dipped in $CaCl_2$ coagulant, modified coating (9, 10); top: fresh sample, (a) outer side, (b) inner side, (c) breaking edge (freeze fracture), tilted 10°; bottom: aged sample (21 days), (d) outer side, (e) inner side, (f) breaking edge (freeze fracture), tilted 10°; 5.0 kV, magnification = 1000 x, wd 10 for outer and inner side, wd 15 for edges 86

Figure 41: SEM images of samples dipped in $Ca(NO_3)_2$ coagulant, modified coating (11, 12); top: fresh sample, (a) outer side, (b) inner side, (c) breaking edge (freeze fracture), tilted 10°; bottom: aged sample (21 days), (d) outer side, (e) inner side, (f) breaking edge (freeze fracture), tilted 10°; 5.0 kV, magnification = 1000 x, wd 10 for outer and inner side, wd 15 for edges 87

Figure 42: SEM images of Sempercare LF 2007, high degree of chlorination, rough surface (1, 2); top: fresh sample, (a) outer side, (b) inner side, (c) breaking edge (RT fracture); bottom: aged sample (21 days), (d) outer side, (e) inner side, (f) breaking edge (freeze fracture); 5.0 kV, magnification = 1000 x, wd 10 for outer and inner side, wd 15 for edges 90

Figure 43: SEM images of Sempercare Edition 2008, high degree of chlorination, rough surface (47); fresh sample, (a) outer side, (b) inner side, (c) breaking edge (RT fracture); 5.0 kV, magnification = 1000 x, wd 10 for breaking edge, outer and inner side 91

Figure 44: SEM images of Sempercare LF 2006, high degree of chlorination, rough surface (3, 4); top: fresh sample, (a) outer side, (b) inner side, (c) breaking edge (RT fracture), wd 10; bottom: aged sample (21 days), (d) outer side, (e) inner side, (f) breaking edge (freeze fracture), wd 15; 5.0 kV, magnification = 1000 x, wd 10 for outer and inner side 92

Figure 45: SEM images of Sempercare Edition 2008, high degree of chlorination, smooth surface (48); fresh sample, (a) outer side, (b) inner side, (c) breaking edge (RT fracture); 5.0 kV, magnification = 1000 x, wd 10 for breaking edge, outer and inner side 93

Figure 46: SEM images of Hartmann's Peha Soft, high degree of chlorination, smooth surface (35, 36); top: fresh sample, (a) outer side, (b) inner side, (c) breaking edge (RT fracture); bottom: aged sample (17 days), (d) outer side, (e) inner side, (f) breaking edge (RT fracture); 5.0 kV, magnification = 1000 x, wd 10 for outer and inner side, wd 15 for breaking edges 94

Figure 47: SEM images of Sempermed Supreme, high degree of chlorination, modified coating (50); fresh sample, (a) outer side, (b) inner side, (c) breaking edge (RT fracture); 5.0 kV, magnification = 1000 x, wd 10 outer and inner side, wd 15 for breaking edge 95

Figure 48: SEM images of Supreme HCl/NaOCl, dry powder (27, 28); top: fresh sample, (a) outer side, (b) inner side, (c) breaking edge (freeze fracture); bottom: aged sample (21 days), (d) outer side, (e) inner side, (f) breaking edge (freeze fracture), tilted 10°; 5.0 kV, magnification = 1000 x, wd 10 for outer and inner side, wd 15 for edges 96

Figure 49: SEM images of Supreme HCl/NaOCl, modified coating (29, 30); top: fresh sample, (a) outer side, (b) inner side, (c) breaking edge (freeze fracture), tilted 10°; bottom: aged sample (21 days), (d) outer side, (e) inner side, (f) breaking edge (freeze fracture), tilted 10°; 5.0 kV, magnification = 1000 x, wd 10 for outer and inner side, wd 15 for edges 97

Figure 50: ^{1}H-NMR spectrum of substance 1 100

Figure 51: ^{13}C-NMR spectrum of substance 1 101

Figure 52: ^{1}H-NMR spectrum of substance 2 102
Figure 53: ^{13}C-NMR spectrum of substance 2 103
Figure 54: ^{1}H-NMR spectrum of substance 3 104
Figure 55: ^{13}C-NMR spectrum of substance 3 105
Figure 56: EI-MS spectrum of substance 3 106
Figure 57: FTIR spectra of substance 5 109
Figure 58: HRMS data of the “mixed fractions” of substance 5 110
Figure 59: EI-MS total ion chromatogram and selected ion traces of melamine in $CuInS_2$ thin films prepared at 200°C (4 eq thiourea) (top: total ion current, middle: ion trace molecular ion, bottom: ion trace fragment ion ($C_2H_5N_4$)) 112
Figure 60: EI-MS spectrum of indium *O*-2,2-dimethylpentan-3-yl dithiocarbonate 114
Figure 61: EI-MS spectrum of copper *O*-2,2-dimethylpentan-3-yl dithiocarbonate 115
Figure 62: EI mass spectrum of 2,2'-(thieno[3,2-*b*]thiophene-2,5-diyl)bis(thiophene-3-carboxylate) 119
Figure 63: HRMS of TTTT (compound 5) 120
Figure 64: EI mass spectrum of indium *O*-2,2-dimethylpentan-3-yl dithiocarbonate 122

8.4 List of Schemes

Scheme 1: Synthesis of substance 1 59
Scheme 2: Synthesis of substance 2 60
Scheme 3: Synthesis of substance 3 61
Scheme 4: Synthesis of substance 4 62
Scheme 5: Synthesis of TTTT 5 63
Scheme 6: Reaction pathway leading to TTTT 99
Scheme 7: Trimerisation of dicyandiamide 113
Scheme 8: Structures of novel metal-xanthates 113

8.5 List of Tables

Table 1: Typical composition of natural rubber [6] 14
Table 2: Characteristics of different mass analysers [94] 50
Table 3: Chemicals 55
Table 4: Investigated latex samples - Semperit 57
Table 5: Investigated latex samples - other companies 58
Table 6: Investigated, not aged latex samples 58
Table 7: Overview of non-chlorinated latex samples 66
Table 8: Overview on chlorinated (low degree) samples 80
Table 9: Overview on samples with a high degree of chlorination 89
Table 10: Assignment of absorptions observed in the FTIR spectra of compound 5 108